

Structural and Biochemical Characterization of an Archaeal ParA Protein

by

Jeehyun Lee

Department of Biochemistry  
Duke University

Date: \_\_\_\_\_

Approved:

\_\_\_\_\_  
Maria A Schumacher, Supervisor

\_\_\_\_\_  
David C Richardson

\_\_\_\_\_  
Richard G Brennan

\_\_\_\_\_  
Harold P Erickson

Dissertation submitted in partial fulfillment of  
the requirements for the degree of Doctor  
of Philosophy in the Department of  
Biochemistry in the Graduate School  
of Duke University

2015

ABSTRACT

Structural and Biochemical Characterization of an Archaeal ParA Protein

by

Jeehyun Lee

Department of Biochemistry  
Duke University

Date: \_\_\_\_\_

Approved:

\_\_\_\_\_  
Maria A Schumacher, Supervisor

\_\_\_\_\_  
David C Richardson

\_\_\_\_\_  
Richard G Brennan

\_\_\_\_\_  
Harold P Erickson

An abstract of a dissertation submitted in partial  
fulfillment of the requirements for the degree  
of Doctor of Philosophy in the Department of  
Biochemistry in the Graduate School of  
Duke University

2015

Copyright by  
Jeehyun Lee  
2015

## Abstract

DNA partition or segregation is the process that ensures the stable inheritance of genomic material. The majority of the bacterial plasmid and some chromosomal partition systems utilize ParA Walker-box-based partition systems. These systems require three components: a DNA centromere site, the ParA ATPase, and the ParB centromere binding protein. ParB binds to the centromere to form the partition complex, which then recruits the motor protein ParA. ParA mediates the partition of replicated DNA by a still poorly understood mechanism. Notably, recent data indicates that ParA Walker-box-based partition systems are employed not only by bacterial plasmids and chromosomes but also DNA elements in archaea. The work in this thesis focused on a homolog of the ParA protein from the first identified archaeal plasmid partition system, located on the plasmid pNOB8. pNOB8 plasmid is harbored in the thermophilic archaeon, *Sulfolobus solfataricus*. The goals of this work were to structurally and biochemically characterize the ParA homolog to gain insights into its function.

Towards these goals, the structure of the ParA homolog was solved by X-ray crystallography in its apo and ADP bound states to resolutions of 2.45 Å and 2.73 Å, respectively. The overall structure was similar to bacterial ParA proteins. We next demonstrated that, similar to bacterial ParA proteins, this ParA homolog harbored ATP-dependent nonspecific DNA capabilities by using fluorescence polarization based DNA binding assays. By mutating the residues in the deviant Walker A motif, we were able to demonstrate the importance of ATP binding in its DNA binding function. Moreover,

characterization of ATP and ADP binding were performed using ITC. Finally, we observed that ParA was able to form polymers in the presence of ATP, using negative stain electron microscopy. Our findings provide evidence that ParA Walker-box-based partition systems, which are the most common systems in bacteria, appear to also be found in archaea.

# Contents

Abstract .....	iv
List of Tables .....	x
List of Figures .....	xi
List of Abbreviations .....	xiv
Acknowledgements .....	xvi
1. Introduction .....	1
1.1 Introduction to DNA partition .....	1
1.2 Type II partition system: Actin-like ParM and ParR move plasmid by insertional polymerization mechanism.....	3
1.3 Type III partition system: Tubulin/FtsZ-like TubZ and TubR move plasmid by tram-like mechanism.....	5
1.4 Type I partition system.....	6
1.4.1 Role of ParA in Type I partition .....	7
1.4.2 ParA has ATP-dependent polymerization and nonspecific DNA binding activities .....	8
1.4.3 CBP has a critical role in stimulating the ATPase activity of ParA .....	9
1.4.4 Models for Type I partitioning.....	10
1.4.5 Chromosomal ParA.....	12
1.5 Archaeal DNA partition system.....	13
1.5.1 General introduction to Archaea.....	13
1.5.2 <i>Sulfolobus solfataricus</i> .....	14
1.5.3 DNA partition machinery in pNOB8 plasmid .....	15
Chapter 2. Crystallography .....	31

2.1 Why X-rays? .....	31
2.2 Why Crystals? .....	32
2.3 Symmetry.....	32
2.4 How does diffraction happen? .....	33
2.4.1 Bragg's Law .....	33
2.4.2 Ewald sphere.....	34
2.5 How do we go from x-ray diffraction data to electron density maps?.....	35
2.6 Phase Determination.....	37
2.6.1 Isomorphous replacement.....	37
2.6.2 MAD (Multiwavelength Anomalous Dispersion).....	38
2.6.3 Locating heavy atoms in the unit cell- Patterson map.....	41
2.6.4 Molecular Replacement (MR).....	42
2.7 After obtaining the initial map .....	43
Chapter 3. Structural studies on ParA .....	56
3.1 Structure determination of ParA structures .....	58
3.2 Overall structure of ParA .....	58
3.3 The insert region.....	59
3.4 ParA shares a set of conserved nucleotide binding motifs with other bacterial Walker-type family proteins.....	60
3.5 Dimerization interface .....	61
3.6 Structure of ParA-ADP .....	61
3.7 ADP binding site .....	62
3.8 Discussion.....	64
3.9 Experimental Procedures .....	65

Chapter 4. Functional studies of ParA .....	81
4.1. ATP-dependent nonspecific DNA binding studies using fluorescence polarization based DNA binding assays.....	83
4.2. Site-directed mutagenesis studies.....	84
4.2.1 ATP binding site (deviant Walker A motif).....	84
4.2.2 Insert region .....	84
4.2.3 Dimerization interface .....	85
4.3 ATP/ADP binding studies using Isothermal Titration Calorimetry .....	85
4.4. ATP-dependent polymerization of ParA.....	86
4.5 Effect of DNA on ParA polymer formation.....	86
4.6 Discussion.....	87
4.6.1 DNA binding by ParA and ParA homologs.....	87
4.6.2 Assembly of proteins in the Walker-type family of proteins.....	89
4.7 Experimental procedures .....	92
Chapter 5. Discussion and Conclusion .....	105
5.1 Speculative Model for archaeal ParA mediated partition .....	106
5.2 Comparison with closely related Min System in E. coli .....	106
5.3 ParA-like ATPases in other processes .....	107
5.4 Future Directions.....	108
Appendix. Protein-protein interaction studies of RacA and DivIVA .....	110
Introduction.....	110
Result.....	112
Discussion.....	113
Experimental Procedures .....	113

References .....	119
Biography .....	128

## List of Tables

Table 1. Nomenclatures of ParA and ParB homologs.....	24
Table 2. Comparison between Type Ia and Type Ib <i>par</i> loci.....	25
Table 3. Seven crystal lattice system.....	48
Table 4. The 14 Bravais lattices.....	49
Table 5. Crystallographic statistics for ParA apo and ParA-ADP structures .....	80
Table 6. DNA binding studies of ParA mutants.....	99
Table 7. Primers used for site-directed mutagenesis .....	104

## List of Figures

Figure 1. General mechanism of DNA partition .....	18
Figure 2. Genetic organization of <i>par</i> loci .....	19
Figure 3. The structures of ParM and ParR- <i>parC</i> partition complex .....	20
Figure 4. The pushing mechanism of plasmid partition by Type II <i>par</i> system.....	21
Figure 5. Structures of TubZ and TubR .....	22
Figure 6. DNA partition by Type III <i>par</i> system.....	23
Figure 7. Size comparison between ParA homologs.....	26
Figure 8. Position of plasmids maintained by Type I <i>par</i> loci.....	27
Figure 9. Pulling mechanism by Type I <i>par</i> system.....	28
Figure 10. Comparison between two models for Type I DNA partition .....	29
Figure 11. Phylogenetic tree of life showing three domains of life.....	30
Figure 12. The overview of X-ray crystallography.....	45
Figure 13. Crystal lattice.....	46
Figure 14. Unit cell .....	47
Figure 15. Derivation of Bragg's Law .....	50
Figure 16. Ewald's sphere describes diffraction in the reciprocal space .....	51
Figure 17. Isomorphous Replacement.....	52
Figure 18. Anomalous scattering by the heavy atom.....	53
Figure 19. Fluorescence scan of the Selenium.....	54
Figure 20. A: Harker construction of SIRAS B: Harker construction of MAD. ....	55
Figure 21. Sequence alignment of pNOB8 ParA and the ParA homolog.....	68
Figure 22. Overall structure of ParA .....	69

Figure 23. Structure comparisons of ParA homologs .....	70
Figure 24. The insert region .....	71
Figure 25. Multiple sequence alignment of pNOB8 ParA and other ParA homologs. ....	72
Figure 26. The Dimerization interface.....	73
Figure 27. Oligomeric state of ParA in solution determined by size exclusion chromatography.....	74
Figure 28. Comparison between apo ParA and Par-ADP structures .....	75
Figure 29. The ADP binding site.....	76
Figure 30. Close up view of the ADP binding site .....	77
Figure 31. Loop change upon ADP binding.....	78
Figure 32. Purification and crystallization of ParA .....	79
Figure 33. ATP-dependent nonspecific DNA binding activity of ParA.....	96
Figure 34. Structure based site-directed mutagenesis studies.....	97
Figure 35. Site-directed mutagenesis studies on deviant Walker A motif.....	98
Figure 36. ITC isotherms of ATP binding and ADP binding of ParA .....	100
Figure 37. ATP-dependent polymerization of ParA .....	101
Figure 38. ATP-dependent polymer formation at 1 $\mu$ M protein concentration.....	102
Figure 39. Negative stain electron micrographs of ParA incubated with ATP in the absence and presence of DNA <i>in vitro</i> . .....	103
Figure 40. Schematic figure of the speculative model for archaeal ParA mediated partition.....	109
Figure 41. Chromosome segregation during sporulation in <i>B. subtilis</i> .....	115
Figure 42. Constructs of DivIVA (59-164) and RacA (70-184) used for the interaction studies.....	116
Figure 43. ITC isotherms of DivIVA and RacA interactions.....	117

Figure 44. ITC control experiments. .... 118

## List of Abbreviations

ATP: Adenosine-5'-triphosphate

ADP: Adenosine-5'-diphosphate

AMP-PNP: Adenosine-5'-( $\beta,\gamma$ -imido)triphosphate, an ATP analog

B834(DE3): Methionine auxotroph for labeling target proteins with selenomethionine

BSA: Buried surface area

BL21(DE3): *E. coli* expression strain carrying T7 RNA polymerase and lysozyme gene

CBP: Centromere binding protein

DNA: Deoxyribonucleic acid

DTT: Dithiothreitol

*E. coli*: *Escherichia coli*

EM: Electron microscopy

FP: Fluorescence polarization

His-tag: Hexa-histidine tag

IPTG: Isopropyl- $\beta$ -D-thio-galactoside

ITC: Isothermal titration calorimetry

$K_d$ : Dissociation constant

MAD: Multiwavelength anomalous diffraction

MANT-ATP: 2'(3')-O-(N-Methylanthraniloyl)-Adenosine 5'-Triphosphate

Mg: Magnesium

Ni: Nickel

NTPase: Nucleotide triphosphatase

OD<sub>600</sub>: Optical density at 600 nm

PDB: Protein data bank

PEG: Polyethylene glycol

pET: Prokaryotic expression vector with T7 promoter and *lacI*

pH: Power of hydrogen

P-loop: Phosphate binding loop

RMSD: Root mean square deviation

S75: Superdex-75

SDS-PAGE: Sodium dodecyl sulfate-polyacrylamide gel electrophoresis

## Acknowledgements

I would like to sincerely thank my mentor, Dr. Maria Schumacher, for her guidance and support. She has encouraged me to be independent and confident as a scientist. I would also like to thank all my committee members, Dr. Richard Brennan, Dr. David Richardson, and Dr. Harold Erickson, for their valuable insights and suggestions for my work.

All the past and present members in the Schumacher Lab have helped me develop my project and thesis. I would like to acknowledge Dr. Schumacher for collecting the MAD data and helping with the determination of the ParA apo structure. And also, this document was thoroughly edited by Dr. Schumacher. Nam had been helpful with the model building and refinement process. I would like to give him special thanks for all the support and help he had provided me throughout my years of study.

I was really lucky to have Porsha, Bonnie, and Bob as my lab mates. I feel truly grateful that I've got to spend my years in the lab with such a good people. I would also like to thank members in the Brennan Lab. In particular, Jungki had been helpful with all the biochemical experiments in the lab and also been supportive with life at Duke as an international student.

I would also like to acknowledge Sara Milam and Desmond Moore from the Erickson Lab for helping and performing the negative stain EM experiments. I would also like to thank Amy, Margot, Peggy, Betty, Sharon, Ester and Marsha for all the administrative work that had to be done and just for being so kind and friendly.

I would like to thank Dr. Ilhwan Kim and Chuljin Sunbae for all the help and support from the beginning of my studies, and also each step of the way. I would also like to thank Prof. Sangkee Rhee and Yangshin unnie in Korea for all your support.

Special thanks to friends at Duke, Kyuseon, Jiyeon, Sumi Unnie, Jihyun, Taerog and friends at Hanmaum Church, especially Pastor Choi, Samonim, Heeeun, Tori Unnie who were like family to me through the good and bad times, being far away from home.

To my parents, thank you for your constant encouragement and love. I am also grateful to my sister and my baby brother who have always been supportive. I miss you guys everyday. Finally, to my loving husband, Namina Paik, I am extremely grateful for the love and support you have provided me even through the difficult times.

# 1. Introduction

## 1.1 Introduction to DNA partition

DNA partition is the process that ensures the newly replicated DNA is accurately distributed to each daughter cell during cell division. This process is essential for the faithful inheritance of the genome and is necessary for the survival of organisms across all kingdoms. While the general mechanism behind eukaryotic chromosome segregation has been well characterized, less has been known about this process in bacteria and essentially nothing is known about the molecular basis of DNA segregation in archaea. High copy number plasmids in bacteria rely on passive diffusion. By contrast, low copy number plasmids in bacteria, as well as bacterial chromosomes, need to be actively partitioned into daughter cells prior to cell division. The process and machinery required for bacterial chromosome segregation are not well characterized and appear to vary significantly from species to species. In contrast, low copy plasmids utilize partition (*par*) systems, which require only three components for partitioning: a nucleotide triphosphatase (NTPase), a centromere binding protein (CBP), and a DNA centromere site (Schumacher, 2008). The simplicity of these *par* systems makes them excellent models to study DNA partition at the molecular level.

The general mechanism of plasmid partition involves three general steps (Figure 1). First, binding of the CBP to the centromere leads to the formation of the partition complex. Plasmid pairing then takes place by interactions between two partition

complexes. Next, the partition complexes are recognized by the motor protein (NTPase), which somehow physically separates the replicated plasmids to opposite cell poles. The timing of plasmid segregation appears to be different depending on the bacterial growth rate and it may also vary with the type of *par* system and the plasmid. Hence, this aspect of DNA segregation remains a subject of debate. Three types of *par* systems have been classified according to the nature of the NTPases (Gerdes et al, 2000). Type I systems use an NTPase called ParA which has a deviant Walker box motif, Type II systems use an actin-like proteins called ParM, and Type III systems utilize TubZ, which contains a tubulin-like fold. As shown in Figure 2, these *par* loci share similar genetic organizations. Notably, all three types of NTPases have been shown to form nucleotide-dependent polymers. However, each type of *par* system utilizes different molecular mechanisms, which will be discussed in more detail later in this chapter.

The DNA segregation mechanism of archaea, the third domain of life, has been far less characterized than that of bacteria. Only two partition systems have been identified in archaea; the cassette driving partition of the pNOB8 archaeal plasmid and that mediating segregation of the *S. solfataricus* chromosome. Notably, both employ putative ParA-like proteins. My thesis work focused on a homolog of the pNOB8 ParA protein. This protein contains conserved motifs found in bacterial ParA proteins, so-called Walker box motifs, which drive Type I partition. However, before I describe these systems, I will first introduce the Type II and Type III systems, which are the best understood from a molecular standpoint. This will be followed by a detailed description

of Type I systems, which are notably the most abundant partition systems in bacteria and also appear to be utilized by archaea.

## **1.2 Type II partition system: Actin-like ParM and ParR move plasmid by insertional polymerization mechanism**

Type II partition systems are the best understood among the three types of plasmid segregation systems. The ParMRC plasmid partitioning apparatus was originally identified on the multiple antibiotic resistance plasmid R1 from *E. coli* (Gerdes et al, 1985). Type II systems utilize NTPases called ParM and CBPs called ParR. Although ParM has low sequence identity with actin, its fold and domain arrangements are very similar to actin. The actin fold is composed of two domains with a nucleotide-binding pocket in the interdomain cleft (Figure 3A) (Popp et al, 2008; van den Ent et al, 2002). ParM forms actin-like filaments in the presence of ATP that are dynamically unstable (Figure 3B). Indeed, these filaments form and fall apart, unless each filament end is capped by a ParR-*parC* nucleoprotein complex. Once each end is capped, the ParM filaments grow by the insertional polymerization of additional ParM molecules at the ParM-ParR-*parC* interface. The bidirectional elongation of ParM filaments between the two ParR-*parC* complexes then push the ParR-*parC* bound plasmids to opposite cell poles (Figure 4) (Campbell & Mullins, 2007; Garner et al, 2004; Moller-Jensen et al, 2007; Salje et al, 2009). A recent structural study of the ParR-centromere partition complex from pSK41 plasmid revealed key insights into this capture and stabilization mechanism (Figure 3C) (Schumacher et al, 2007). Specifically, the structure of the first full length

partition complex, that of the Type II ParR-*parC* complex from the multidrug resistance plasmid pSK41, revealed that six dimers of dimers of ParR assemble into a continuous helical structure with the DNA wrapped around its outside. The N-terminal, basic DNA-binding domain of ParR is located at the helix exterior and interacts with the DNA while the C-terminal tails, which were shown to bind ParM, face inward toward the center of the helix. The pore dimensions of this complex are suitable for making interactions with ParM filaments, explaining how it could act as a filament cap.

The *in vitro* reconstitution of the Type II partition system from R1 plasmid demonstrated that the three-component *par* system is sufficient for DNA partition without any additional factors from the host. A DNA fragment containing centromere-like region was attached to beads and mixed with ParR and ParM, and filament assembly was induced by addition of ATP. Short but dynamic ParM filaments were extended from the *parC* bead surface, however as soon as the two *parC* beads came into proximity, indicating both ends of the ParM filament are interacting with the ParR-*parC* complex, the filament started growing and pushed the two beads apart. It was also observed that elongation was symmetrical and bipolar and occurred at the interface between ParM and the ParR-*parC* complex (Garner et al, 2007).

The dynamic instability of ParM is reminiscent of eukaryotic tubulin, which indicates that eukaryotic and prokaryotic cells have evolved functionally in very similar ways to deal with the essential process of DNA segregation.

### **1.3 Type III partition system: Tubulin/FtsZ-like TubZ and TubR move plasmid by tram-like mechanism**

Type III systems are characterized by GTPases called TubZ that have tubulin/FtsZ like folds (Ni et al., 2010). Further, TubZ has been demonstrated to polymerize in a GTP-dependent manner and undergo treadmilling. This phenomenon occurs when subunits are added at the plus end of the polymer and lost at the minus end, resulting in the polymer appearing to move across a substratum (Chen & Erickson, 2008). TubR is a centromere binding protein, which forms a highly intertwined dimer and contains a winged helix-turn-helix (HTH) motif (Huffman & Brennan, 2002). Studies showed that TubR has structural similarity to the ArsR family of winged-HTH transcriptional repressors (Ni et al., 2010). However, TubR has an unusual HTH-DNA interaction mode. Instead of inserting into the major groove, the recognition helices of TubR mediate dimerization. Only the N-termini of the recognition helices appear to contact DNA with the wings providing most of the contacts to the DNA (Ni et al, 2010). This is different from other canonical HTH motifs, in which the  $\beta$ -strand acts as the wing while the recognition helices insert deeply within the DNA major grooves (Figure 5B) (Huffman & Brennan, 2002; Pabo & Lewis, 1982).

The crystal structure of TubZ revealed a flexible C-terminal tail (Figure 5A) and biochemical studies showed that this basic tail interacts with the acidic TubR dimer face (Ni et al, 2010). These combined findings led our laboratory to propose a tram-like model for Type III partition (Ni et al., 2010) (Figure 6). In this model, the TubR-plasmid

complex attaches to the TubZ filaments via interactions between TubR and the C-terminal tail of the TubZ filament. GTP hydrolysis within the TubZ filament causes treadmilling, leading to elongation at the plus end and retraction at the minus end. This results in the TubR-plasmid complex being transported to cell poles. Consistent with this model, subsequent EM structures of the TubZ polymer revealed double stranded filaments with the C-terminal tail exposed to the surface of the filaments, optimal for interaction with TubR (Aylett et al., 2010).

#### ***1.4 Type I partition system***

Type I systems are the most common partition systems in bacterial plasmids and chromosomes. These cassettes encode an ATPase called ParA with a deviant Walker A box motif and a CBP called ParB. The nomenclature of Type I ATPases is confusing. Hence, the names of various ParA and ParB homologs are outlined in Table 1. The Walker-type family of proteins contain a highly conserved sequence called the Walker A motif (GxxGxGKS/T), which is involved in ATP binding. The protein sequence forms a glycine-rich loop that is often preceded by a  $\beta$ -strand and followed by a  $\alpha$ -helix. It is also known as a P-loop, or a phosphate-binding loop. A deviant Walker A motif is different from the classic Walker A motif in that it has a second lysine near the N-terminal end of the motif (xKGGxxKS/T). This second lysine residue is called the signature lysine and is known to be essential for hydrolysis of ATP (Lutkenhaus & Sundaramoorthy, 2003). Studies have shown that mutations in the ATP binding motif of different ParA proteins eliminate partition activities and result in plasmid instability, suggesting that this motif

plays a crucial role in DNA segregation (Ebersbach & Gerdes, 2004; Leonard et al, 2005; Quisel et al, 1999).

Type I systems can be further divided into two subtypes based on the sizes and sequences of the ParA and ParB proteins (Schumacher, 2008). Type Ia systems include large ParA (321-420 residues) and ParB (312-342 residues) proteins and Type Ib cassettes encode small ParA (192-308 residues) and ParB (46- 131 residues) proteins. Type Ia ParA proteins contain regulatory N-terminal regions that bind to its promoter, thus functioning in transcription autorepression (Dunham et al, 2009). In contrast, Type Ib ParA proteins lack this regulatory N-terminal DNA binding region (Figure 7). Instead, the CBP binds to the operon promoter and regulates the transcription of the operon. These differences between Type Ia and Type Ib *par* system has been summarized in Table 2.

#### **1.4.1 Role of ParA in Type I partition**

One important characteristic of Type I partition is the resultant equal distribution and positioning of plasmids in the cell by this system. Plasmids maintained by the Type I *par* locus are positioned roughly at midcell or one-quarter and three-quarter positions which are the future division sites of the daughter cells (Figure 8) This equally spaced positioning of plasmids is observed regardless of the plasmid focus number (Ebersbach et al, 2006). Studies using immunofluorescence and fluorescent-protein tagged fusions have shown co-localization of different ParA homologs with the nucleoid (Adachi et al, 2006; Ebersbach & Gerdes, 2004; Lim et al, 2005; Marston & Errington, 1999; Quisel et al,

1999). Different ParA proteins were also observed to have a dynamic oscillation property across the nucleoid (Lim et al, 2005; Marston & Errington, 1999; Quisel et al, 1999). Furthermore, it was revealed that a mutation in the Walker box motif prevents this movement and further leads to destabilization of plasmids (Ebersbach & Gerdes, 2004). These studies suggest a correlation between ParA and the plasmid movement.

ParA seems to play a direct role of movement in plasmid segregation, perhaps by providing the motive force required for active plasmid segregation. A number of studies have shown that the function and the behavior of ParA is regulated by its nucleotide bound state and that the ATP bound form is the active state for partition, which as will be discussed, involves nonspecific DNA binding. Cycling of different nucleotide-bound states seems to allow the dynamic movement of ParA proteins on the nucleoid.

#### **1.4.2 ParA has ATP-dependent polymerization and nonspecific DNA binding activities**

Type Ib ParA like proteins are better understood. Indeed, recent structural and functional studies on the ATPase, ParF showed that it is monomeric in its apo form and becomes a nucleotide sandwich dimer upon ATP binding (Schumacher et al, 2012). This has led to a dimer switch mechanism of partition in which ATP binding forms the partition active dimer. By contrast, Type Ia ATPases are more complex. Studies in our lab on the P1 ParA and P7 ParA proteins show that they harbor long N-terminal  $\alpha$ -helices that function in dimerization in their apo form and ATP binding appears to stabilize a specific dimeric conformation active for partition (Dunham et al, 2009). Why

the ATP bound ParA form is active for partition has been less clear and indeed, controversial. Early studies demonstrated that several Type I ATPases can form filament bundles *in vitro* in the presence of ATP and Mg<sup>2+</sup> (Barilla et al, 2005; Bouet et al, 2007; Bouet & Funnell, 1999; Ebersbach et al, 2006; Lim et al, 2005). This led to the hypothesis that ATP-dependent polymerization might drive DNA segregation, but how ParA polymerization may contribute to partitioning has been less clear. One unusual finding that has been shown to be incontrovertibly important for Type I partition is the fact that nonspecific DNA binding by ParA proteins in the presence of ATP is required for partition (Havey et al, 2012; Vecchiarelli et al, 2010). This nonspecific DNA binding property allows ParA to bind to the nucleoid DNA, which apparently acts as a track for ParA movement between cell poles. Mutagenesis studies on the ParA proteins, SopA and Soj, revealed that inhibition of their DNA binding activities abrogated partition (Hatano et al, 2007; Hester & Lutkenhaus, 2007).

#### **1.4.3 CBP has a critical role in stimulating the ATPase activity of ParA**

ParB proteins bind site specifically and cooperatively to centromeric DNA that consists of either multiple direct or inverted repeats near the *par* operon. Multiple ParB proteins assemble on the centromere repeats to form a higher order nucleoprotein complex, the partition complex. In contrast to ParA, Type I CBPs show little to no sequence homology. However, examining the structures of Type Ib CBP, *E. coli* TP228 ParG and *Streptococcus pyogenes* pSM19035  $\omega$  revealed that both proteins contain RHH (ribbon-helix-helix) folds despite the lack of sequence homology (Golovanov et al, 2003;

Murayama et al, 2001). Type Ia CBPs are more complex and consist of three domains: an N-terminal NTPase binding domain, a central helix-turn-helix (HTH) domain, and a C-terminal dimer-domain (Schumacher & Funnell, 2005).

Several studies revealed that the N-terminus of the CBP partner stimulates the ATPase activity of ParA. Type Ib ParG contains a flexible N-terminal arm with a conserved arginine that functions in interacting with ParF and stimulating ATP hydrolysis (Golovanov et al, 2003; Pratto et al, 2008). The role and the mechanism of ATP hydrolysis of ParA proteins are not well understood (Pratto et al, 2008).

#### **1.4.4 Models for Type I partitioning**

Although *par* loci encoding ATPases with Walker box motifs were discovered almost 30 years ago, the investigation into the dynamics of how the components work together to facilitate partitioning has only recently begun. The ability to form filaments originally suggested that Type I systems may use similar mechanisms for partition as Type II or Type III systems. However, there is no structural or sequence similarity between ParA and ParM. And strikingly, nonspecific DNA binding activity has only been observed for Walker-type ATPases, and as noted, has been shown to be essential for their segregation.

Based on the previous studies showing ATP mediated polymerization of ParA proteins, Gerdes et al. proposed a pulling mechanism (Ringgaard et al, 2009). According to this model, ATP bound ParA binds the host nucleoid DNA and forms filaments. When this growing filament encounters the centromere-bound ParB, its ATPase activity

is stimulated by ParB. Conversion of ParA-ATP to ParA-ADP causes the depolymerization and detachment of ParA from the nucleoid. This retracting polymer is thought to provide the pulling force for plasmid movement (Figure 9). Several studies appear to support this pulling mechanism (Hatano et al, 2007; Ringgaard et al, 2009; Sengupta et al, 2010), however, more recent data has called polymerization based Type I partition mechanisms into question as detailed below.

More recently, a diffusion ratchet mechanism has been proposed for P1 plasmid segregation (Figure 10B). This model does not rely on ParA polymerization. Instead, P1 ParA undergo a slow, multi-step conformational transition upon ATP binding that allows ParA dimers to independently bind to nucleoid DNA. Then ParA-ATP dimers tether the plasmids to the nucleoid surface by the interaction with the partition complex. Once ParB stimulates ParA's ATPase activity, ParA is released from the nucleoid. The time delay induced by the slow conformational change combined with the ATP hydrolysis activity of ParA creates a dynamic concentration gradient of ParA dimers that provide the motive force for the plasmid movement (Vecchiarelli et al, 2010).

The fundamental difference between two models is the presence and absence of ParA polymerization (Figure 10). Whether ParA polymerization/depolymerization is involved or not is still controversial, however both models rely on the ability of ParA to bind DNA nonspecifically and hydrolyze ATP to facilitate plasmid movement. The role of ATP hydrolysis seems to be central to the partitioning mechanism.

### 1.4.5 Chromosomal ParA

Many bacterial chromosomes encode Type I *par* loci. It was shown that chromosome-encoded *par* loci is essential in *Caulobacter crescentus* (Toro et al, 2008) and *Vibrio cholera* (Fogel & Waldor, 2006). However, these loci are generally non-essential in other bacteria. In growing cells of *B. subtilis*, deletion of *soj* had no effect on chromosome segregation (Marston & Errington, 1999) and similarly, deletion of the *par* locus in Gram-negative bacteria had only mild defects in chromosome segregation (Lewis et al, 2002). Although there is no evidence that the chromosomal *par* locus is required for segregation of bacterial chromosomes, it has been shown that the locus can be utilized to maintain unstable plasmids (Yamaichi & Niki, 2000). This suggests that the locus can still perform partitioning functions.

ParA may not play an essential role in chromosome segregation in the vegetative growth of *B. subtilis*, however recent studies have revealed that Soj (ParA homolog in *B. subtilis*) plays an indirect role during sporulation by complementing an independent origin segregation mechanism that involves the RacA protein, which is expressed early in sporulation. RacA is a DNA binding protein that has been shown to mediate chromosome segregation. The protein binds to the *oriC* region of the chromosome and is recruited to the cell pole by DivIVA, to act as a bridge between the chromosome and the cell pole. Deletion of both Soj and RacA had deleterious effect on chromosome segregation, which suggest that RacA and Soj-Spo0J play redundant roles in the origin segregation during sporulation. How RacA may play a role in the chromosome

segregation process is discussed in the Appendix.

## ***1.5 Archaeal DNA partition system***

### **1.5.1 General introduction to Archaea**

In contrast to the amount of knowledge concerning DNA segregation in eukaryotic and bacterial cells, very little is known about the components and the mechanisms of this fundamental process in archaea, the third domain of life. Archaea are highly diverse and abundant. A number of species in archaea are extremophiles that thrive under conditions of extreme heat, acidity, salinity and/or pressure (Pikuta et al, 2007). They are abundant in harsh environments such as hot springs, inside the digestive tracts of cows, and in methane-producing marine life. Surprisingly, they are not only restricted to extreme environments but also thrive abundantly and globally in different aquatic and terrestrial environments under non-extreme conditions (Robertson et al, 2005).

Archaea was not recognized as a major domain of life until quite recently. They used to be classified as prokaryotes up until 40 years ago when the tripartite tree was established based on the pioneering work of Carl Woese who utilized sequence comparisons of the 16S rRNA and 18S rRNA as indicators for molecular evolution (Woese & Fox, 1977). Figure 11 is the phylogenetic tree that illustrates the three domains of life, Eukarya, Bacteria, and Archaea. Archaea has unique lipid compositions in the membrane that distinguishes itself from other life forms. Archaeal membranes contain ether-linkages while those of bacteria and eukaryotes contain ester-linkages.

Archaea are also described to have a mosaic of eukaryal and bacterial features. For example, archaea do not have a nucleus with a nuclear envelope like eukaryotes, however it has been shown that archaeal proteins that are required for replication, transcription, and translation are more similar to eukaryal proteins than bacterial proteins. In contrast, proteins involved in metabolic pathways and regulatory functions generally are more similar to those in bacteria. This genetic mosaicism makes archaea a good model to study evolution. Currently, three main branches of archaea have been recognized at the phylum level: Euryarchaeota, Crenarchaeota, and Korarchaeota (Brochier-Armanet et al, 2008; Woese et al, 1990)

### **1.5.2 *Sulfolobus solfataricus***

All members of the order Sulfolobales are thermoacidophiles of the crenarchaeal branch of archaea. It is an aerobic crenarchaeon that grows optimally at 80 °C and pH 2-4. The cell walls are composed of surface layer (S-layer) proteins that have been known to maintain cell integrity even in harsh growth conditions. *Sulfolobus* species have become important model organisms to study hyperthermophiles and archaea in general for their qualities. *Sulfolobus solfataricus* is the most widely studied organism and has been used as a model for research on mechanisms of DNA replication, the cell cycle, chromosomal integration, and transcription. Importantly, its genome has been completely sequenced in 2001. The genome is 3 Mb in size and encodes 2,977 proteins. Among the encoded proteins, 40% were found to be archaeal-specific, 12% bacterial-specific, and 2.3% eukaryal-specific, and the last one-third of the proteins currently have

no homologs in common with other sequenced genes. The predicted proteins encoded on the genome also revealed that components putatively required for DNA replication, DNA repair and recombination, the cell cycle and transcription appear related to their eukaryotic counterparts. (She et al, 2001).

Light microscopy studies of the nucleoid structure and distribution of *Sulfolobus* revealed that the nucleoids are highly organized during exponential growth and are unstructured during stationary-phase (Poplawski & Bernander, 1997). Similar to bacteria, archaea lack a true nucleus for nuclear DNA organization. In *Sulfolobus solfataricus*, four nucleoid-associated proteins (NAPs) have been identified so far (Alba, Sso10a, Cren7, and Sso7d) for compaction and organization of their genomic DNA (Driessen & Dame, 2011; Edmondson et al, 2004; Guo et al, 2008; Kahsai et al, 2005; Wardleworth et al, 2002). The same light microscopy studies also observed different localizations of the nucleoid at different stages of partition. The considerable time intervals between the termination of chromosome replication and the completion of nucleoid separation appeared similar to the G<sub>2</sub> phase in eukaryotic cells. This suggest that nucleoid processing in *Sulfolobus* may display both bacterial and eukaryotic traits (Poplawski & Bernander, 1997).

### **1.5.3 DNA partition machinery in pNOB8 plasmid**

Although plasmids occur widely in the archaeal domain and several have been isolated and partially characterized, very little is known about their mechanisms of maintenance, copy number control, or conjugation (Zillig et al. 1996). The first archaeal conjugative plasmid, pNOB8, was isolated from the thermophilic archaeon *Sulfolobus*

isolate, NOB8H2 (Schleper et al, 1995). The pNOB8 plasmid is a multicopy plasmid, about 41 kb in size, and contains a well-conserved cluster of genes involved in the horizontal gene transmission. The plasmid also harbors genes encoding proteins that have sequence similarity to bacterial ParA and ParB proteins. Recently, a segregation cassette on the pNOB8 plasmid was identified and was shown to be required for plasmid maintenance. This segregation cassette is similar to the bacterial system in that it encodes putative ParA-like and ParB-like proteins. Additionally, the cassette contains a third required protein component called AspA. AspA encodes a putative DNA-binding protein. This archaeal segregation cassette is atypical in that it has a tricistronic architecture.

It was recently shown that the *Sulfolobus solfataricus* chromosome harbors a segregation cassette that encodes two proteins, SegA and SegB. The SegA protein shows homology to bacterial ParA proteins, while the SegB protein shows no homology to any known protein (Kallioma-Sanford et al, 2012). These findings suggest that the general bacterial chromosomal and plasmid partition system may be conserved in the archaeal system. Studies on these archaeal systems will likely provide important linkages to DNA segregation in the bacterial and eukaryotic domains of life.

Here, we have focused on studying a homolog of the archaeal pNOB8 ParA. The aim of this work is to structurally and biochemically characterize the protein. In Chapter 2, I explain some of the basic principles of X-ray crystallography, which is the main approach used in this work. In Chapter 3, crystal structures of ParA in its apo state and

ADP bound state are analyzed and discussed. These studies provide some insight into how nucleotide binding affects ParA function. Along with structural studies, we performed biochemistry studies using fluorescence polarization (FP) based DNA binding assays and isothermal titration calorimetry (ITC) to characterize the ATP-dependent nonspecific DNA binding properties of the protein. These are described in Chapter 4. Moreover, the ATP-dependent polymer formation behavior of ParA is examined in this chapter. In Chapter 5, we discuss the similarities between Walker-box based proteins in cellular processes involving transport. Finally, in the Appendix, we describe our initial investigation of protein-protein interactions between RacA and DivIVA using ITC.

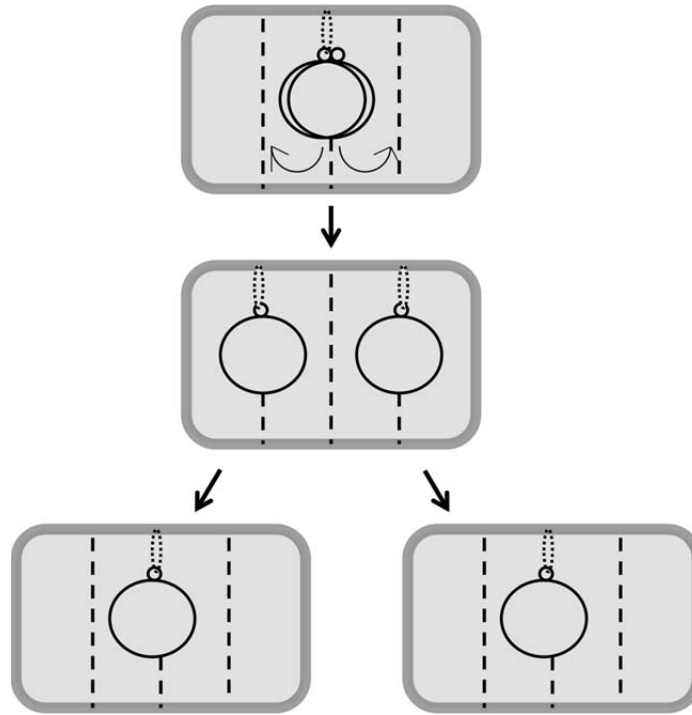


**Figure 1. General mechanism of DNA partition**

Schematic figure showing the general steps of plasmid partition. Large circles represent the plasmids and small circles represent the partition complexes. First, the centromere binding protein binds to the centromere to form the partition complex. Then plasmid pairing takes place by the interactions between the two partition complexes. This partition complexes are then recognized by the NTPase, which plays the mechanical role and physically separates the newly replicated plasmid to the opposite cell poles (Schumacher, 2012).

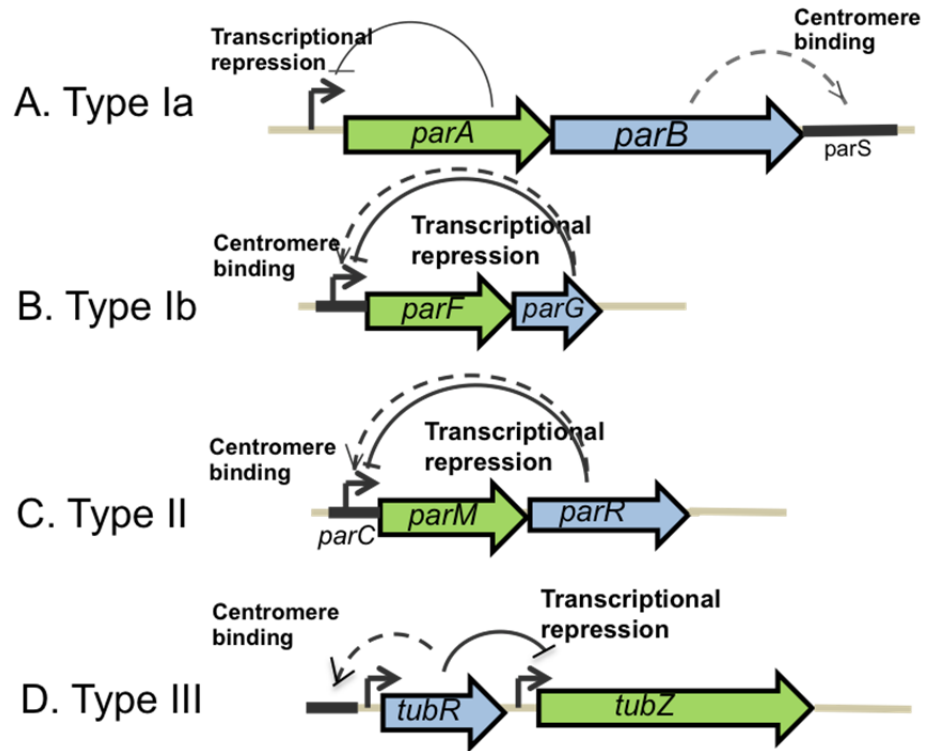
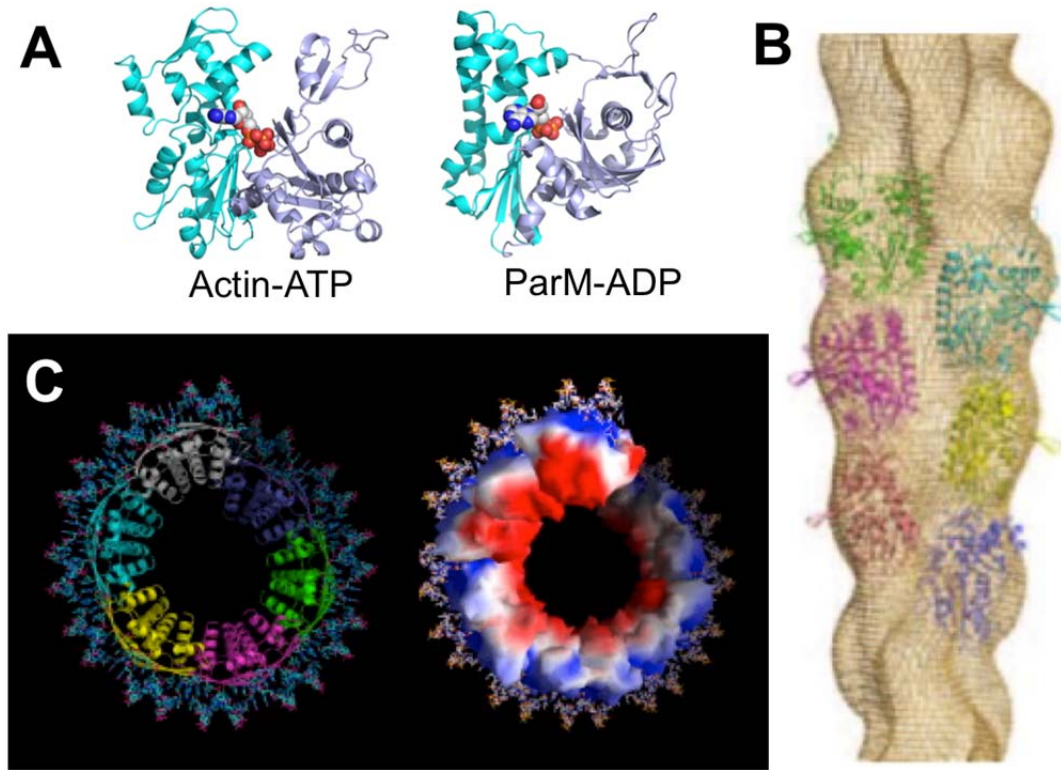


Figure 2. Genetic organization of *par* loci

Green arrows represent genes encoding NTPases and blue arrows represent genes encoding the centromere-binding proteins. Centromere-like DNA is shown as black solid bars. Solid arcs indicate the regulation of promoter activity and dashed arcs indicate the formation of partitioning complex (Gerdes et al, 2010).



**Figure 3. The structures of ParM and ParR-*parC* partition complex**

A: Monomeric structures of Actin-ATP (pdb: IYAG) and ParM-ADP (pdb: 1MWM). The nucleotides are colored by the element and shown in spheres at the interdomain cleft of both structures. B: A low-resolution reconstruction of the ParM filament. Individual monomers fitted in the map are shown in a ribbon representation (Salje 2010). C: The structure of ParR/*parC* partition complex of pSK41. The N-terminal domain of ParR is bound to its cognate *parC* centromere forming a continuous helix consisting of six dimers-of-dimers in one turn. On the right is an electrostatic surface representation of the partition complex. Blue represents electropositive surfaces and red represents electronegative surfaces (Schumacher 2007).

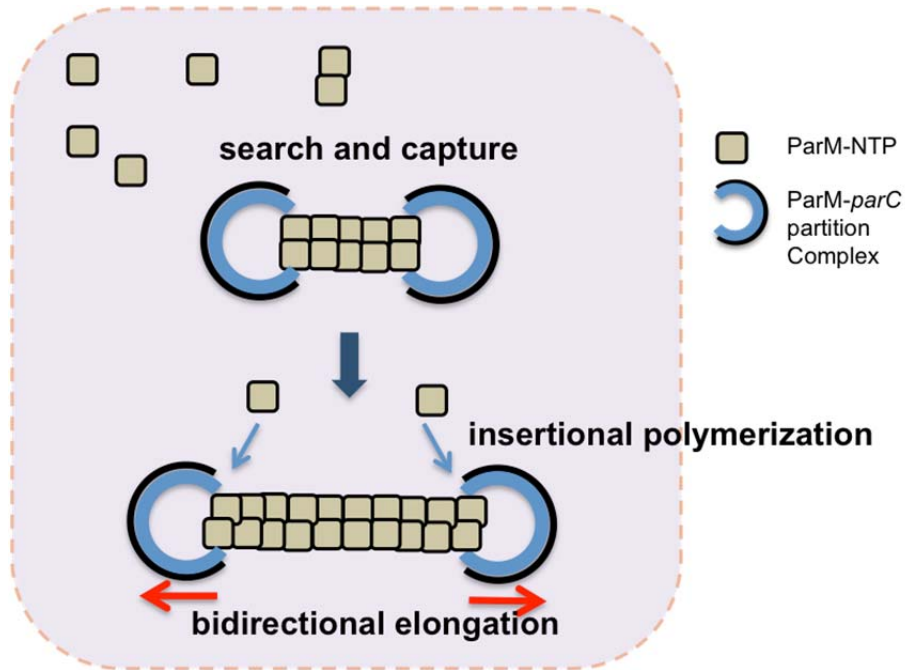


**Figure 4. The pushing mechanism of plasmid partition by Type II *par* system**

ParM polymerizes in the presence of ATP, which either undergoes a catastrophic disassembly following ATP hydrolysis or becomes capped by a ParR-*parC* complex. Once the ParM filament becomes capped at both ends by the ParR-*parC* partition complexes, it becomes stabilized and then pushes both plasmids to opposite cell poles by bidirectional elongation (Salje et al, 2010).

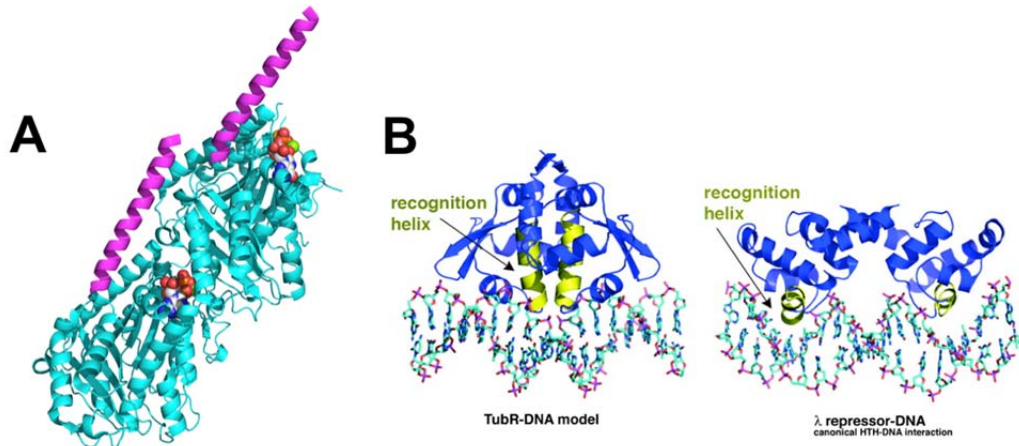


**Figure 5. Structures of TubZ and TubR**

A: Ribbon diagram of Chain A and B of TubZ-GTPYS (pdb: 2XKA). The C-terminal tail is colored in magenta. B: Left is the ribbon diagram of the TubR-DNA complex structure with the recognition helices colored in yellow. Right is the ribbon diagram of the  $\lambda$  repressor-DNA complex showing a canonical HTH-DNA interaction with the recognition helices colored in yellow (Ni, L. et al. PNAS 2010).

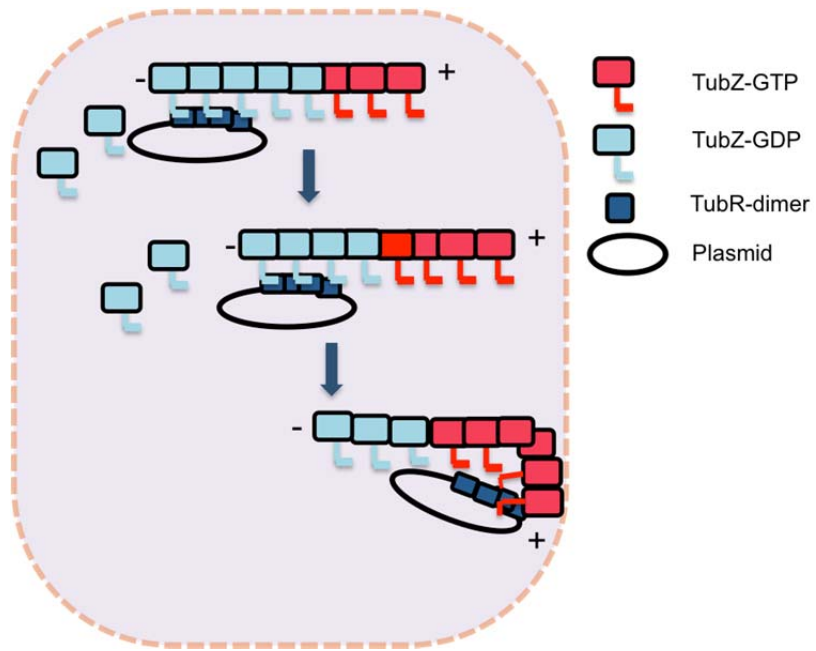


**Figure 6. DNA partition by Type III *par* system**

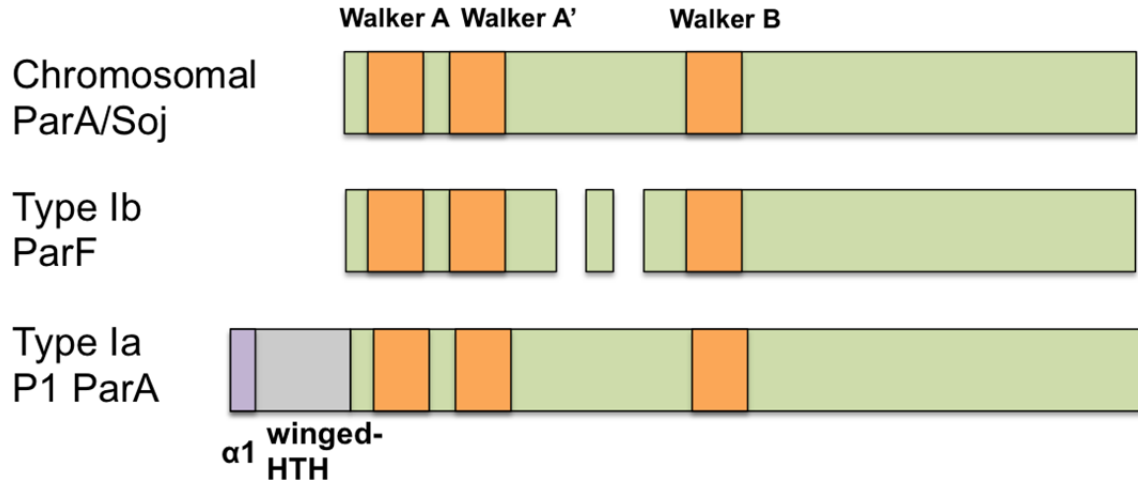
TubR first binds to its centromere on one of the replicated pBtoxis plasmids, and then contacts the TubZ C-terminal region of a treadmilling TubZ filament. TubZ subunits are lost at the – end and are added to the + end. TubR-plasmid is carried along the growing TubZ filament by TubR-TubZ interaction until it reaches the cell pole and is knocked off when it comes in contact with the membrane at the cell pole (Schumacher, 2012).

Table 1. Nomenclatures of ParA and ParB homologs

<b>ParA homologue</b>	<b>ParB homologue</b>	<b>Plasmid/Chromosome</b>
ParA	ParB	<i>E. coli</i> P1 plasmid, pB171 plasmid
SopA	SopB	<i>E. coli</i> F plasmid
ParF	ParG	<i>E. coli</i> TP228 Plasmid
δ	ω	<i>Streptococcus pyogenes</i> pSM19035
Soj	Spo0J	<i>B. subtilis</i> chromosome

**Table 2. Comparison between Type Ia and Type Ib *par* loci**

<b>Type Ia</b>	<b>Type Ib</b>
Larger (size: 321-420 aa)	Smaller (size: 192-308 aa)
ParA has role in transcription autoregulation	Centromere binding protein carries out transcription autoregulation
Extra N-terminal DNA-binding motif (winged-HTH) $\alpha 1$ for dimerization	Do not contain HTH-motif Do not contain $\alpha 1$
P1 ParA, F SopA	pB171 ParA, TP228 ParF



**Figure 7. Size comparison between ParA homologs**

ParA homologs share nucleotide binding motifs, Walker A Box, Walker A' Box, and Walker B Box, which are indicated by orange blocks. Type Ia ParA proteins have an N-terminal winged-HTH DNA motif for DNA binding to its promoter, and  $\alpha 1$  for dimerization function, and thus are larger than both Type Ib and chromosomal ParA homologs.

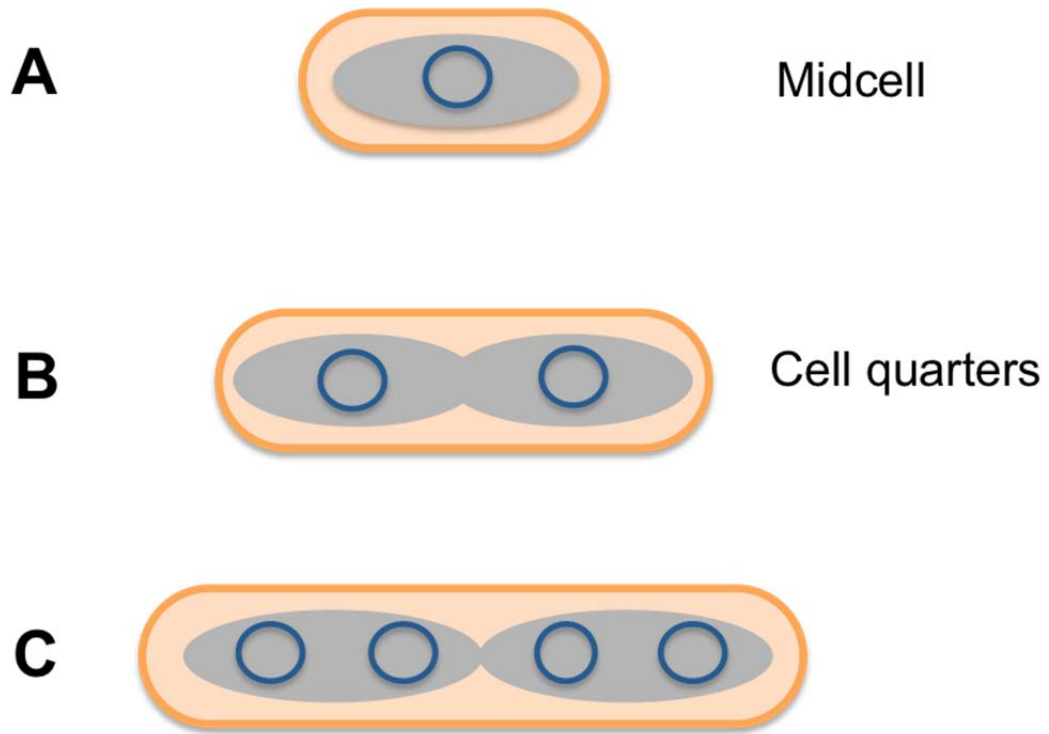


**Figure 8. Position of plasmids maintained by Type I *par* loci**

Schematic figure showing equally spaced positioning of plasmids over the nucleoid. A: The plasmid is localized at mid-cell in newborn cells B: After replication, the plasmids migrate to one quarter and three quarter positions of the cell during cell division. C: Equal distance positioning is observed even after the amplification of the plasmid copy numbers. (Szardenings et al, 2011).

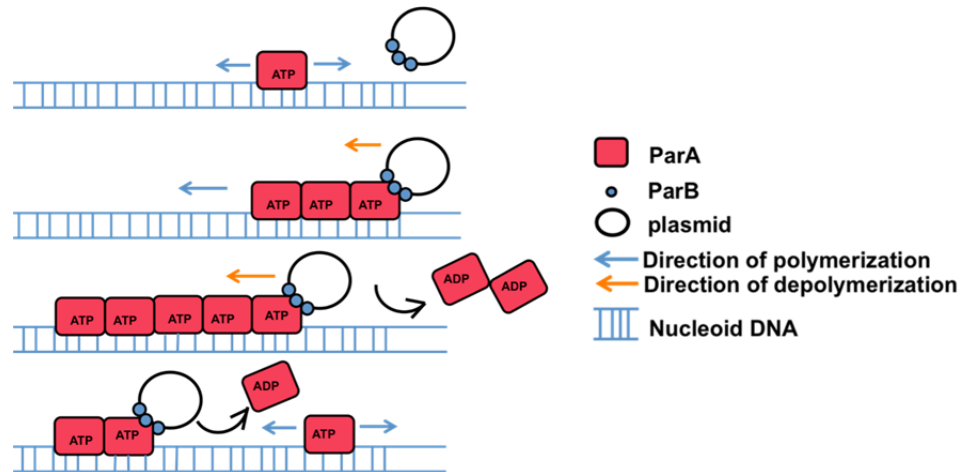


**Figure 9. Pulling mechanism by Type I *par* system**

1) ParA-ATP dimer binds to the nucleoid DNA, leading to the formation of ParA filaments. 2) Growing filament contacts the plasmid bound ParB (the partition complex). 3) ParB stimulates the ATPase activity of ParA at the end of the filament. ParA-ADP is released from the nucleoid DNA, leading to retraction of the polymer. 4) Plasmid can either drop off or continue to be attached to the end of the depolymerizing filament. ParA-ADP subunits released by the partition complex is rejuvenated to ParA-ATP and the cycle repeats (Ringgaard et al, 2009).

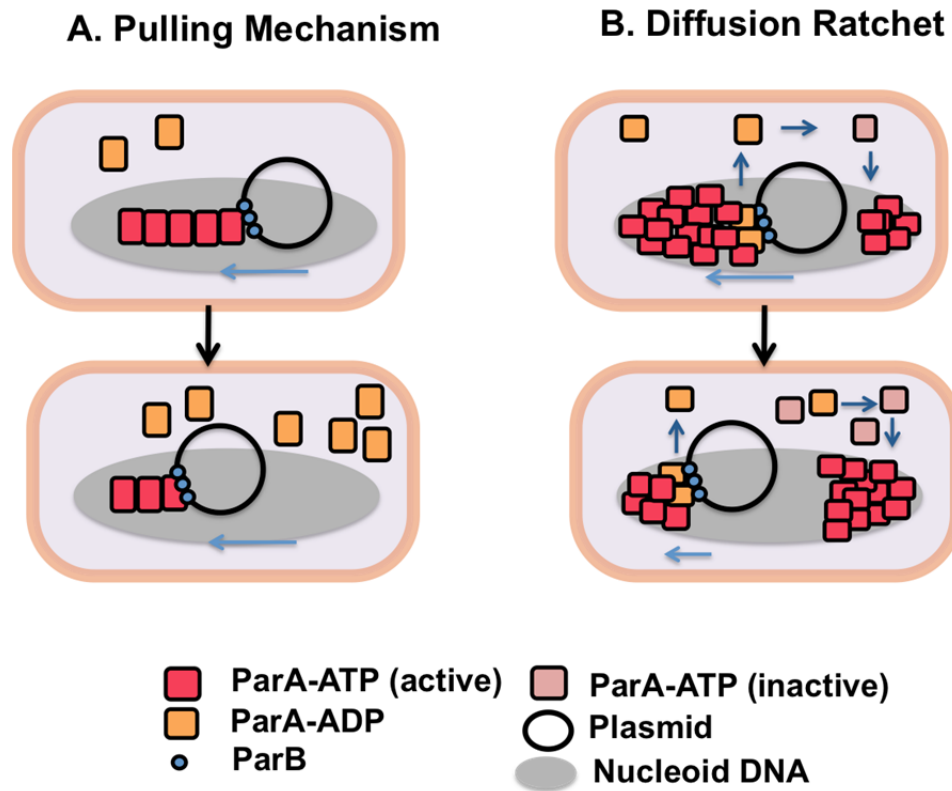


**Figure 10. Comparison between two models for Type I DNA partition**

A: Pulling mechanism (Ringgaard et al, 2009). In this model, the pulling force for plasmid movement is provided by the retraction of the ParA filaments. B: Diffusion ratchet mechanism (Vecchiarelli et al, 2010). This mechanism does not rely on ParA polymerization, but instead the pulling force is towards regions of high ParA concentration where a greater number of ParA-ParB bonds can be formed. Time delay caused by ParA's a slow multi-step conformation transition upon ATP binding, combined with stimulation of ParA's ATPase activity by ParB bound to plasmid, generate an uneven distribution of the nucleoid-associated ParA and provide the motive force.

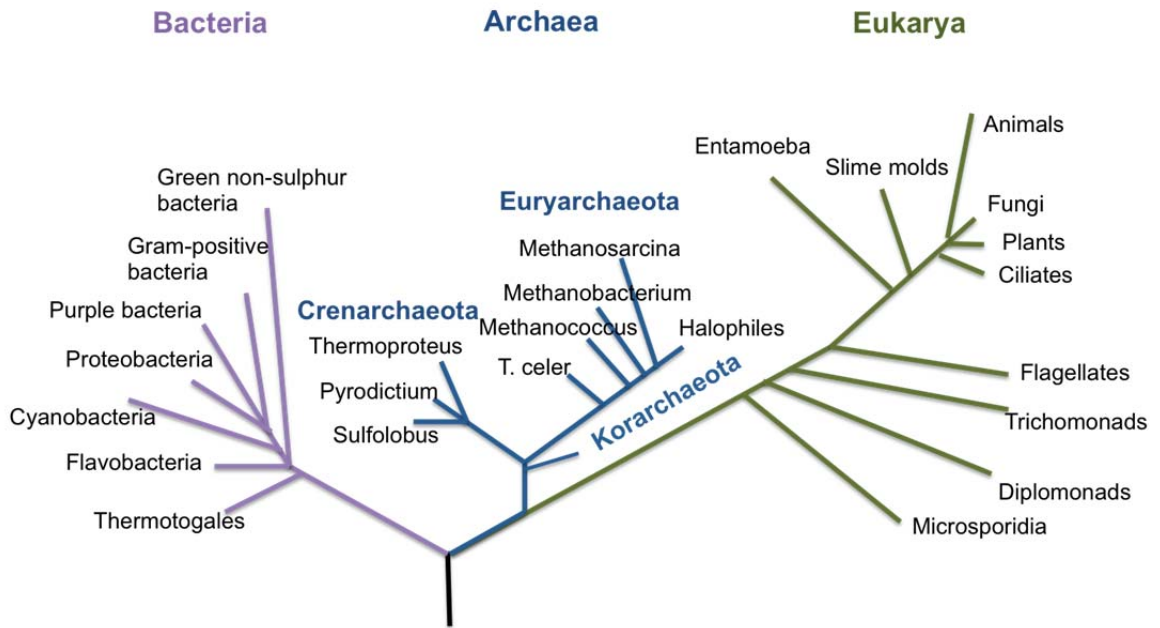


**Figure 11. Phylogenetic tree of life showing three domains of life**

A phylogenetic tree based on RNA data and proposed by Carl Woese (Woese & Fox, 1977) showing the separation of Bacteria, Archaea, and Eukaryota. The exact relationships of the three domains are still being debated (Image adapted from NASA Astrobiology Institute).

## Chapter 2. Crystallography

X-ray crystallography is a method used to determine the three dimensional structure of a macromolecule. The technique can be applied to studying the macromolecules such as DNA, RNA or assemblies of molecules such as viruses and ribosomes, however in this chapter, I will refer only to proteins. The method allows a direct visualization of protein structures with details of individual atoms that can provide an enhanced understanding of how the protein may function in the cell.

### 2.1 Why X-rays?

In order for an object to be visualized under a light microscope, there is a limit to how small an object can be. It cannot be smaller than the wavelength ( $\lambda$ ) of the light, which is the electromagnetic radiation with wavelengths of 400-700 nm. Thus, to be able to see the individual atoms in a protein where the atoms are separated by a distance of only about 0.15 nm (or 1.5 Å), electromagnetic radiation of this wavelength needs to be used. X-ray falls in this wavelength range in the electromagnetic spectrum.

When the object is irradiated with light, it causes the incident radiation to be diffracted. The lens on a microscope focuses the diffracted beam and magnifies it to form an enlarged image (Figure 12A). However, there are no X-ray lens available to physically focus the diffracted X-rays, so computers are used instead to simulate an image-constructing lens. After the X-ray diffraction is recorded using a detector, the directions and the intensities of X-ray beams are analyzed by a computer to produce an image of the cell's content, which is then interpreted as an electron density map.

Crystallographers can then build the atomic model into the electron density map (Figure 12B).

## **2.2 Why Crystals?**

In order to determine a protein structure by X-ray crystallography, first the protein of interest must be purified and crystallized to produce high quality crystals. A crystal is a periodic arrangement of molecules in a lattice (Figure 13). Then, why do we need a crystal? While the X-ray diffraction from a single molecule would be too weak to detect and measure, a crystal, which arranges a significant number of identical molecules in a regular and periodic way, acts to magnify the signal. A repeating unit in this three dimensional regular array is called a unit cell. A Unit cell has six parameters to describe its dimensions- three intersecting edges (length) of the unit cell ( $a$ ,  $b$ ,  $c$ ) and the angles between them ( $\alpha$ ,  $\beta$ ,  $\gamma$ ). The angle  $\alpha$  is between  $\mathbf{b}$  and  $\mathbf{c}$  cell edges,  $\beta$  is between  $\mathbf{a}$  and  $\mathbf{c}$ , and  $\gamma$  between  $\mathbf{a}$  and  $\mathbf{b}$  (Figure 14). The lattice is an infinite repetition of the unit cell.

## **2.3 Symmetry**

A lattice has an infinite array of points where the environment of any point is identical to the environment of any other point. This expresses the translational periodicity within a crystal with the systematic repetition. There are seven basic crystal systems defined by the relations between the axes and the angles of the unit cell, and their minimal internal symmetry to fill an infinite space (Table 3). Additional translations are allowed to create 14 Bravais Lattices, which belong to the seven crystal

systems (Table 4). In a primitive lattice, the corners of the unit cell can serve as the equivalent positions. However, in Bravais lattice system, equivalent points are expanded to those to C (base-centered), I (body-centered), and F (faced-centered), which give the additional translational symmetry to the unit cell. The asymmetric unit is the smallest unit (unique volume) needed to generate the whole entire unit cell only by applying the symmetry operations. The combination of symmetry operators (rotations and translations) and the lattices that characterize a crystal is called a space group. Symmetry operations together with the additional translations allow 230 space groups in total, but of those only 65 are chiral which is suitable for macromolecules such as proteins.

## ***2.4 How does diffraction happen?***

### **2.4.1 Bragg's Law**

Within the crystal lattice, infinite sets of regularly spaced planes can be drawn through the lattice points. These planes are considered to be the source of diffraction. A set of equivalent, parallel lattice planes is designated by a set of three numbers called the Miller indices ( $h, k, l$ ). The index  $h$  is equivalent to the number of parts into which a set of planes cut the  $a$  edge of each cell. Similarly, the index  $k$  and  $l$  define the number of parts into which the  $b$  and  $c$  edges of each cell are cut. Diffraction takes place when the scattered X-rays from successive planes constructively interfere (are in phase). As illustrated in Figure 15, for the two reflected rays to be in phase, the path difference between waves scattered by the adjacent lattice planes must be an integral multiple of the wavelengths. This is referred to as Bragg's law and is expressed as:

$$n\lambda=2d\sin\theta$$

(d: the perpendicular distance between two lattice planes,  $\lambda$ : wavelength of the incident wave,  $\theta$ : the angle between the incident ray and the lattice planes).

### 2.4.2 Ewald sphere

A reflection (h, k, l) from diffraction space originates from the set of planes (h, k, l). Miller indices also specify a vector in reciprocal space perpendicular to these planes in the real space, with interplanar distance equal to the reciprocal of the spacing between the Bragg planes ( $1/d_{hkl}$ ). There is an inverse relationship between the dimensions in real space and the dimensions in reciprocal space. Lattice in the diffraction pattern dimensions are inversely proportional to the dimensions of the real lattice. The unit cell in the reciprocal lattice can be described with axes,  $a^*$ ,  $b^*$ , and  $c^*$ . This inverse relationship can be explained in more detail using the Ewald sphere.

The Ewald sphere is basically a geometric construction and a useful means to understand the relationship between diffraction and reciprocal space. The Ewald construction integrates the scalar (Bragg's law) and the vector (Miller index) description of the diffraction process (Figure 16). First, draw a sphere with the radius of  $1/\lambda$  (for convenience) and imagine the real crystal to sit at the center of the sphere. The X-ray beam comes from the left and the unscattered beam passes through the crystal and the point where it reaches the sphere surface is the origin of the reciprocal space. The incident ray and the diffracted ray are both at an angle  $\theta$  from a set of Bragg planes in

the crystal. In order for the diffraction in the reciprocal space to occur, the diffracted ray must contact with the surface of the Ewald sphere. The angle between the incident and the diffracted ray is  $2\theta$  and the vector connecting the reciprocal space origin and the diffraction point is the diffraction vector  $\mathbf{S}$ , which satisfies the Bragg equation in vector form. The length of the vector is  $2(1/\lambda)\sin\theta$ , which equals to  $1/d$  by Bragg's law, which is also the length equal to the reciprocal of the spacing between the Bragg planes. A single recording of diffraction at a fixed crystal orientation only sample a limited number of reciprocal lattice points. Thus, the crystal needs to be systematically rotated in order to move more reciprocal lattice points through the Ewald sphere to be sampled.

## ***2.5 How do we go from x-ray diffraction data to electron density maps?***

Each reflection in the diffraction pattern is a diffractive contribution from all atoms in the unit cell which is a wave consisting of amplitude and phase. The structure factor is a mathematical function describing the amplitude and phase of a wave diffracted from the crystal lattice planes defined by Miller Indices, (h, k, l).

$$F_{hkl} = |F_{hkl}|e^{i\alpha_{hkl}} = \sum_j f_j e^{2\pi i(hx_j+ky_j+lz_j)}$$

This equation describes the structure factor as the sum of all atomic scattering contributions in a unit cell in the direction defined by  $hkl$ . In the above equation,  $x_j, y_j, z_j$  are the positional coordinates of the  $j$ th atom,  $f_j$  is the scattering factor of the  $j$ th atom, and  $\alpha_{hkl}$  is the phase of the diffracted beam. Since it is the electrons that are

scattering x-rays, the scattering factor can be thought of in terms of the electron density  $\rho$  throughout the molecule. Rewriting the equation from the above in terms of  $\rho$ :

$$F_{hkl} = \int_V \rho(x, y, z) e^{2\pi i(hx+ky+lz)} dV$$

Here, the structure factors for the various points in the reciprocal lattice correspond to the Fourier transform of the electron density distribution within the unit cell of the crystal. Because the Fourier transform is reversible, the electron density can be regenerated from the structure factors using an inverse Fourier transform.

$$\rho(x, y, z) = \frac{1}{V} \sum_h \sum_k \sum_l |F_{hkl}| e^{ia_{hkl}} e^{-2\pi i(hx+ky+lz)}$$

The goal of the crystallographic experiment is to determine the  $\rho(x, y, z)$ , the electron density for all  $x, y, z$  in the unit cell, and thus obtain the image of the unit cell contents. What we measure during the experiment is the positions and the intensities of the reflections. In the equation,  $|F_{hkl}|$  can be obtained from the experiment because the amplitude of the structure factors are proportional to the square root of the measured intensities. However the phase is lost during data collection. In order to determine the electron density distribution in the crystal, the phase problem needs to be solved.

Some of the methods that are commonly used to determine the phase are Single Isomorphous Replacement (SIR) / Multiple Isomorphous Replacement (MIR), Single-wavelength Anomalous Dispersion (SAD) / Multiwavelength Anomalous Dispersion (MAD), and Molecular Replacement (MR).

## **2.6 Phase Determination**

### **2.6.1 Isomorphous replacement**

This method involves heavy atom substitution of a native crystal or protein to solve the phase problem. Since different atoms contribute to the scattered intensity in proportion to the square of the number of electrons they contain, introducing the heavy atoms into the protein will change the scattered intensity significantly. Heavy-atom derivative crystals are prepared by soaking the native protein crystals in a buffer containing a heavy-atom compound. The differences in the diffracting intensities of the data between the native crystal and the derivative crystal will largely reflect the scattering contribution of the added heavy atoms. The differences between the scattering powers can be used to compute a difference Patterson map for determination of the heavy atom locations, which can then be used to calculate their contribution to the structure factors. A more detailed explanation of how heavy atom sites are determined will be described later in this chapter.

The native and derivatized crystals should be isomorphous which means that the heavy atoms must not disturb the crystal packing or the unit cell dimensions. The structure factor for the derivative crystal ( $F_{PH}$ ) is equal to the sum of the protein structure factor ( $F_P$ ) and the heavy atom structure factor ( $F_H$ ) (Figure 17A).

$$F_{PH} = F_P + F_H$$

We can solve this vector equation for  $F_P$ , and obtain the phases of the protein structure by using the Harker diagram (Figure 17B).  $|F_{PH}|$  and  $|F_P|$  are already known

from the measurement of the reflection intensities  $I_{PH}$  and  $I_P$ . To construct the Harker diagram, first draw a circle with a radius of  $|F_P|$ , centered at the origin. The circle indicates all the vectors that would be obtained with all the possible phase angles for  $F_P$ . Next, draw another circle with radius of  $|F_{PH}|$  centered at a point offset by vector  $F_h$  (the amplitude and the phase of  $F_h$  is already calculated from the positions of the heavy atoms). The two circles intersect at two points where two possible solutions are given for the phase values for  $F_P$ , corresponding to two vectors,  $F_P(a)$  and  $F_P(b)$ . In principle, the twofold phase ambiguity can be resolved by preparing a second derivative crystal with heavy atoms that bind at different sites.

### **2.6.2 MAD (Multiwavelength Anomalous Dispersion)**

MAD is an approach used to solve the phase problem by collecting datasets from a single crystal at multiple wavelengths in order to maximize the absorption and the dispersive effects of anomalous scattering atoms. For this reason, it requires a tunable X-ray source at the synchrotron. Selenium is a particularly good anomalous scatterer and it can be incorporated into the proteins by over-expressing them in strains of *E. coli* that are auxotrophic for methionine. The host cells are grown in minimal media supplemented with amino acids and using selenomethionine in place of methionine.

Absorption curves for heavy elements are not smooth curves, but exhibit distinct, step-like features. This sudden change in absorption as a function of wavelength ( $\lambda$ ) is called an absorption edge. Friedel's Law holds that the intensity of the reflection ( $h, k, l$ ) is the same as that of the reflection ( $-h, -k, -l$ ).

$$|F_H(hkl)| = |F_H(-h-k-l)|$$

However, as a result of this absorption, a shift in amplitude and phase takes place and this causes the breakdown of the Friedel's law. The reflections (h,k,l) and (-h,-k,-l) are no longer equal in intensity and this inequality of symmetry-related reflections is called the anomalous scattering or anomalous dispersion. The anomalous difference between these two reflections ( $\Delta F_H = |F_H(hkl)| - |F_H(-h-k-l)|$ ) can be used to locate the anomalous scatterers (heavy atoms) by the difference Patterson function. Figure 18B shows the breakdown of the Friedel pair. Anomalous scattering by the heavy atom is expressed as:

$$f(\lambda) = f_0(S) + f'(\lambda) + if''(\lambda) \quad (f': \text{real}, f'': \text{imaginary})$$

The normal scattering factor  $f_0$  is independent of the wavelength and is what contributes to the normal diffraction. The anomalous scattering factors,  $f'$  and  $f''$  change with the wavelength and represent the anomalous scattering that occurs at the absorption edge.  $f'$  is the dispersive term and  $f''$  is the absorption term and is 90° in advance (Figure 18A).

For a successful MAD experiment, three or more consecutive data sets are collected from the same crystal at different wavelengths around the X-ray absorption edge of the anomalous scatterer. Figure 19 shows the absorption edge of Selenium.  $\lambda_1$  is the inflection point where  $f'$  is the minimum,  $\lambda_2$  is the peak where  $f''$  is the maximum, and  $\lambda_3$  is the high energy remote.

Once the MAD dataset is collected, we can obtain the information of changes in the scattering power of the heavy atom as in Isomorphous Replacement, along with the anomalous scattering differences. In other words, the MAD experiment can be treated as a SIRAS (Single Isomorphous Replacement with Anomalous Scattering) experiment, which is a combination of Isomorphous Replacement and anomalous dispersion. Three datasets must be collected for this kind of experiment:

- (1) one for native crystal
- (2) one for the heavy-atom derivative at the same wavelength as (1)
- (3) one for the heavy-atom derivative that results in maximal anomalous scattering

(1) and (2) are used to calculate the difference Patterson to locate the heavy atoms in the unit cell and then calculate  $F_H$ . (3) is used to determine  $F_{PH}$  from the non-equivalent Friedel pair intensities due to anomalous scattering. Protein phases are then calculated by the relation:  $F_p = F_{PH} - F_H$ . However in the MAD experiment, all these datasets at different wavelengths are collected from a single crystal, which helps overcome the non-isomorphism problem, which occurs in MIR when data are collected on separate crystals for the native and derivative data. In MAD,  $\lambda_3$  and  $\lambda_1$  can be used in Patterson analyses to extract the dispersive (isomorphous) differences and the Friedel pairs at  $\lambda_2$  can be employed to determine the anomalous heavy atom contributions. Phases for the protein structure can be determined by the Harker construction, similar to Isomorphous replacement experiments (Figure 20).

### 2.6.3 Locating heavy atoms in the unit cell- Patterson map

The heavy-atom coordinates are determined using a Fourier sum called the Patterson function  $P(u,v,w)$ .

$$P(u, v, w) = \frac{1}{V} \sum_h \sum_k \sum_l |F_{hkl}|^2 \cos 2\pi(hu + kv + lw)$$

The Patterson function is a Fourier sum with intensities as coefficients. Since the Patterson function only requires intensities but not phases, it can be computed from any crystallographic data set. Patterson maps display peaks at locations corresponding to vectors between atoms. For a relatively small numbers of atoms, it is possible to work out the original positions of the atoms that would give rise to the observed Patterson peaks.

In order to obtain the Patterson function for the heavy atoms in the derivative crystals, a difference Patterson function can be calculated, in which the amplitudes are the difference between the structure factor amplitudes with and without the heavy atom. This reflects the contribution of the heavy atom alone:  $(|F_{PH}| - |F_P|)^2$ . In addition, when using the anomalous difference to solve the phases, the heavy atom sites can be located by an anomalous difference Patterson map. The observable anomalous difference,  $\Delta F_H$  is expressed as  $\Delta F_H = ||F_H(hkl)| - |F_H(-h-k-l)||$ , which describes the difference between the amplitudes of the structure factor for the reflections (h,k,l) and (-h,-k,-l).

## 2.6.4 Molecular Replacement (MR)

This method relies on having a structure available that is homologous to that you are trying to solve. The homologous structure is used as a search model and is used to calculate an initial set of phases. To place the model structure in the correct orientation and position in the unit cell, the model is first rotated and then translated into the optimal overlap position. The process of finding the MR solution involves solving for three rotation angles and three vector values, a total of six parameters. For computational efficiency, this six-dimensional problem can be divided into two three-dimensional problems: 1) the rotation function and 2) translation function. The optimal MR solution can be expressed as  $r' = Mr + v$  ( $r$ =model coordinates,  $M$ =rotation function,  $v$ =translation vector).

First, the Patterson map is calculated from the atomic coordinates of the search model and then compared to the Patterson map from the experimental intensities. As mentioned above, the Patterson map is the result of the Fourier transform of only the intensities, which gives a map of vectors between individual atoms. The intramolecular vectors provide the rotational relationship between the model and the unknown structure and so these can be used to solve the rotation function. And once the rotation function is known, the intermolecular vectors can then be used to solve the translation function.

## **2.7 After obtaining the initial map**

Once the initial electron density map is obtained, the quality and the resolution of the map can be improved by density modification. The term applies to a number of methods such as solvent flattening, histogram matching, and density averaging, which incorporate prior knowledge of proteins and water (solvent content) in crystals to improve the protein phases. For instance, on average, the density in the solvent region is essentially zero. Density modification aims to adjust the electron density to the expectations of how it should generally look.

Once an interpretable electron density map is obtained, an initial model of the protein can be constructed. Refinement improves the initial model by systematically adjusting the atomic coordinates to maximize the agreement between the observed diffraction data and the data calculated from the model. Models are improved by an iterative process involving model (re)building into the electron density (real space refinement), and shifting parameters to improve the fit of the calculated structure factors to the observed data (reciprocal space refinement). Restraints are included to ensure that parameters, such as bond lengths, bond angles, van der Waals contact distance, remain close to known values.

Two maps are useful in the process of refinement. One is the  $2F_o - F_c$  map, which shows the current best estimate of the electron density for the structure, and which the model is usually fit into. The other is the difference map ( $F_o - F_c$  map), which shows the best estimate of the difference between the original data and the current model. It

emphasizes the errors in the current model with the positive density indicating where atoms should be added and the negative density shows where atoms should be removed.

The progress of the refinement process is monitored by the  $R$ -factor, in particular the  $R$ -free, which is the measure of the agreement between the calculated amplitude and the observed amplitude.

$$R = \frac{\sum | |F_{\text{obs}} - F_{\text{calc}}| |}{\sum |F_{\text{obs}}|}$$

$|F_{\text{obs}}|$  is derived from a measured reflection intensity and each  $|F_{\text{calc}}|$  is the amplitude of the corresponding structure factor calculated from the current model.

However, the  $R$ -factor can get trapped in local minima giving the false impression of having a good model. For this reason the free  $R$ -factor ( $R_{\text{free}}$ ) is used to validate the refinement process. Before starting the refinement process, a random subset of about 5-10% of the reflection data is set aside.  $R_{\text{free}}$  gives an independent measure of the refinement process and is an example of statistical cross-validation.

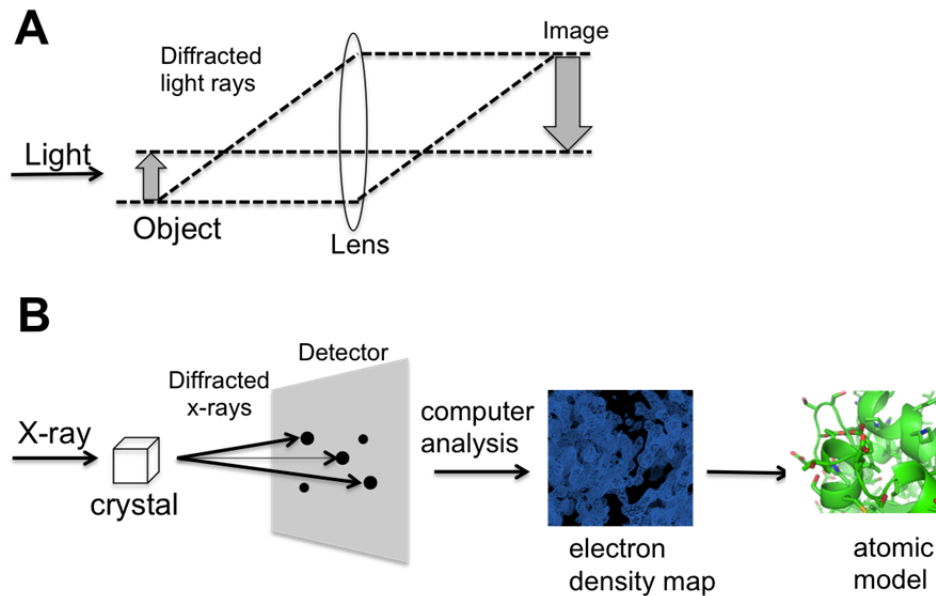


**Figure 12. The overview of X-ray crystallography**

A: In microscopy, the lens collects and focuses the diffracted light from the object and reconstructs a magnified image of the object. B: In X-ray crystallography, the crystal diffracts the X-ray into discrete beams, which produce a spot (reflection) on the detector. After the data collection, the image of the crystal's content is produced and interpreted into the electron density by computer analysis. Adapted from: Rhodes G (2006) Crystallography made crystal clear: a guide for users of macromolecular models.

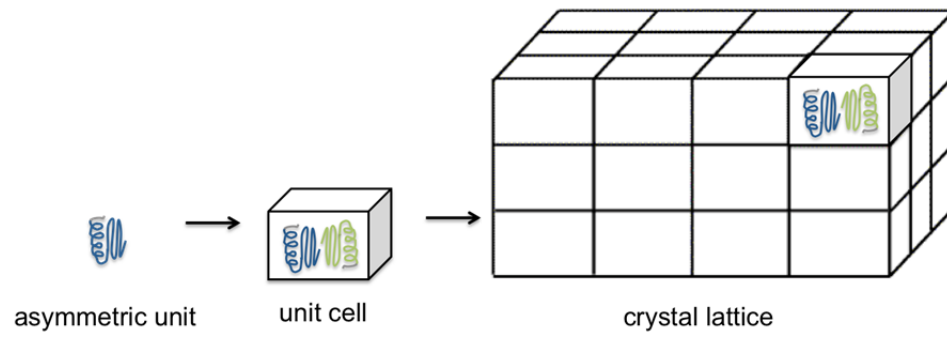


**Figure 13. Crystal lattice**

Asymmetric unit is the smallest unit of a crystal needed to generate the whole entire unit cell by application of the symmetry operations. The crystal is an array of unit cells arranged in a periodic pattern.

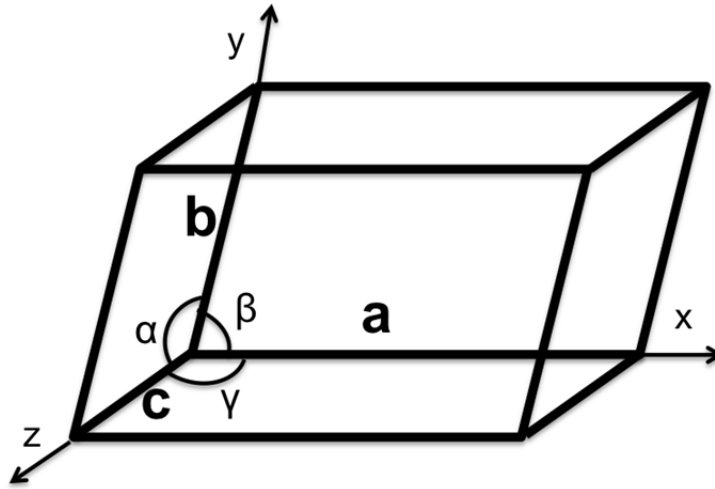


Figure 14. Unit cell

The unit cell has six variables to describe its dimensions, angles  $\alpha$ ,  $\beta$ ,  $\gamma$ , and edges **a**, **b**, **c**.

**Table 3. Seven crystal lattice system**

<b>Crystal system</b>	<b>Axial lengths and angles</b>
Triclinic	$a \neq b \neq c, \alpha \neq \beta \neq \gamma \neq 90^\circ$
Monoclinic	$a \neq b \neq c, \alpha = \gamma = 90^\circ, \beta \neq 90^\circ$
Orthorhombic	$a \neq b \neq c, \alpha = \beta = \gamma = 90^\circ$
Tetragonal	$a = b \neq c, \alpha = \beta = \gamma = 90^\circ$
Trigonal (Rhombohedral)	$a = b = c, \alpha = \beta = \gamma \neq 90^\circ$
Hexagonal	$a = b \neq c, \alpha = \beta = 90^\circ, \gamma = 120^\circ$
Cubic	$a = b = c, \alpha = \beta = \gamma = 90^\circ$

**Table 4. The 14 Bravais lattices**

Capital letters refer to the lattice type, P: primitive, I: body-centered, F: face-centered, C: base-centered, and R: rhombohedral.

<b>Crystal System</b>	<b>Lattice</b>
Triclinic	P
Monoclinic	P, C
Orthorhombic	P, C, I, F
Rhombohedral	R
Tetragonal	P, I
Hexagonal	P
Cubic	P, I, F

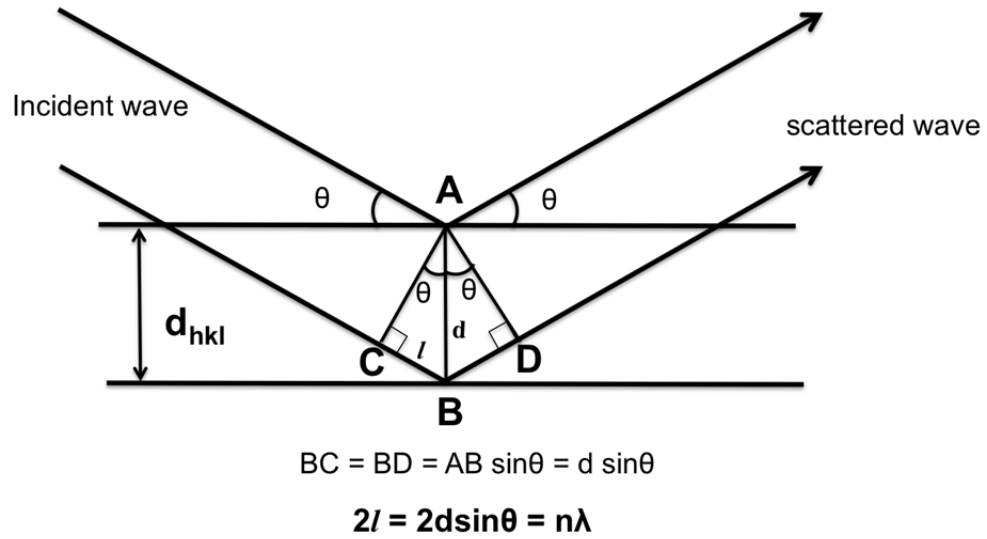


**Figure 15. Derivation of Bragg's Law**

Bragg's Law can be expressed as  $2d\sin\theta=n\lambda$ , where  $d$  is the perpendicular spacing between planes in the lattice,  $\theta$  is the angle between the incident and reflected rays,  $\lambda$  is the wavelength of the incident wave, and  $n$  is an integer. The difference in path length between the rays diffracted from the adjacent planes is twice the distance  $l$ . By simple trigonometry, distance  $l$  is equal to  $d\sin\theta$ . For two rays to diffract in phase,  $2l$  must equal the integral number of the wavelength ( $n\lambda$ ).

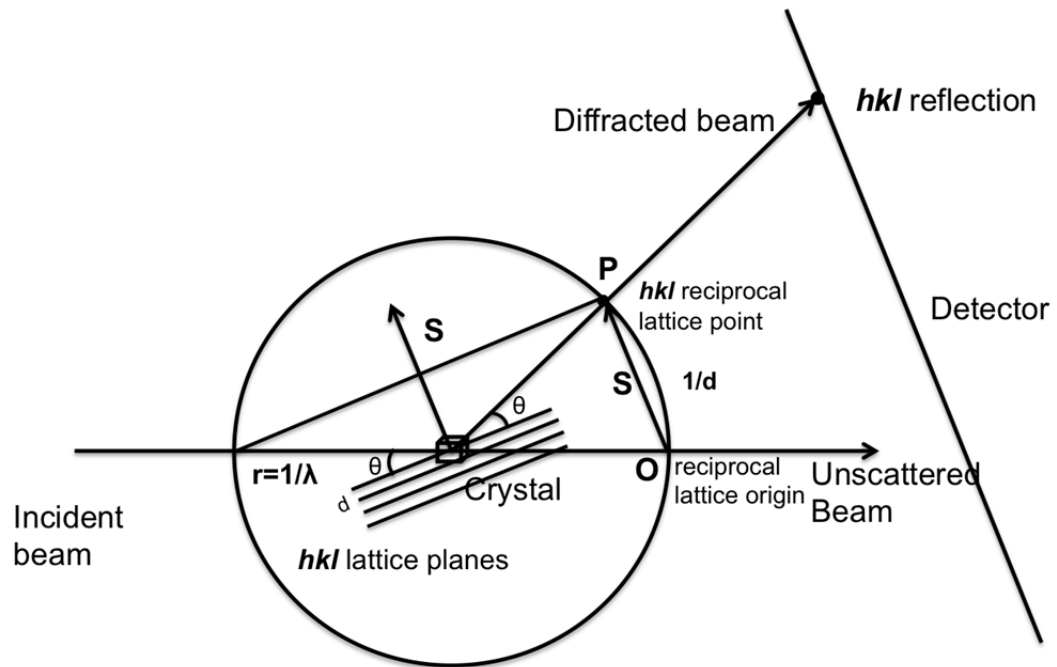


**Figure 16. Ewald's sphere describes diffraction in the reciprocal space**

The sphere has a radius of  $1/\lambda$ . The crystal sits in the center of the sphere. The X-ray beam comes from the left and the unscattered beam passes through the crystal and the point where it reaches the sphere surface is the origin of reciprocal space (O). For a diffraction point in reciprocal space to occur, it must contact with the surface of the Ewald sphere (P). The vector connecting the reciprocal lattice origin and the diffraction point is the diffraction vector,  $\mathbf{S}$  with the length of  $1/d_{hkl}$ . In short, according to Bragg's law, the reflection  $hkl$  in the reciprocal space is the result of the reflection from the set of  $hkl$  lattice planes.

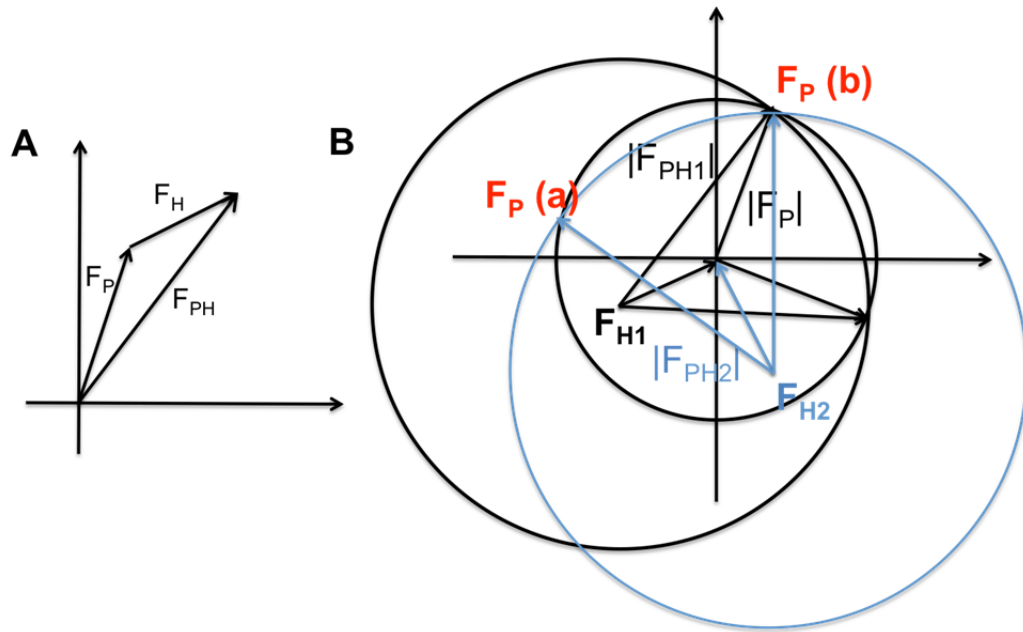


**Figure 17. Isomorphous Replacement**

A: The structure factor for the derivative crystal  $F_{PH}$  equals the sum of the protein structure factor  $F_P$  and the heavy atom structure factor  $F_H$ . B: Harker construction of MIR for determining the native protein phase  $\Phi_P$ . It shows the relationship between the native crystal structure factor  $F_P$  and that of an isomorphous derivative crystal  $F_H$ , which contains a heavy atom that contributes a scattering component  $F_{H1}$ . The circles intersect in two points that represent two solutions for phase of  $F_P$ . A second heavy atom derivative crystal structure  $F_{PH2}$  can solve this phase ambiguity.

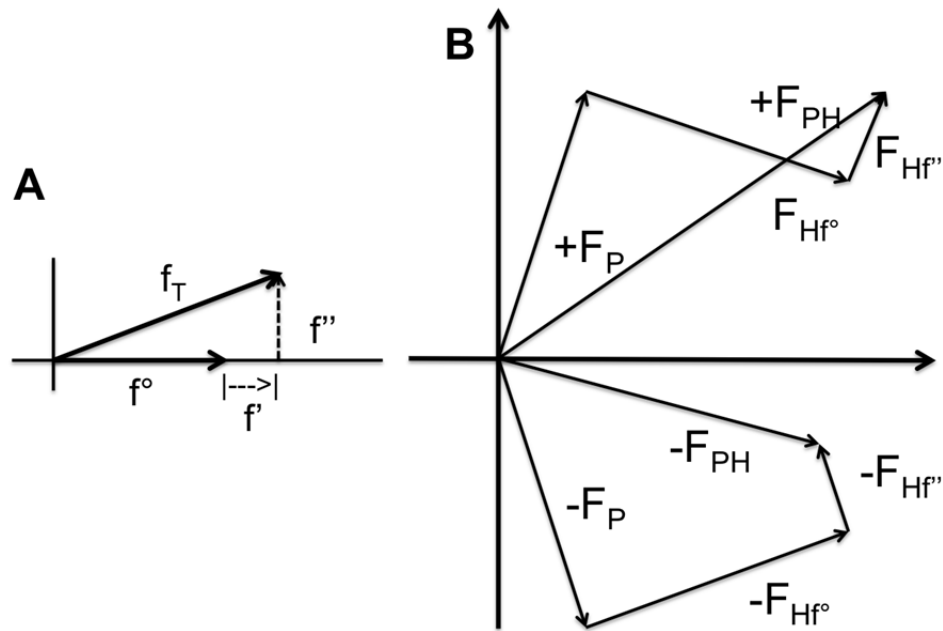


**Figure 18. Anomalous scattering by the heavy atom**

A:  $f_T$ : total scattering factor,  $f^o$ : normal scattering factor,  $f'$ : real component of anomalous scattering,  $f''$ : imaginary component of anomalous scattering. B: The effect of anomalous scattering on the measured structure amplitude is shown here. Anomalous scattering breaks the Friedel's Law. In the absence of anomalous scatterers,  $+F_P$  and  $-F_P$  are symmetric. However, in the presence of anomalous scattering, the imaginary component of  $F_{Hf''}$  always leads  $F_{Hf^o}$  by  $90^\circ$  for both  $+F_P$  and  $-F_P$ , so the center of symmetry no longer holds. ( $+F_{PH} \neq -F_{PH}$ )

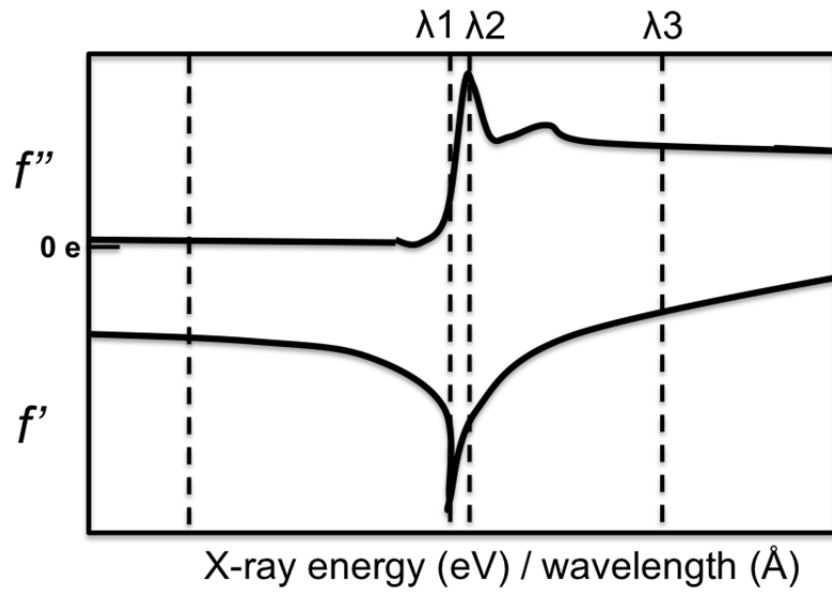


**Figure 19. Fluorescence scan of the Selenium**

It measures the  $f''$  anomalous scattering from the crystal and is used for choosing the wavelengths for a MAD experiment.  $\lambda_1$ : the inflection point where  $f'$  is the minimum.  $\lambda_2$ : the peak where  $f''$  is the maximum.  $\lambda_3$ : high energy remote.

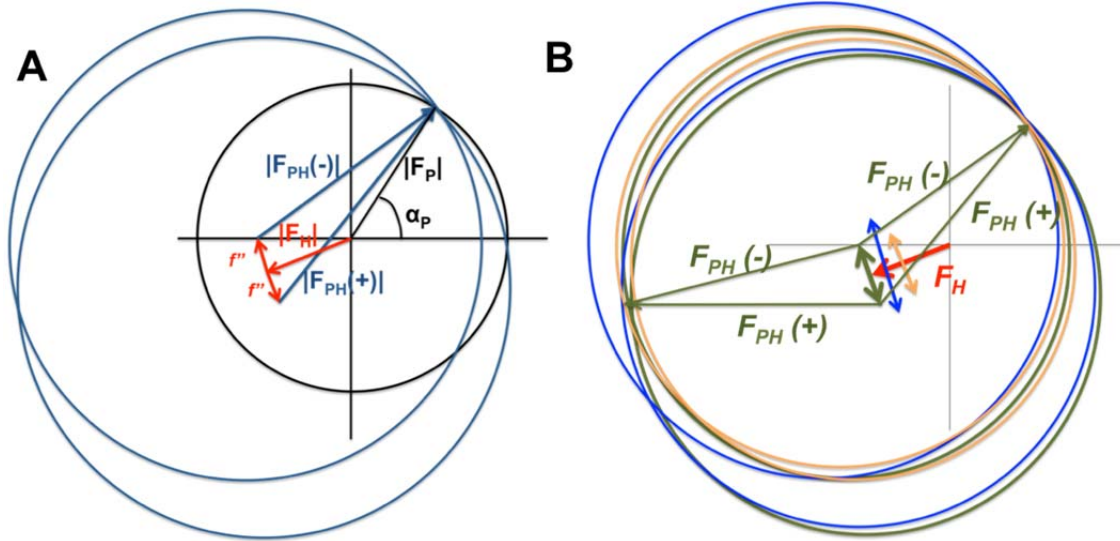


Figure 20. A: Harker construction of SIRAS B: Harker construction of MAD.

## Chapter 3. Structural studies on ParA

ParA is a member of the Walker-type family of ATPases and is responsible for the localization and movement of plasmids and in some cases, chromosomes, during DNA partition. These systems are composed of three components: a DNA centromere site, the ParA ATPase and the ParB centromere binding protein. ParB binds the centromere to form a scaffold, which recruits the motor protein, ParA. In the next step, the ParA protein mediates separation of the replicated DNA. ParA plays an essential role as a motor protein in the active plasmid partition, perhaps by providing the motive force for the movement of replicated plasmids. Multiple Fluorescence Microscopy studies have observed the dynamic movement of ParA over the nucleoid (Ebersbach & Gerdes, 2004; Hatano et al, 2007; Lim et al, 2005; Marston & Errington, 1999; Pratto et al, 2008). SopA from the F plasmid and ParA from the pB171 plasmid were shown to display oscillatory behavior on the nucleoid and notably, this movement required the presence of the cognate centromere binding protein and the centromere-like DNA site (Ebersbach & Gerdes, 2004; Lim et al, 2005). These observations suggest that the dynamic movement of ParA is somehow responsible for DNA partition, however how ParA dynamics would facilitate plasmid movement during the partitioning process is not well understood.

Multiple ParA proteins can form polymers in an ATP-dependent manner *in vitro* (Barilla et al, 2005; Dunham et al, 2009; Ebersbach et al, 2006; Leonard et al, 2005; Lim et al, 2005; Pratto et al, 2008), and they also display ATP-dependent nonspecific DNA

binding activity (Havey et al, 2012; Leonard et al, 2005; Pratto et al, 2008). This suggests that ParA function is regulated by the nucleotide-bound state and that the ATP bound form is the active state in DNA partition. Some studies have suggested that the ATPase activity of ParA is stimulated by a proposed arginine finger found on its partner ParB protein (Barilla et al, 2007; Pratto et al, 2008). This indicates that the cycling of ATP binding and ATP hydrolysis is key to the segregation process.

Notably, this abundant ParA based partition machinery has been shown to function in segregation of both plasmid and chromosomal archaeal DNA. Our work focuses on a ParA homolog similar to the ParA protein from the first identified archaeal plasmid partition system, located on the pNOB8 plasmid harbored in the thermophilic archaeon, *Sulfolobus solfataricus*. Later BLAST analyses revealed that this homolog is a chromosomal ParA from *Sulfolobu islandicus*. The ParA homolog has 60% sequence identity and 82% similarity to the pNOB8 protein as shown in Figure 21. This work focuses on the ParA homolog, which I will simply refer to herein as ParA. The protein sequence of ParA contains a putative Walker box motif and is highly homologous to bacterial ParA proteins, which suggest that archaeal DNA partition may use similar partition mechanisms as bacteria.

To gain insight into the function of ParA in the process of archaeal DNA partition, we solved its crystal structure in the apo and ADP-bound states and performed a series of complementary biochemical studies.

### **3.1 Structure determination of ParA structures**

The structure of the apo ParA was determined at 2.45 Å resolution using MAD phasing of selenomethionine-substituted protein crystals. The crystals belonged to space group P3<sub>1</sub>21, with unit-cell parameters of a=89.1, b=89.1, c=116.6,  $\alpha$ ,  $\beta$  =90°,  $\gamma$  =120°. The structure was refined to a crystallographic *R*-factor of 19.0% and *R*-free of 24.0%.

Subsequently, a ParA-ADP bound state was crystallized and its structure solved to 2.74 Å resolution by molecular replacement using the apo structure as the search model. The ParA-ADP crystal belongs to the space group, P3<sub>2</sub>21 with unit cell dimensions, a, b=90.3, c=61.6,  $\alpha$ ,  $\beta$  =90°,  $\gamma$ =120° and was refined to a crystallographic *R*-factor of 22.9% and *R*-free of 27.7% (Table 5).

### **3.2 Overall structure of ParA**

The 314 residue apo ParA structure revealed a dimer in the crystal. Each ParA subunit is composed of a seven-stranded  $\beta$ -sheet surrounded by twelve  $\alpha$ -helices with the topology:  $\beta$ 1(residues 4-8)-  $\alpha$ 1(17-30)-  $\beta$ 2(34-38)-  $\alpha$ 2(44-49)-  $\alpha$ 3(52-62)-  $\alpha$ 4(71-79)-  $\beta$ 3(84-91)-  $\beta$ 4(96- 104)-  $\alpha$ 5(17-30)-  $\alpha$ 6(122-138)-  $\beta$ 5(141-145)- $\alpha$ 7(154-160)-  $\beta$ 6(163-168)-  $\alpha$ 8(172-190)-  $\beta$ 7(198- 206)-  $\alpha$ 9(211-227)-  $\alpha$ 10(230-223)-  $\beta$ 101(249-252)-  $\beta$ 102(261-264)-  $\alpha$ 11(273-286)-  $\alpha$ 12(298-313) (Figure 22A).  $\beta$ 102(261-264) is only shown in Chain B while this region in Chain A is highly disordered. A structural homology search using DALI (Holm & Rosenstrom, 2010) revealed that ParA has the strongest structural similarity with the Soj protein from *Thermus thermophilus* (PDB: 2bek). The Soj protein contains a canonical Walker-type fold and plays an important role in chromosome segregation in

collaboration with its CBP Spo0J (Leonard et al, 2005). Although the primary sequence identity is 25%, ParA and Soj can be maximally superimposed with a root mean square deviation (RMSD) of 2.3 Å for 208 corresponding C $\alpha$  atoms.

Superimposition of Soj onto ParA revealed high similarity in their overall conformations. Both contain seven  $\beta$ -strands ( $\beta$ 7- $\beta$ 6- $\beta$ 1- $\beta$ 5- $\beta$ 2- $\beta$ 4- $\beta$ 3) along with  $\alpha$ 1,  $\alpha$ 2,  $\alpha$ 7,  $\alpha$ 8,  $\alpha$ 9,  $\alpha$ 13 and the P-loop between  $\beta$ 1 and  $\alpha$ 1 (Figure 23D). ParA also shows structural similarity to other Walker-type family ATPases such as MinD (pdb: 1g3q) (RMSD= 2.3 Å for 207 corresponding C $\alpha$  atoms) (Figure 23C), ParF from TP228 plasmid (pdb: 4e07) (RMSD= 2.3 Å for 194 corresponding C $\alpha$  atoms) (Figure 23E), and ParA from the P1 plasmid (pdb: 3ez7) (RMSD= 2.9 Å for 222 corresponding C $\alpha$  atoms) (Figure 23F). All these ParA structures have an architecture with six  $\beta$  strands, the P-loop, and helices  $\alpha$ 1,  $\alpha$ 2,  $\alpha$ 7,  $\alpha$ 8,  $\alpha$ 9,  $\alpha$ 13. The region where  $\alpha$ 3,  $\alpha$ 4, and  $\alpha$ 5 are located (ParA numbering) varies among all the structures listed above (Figure 23).

### **3.3 The insert region**

Notably, major differences between ParA homolog structures are found in the region consisting of  $\beta$ 3- $\beta$ 4 in the archaeal ParA. Indeed, this region is not found in other bacterial ParA proteins and herein, we call this the insert region ( $\beta$ 3-loop- $\beta$ 4) (Figure 24). It is particularly interesting because additional structures of ParA and pNOB8 ParA determined recently in the Schumacher Lab revealed that the secondary structure of this region varies depending upon its crystal packing environment (Schumacher *et al.*, manuscript under review). This suggests that this region is flexible and may only fold

upon binding to another protein or DNA. The sequence of this region is VENFIHVSKTSKGEVKVSLD and the lysines (in bold) are located in the loop between the two beta strands,  $\beta 3$  and  $\beta 4$ .

### **3.4 ParA shares a set of conserved nucleotide binding motifs with other bacterial Walker-type family proteins**

Walker-type proteins contain a highly conserved sequence called the Walker A motif. Moreover, two additional motifs called the Walker A' and the Walker B are also highly conserved in the proteins of this family. This set of three motifs mediate nucleotide-binding (Koonin, 1993). To investigate whether ParA also contain this set of nucleotide binding motifs, protein sequences from members of the ParA-like family were aligned with that of ParA. ClustalW2 web-based alignment tools (Robert & Gouet, 2014) were used for analysis of sequence homology and conserved residues of the protein sequences including TP228 ParF, Soj from *T. thermophiles*, P1 ParA from *E. coli* and MinD from *P. furiosus*. Figure 25 is the result of the multiple sequence alignment that shows the conserved sequences in red. Indeed, all Walker A, Walker A' and Walker B motifs are shown to be highly conserved among the ParA homologs listed above, and furthermore, the archaeal ParA also shares this conserved set of nucleotide binding motifs.

Deviant Walker box proteins, such as partition ParA proteins, contain a variation of the Walker A motif in which there is an extra lysine, termed the signature lysine, near the N-terminal end of the motif. This residue has been shown to play a role in ATP hydrolysis by these proteins. The structure of the archaeal ParA revealed a clear deviant

Walker A motif (residues 11-18) that forms a glycine rich loop. Moreover, the structure also revealed a Walker A' motif (residues 34-42) and Walker B motif (residues 140-145) both of which are also characteristic of Walker box proteins (Figure 22B).

### **3.5 Dimerization interface**

The total buried surface area (BSA) in the archaeal ParA dimer interface is 1907 Å<sup>2</sup>. This is relatively smaller than the significant BSA observed in the P1 and P7 ParA dimers. However, this difference is at least partly due to the fact that the P1 and P7 ParA proteins harbor an extra N-terminal helix that forms tight dimer contacts. This helix is absent in the archaeal and type Ib ParA proteins. The residues that are involved in the dimerization interface of the archaeal ParA are negatively or positively charged and located primarily on the loops between  $\beta 6$ - $\alpha 8$ ,  $\beta 7$ - $\alpha 10$  and the loop just before  $\alpha 11$  (Figure 26). In particular, there are four salt bridges that seem to stabilize the dimer of ParA. These interactions occur between residues, Glu173-Arg55 and Arg209-Glu269. Size exclusion chromatography analyses on the archaeal ParA protein revealed a calculated mass of 70 kDa, supporting that it is dimeric in its apo form (Figure 32)

### **3.6 Structure of ParA-ADP**

The structure of ParA-ADP contains one subunit in the asymmetric unit and the dimer is generated by crystallographic symmetry. The structure contains some highly disordered regions in  $\alpha 4$  (residues 69-81) and  $\alpha 5$  (residues 105-122), and a partial  $\alpha 6$  (residues 123-129). The apo structure and ParA-ADP dimer superimpose with a root mean square deviation (RMSD) of 0.7 Å (Figure 28). The total buried surface area of the

ParA-ADP dimer is 1673 Å<sup>2</sup>, which is approximately 300 Å<sup>2</sup> smaller than that of the ParA apo structure. Based on comparisons of the two structures, the apo and ADP bound dimers are very similar in their overall structures and oligomeric arrangements. However, there is a subtle difference in the conformation of the loop region near the ADP binding site (residues 256-263). This will be discussed in more detail after the ADP binding site has been described.

### **3.7 ADP binding site**

In the ParA-ADP bound structure, ADP sits in a cavity at the surface created by residues Lys12-Leu20, Ser44, Asp 145, Pro148, Arg206, Leu254-Lys258, and Leu261-Asp263 (Figure 29). Figure 30 shows a close up view of the ParA ADP binding site. The loop after  $\alpha 11$ , composed of residues Ser255-Ser262, extends around the adenine ring. The main chain carbonyl of Ser255 forms hydrogen bond with N6 of adenine. N1 of adenine forms hydrogen bonds with the main chain nitrogen of Asn257 and N7 makes hydrogen bonds with the side chain of Thr19. Non-polar interactions are observed with Leu254, Leu261, and Lys206. The Leu261 side chain extends vertically to the adenine ring to make a hydrophobic contact while the aliphatic atoms of the Lys206 side chain also make non-polar contacts with the adenine moiety. The ribose ring adopts the typical C3'-*endo* conformation. The ADP hydroxyl group at the 2' position is recognized by the main chain carbonyls of Leu261 and Ser262.

The phosphate-binding region reveals the conserved deviant Walker A motif as is shown in Figure 29 (colored in magenta). The P-loop located between  $\beta 1$  and  $\alpha 1$ , is

composed of residues 11-18, and extends around the  $\beta$  phosphate. The main chain amide nitrogen groups of Gly14-Thr18 stabilize the  $\alpha$  and the  $\beta$  phosphates of the ADP moiety. The hydroxyl group of the Thr19 side chain and its main chain amide group recognize the  $\alpha$  phosphate. The signature lysine in crystal structures of ParA-like family proteins make intersubunit phosphate contacts with the nucleotide bound in the adjacent subunit. In the ADP bound structure of ParA, the signature lysine (Lys12) is too far from the ADP bound in the adjacent subunit (distance: 7.56 Å) to make this intersubunit contact.

The Walker A' motif, adjacent to Walker A motif, is located at  $\beta 2$  (residues 34-42). The, highly conserved Asp40 of this motif interacts indirectly with the Mg ion through a water molecule. This conserved Asp residue is known to be the sensor of ATP binding/hydrolysis. The Walker B motif, with the conserved sequence, hhhhD (h=hydrophobic residues) is known to contain a conserved acidic residue Asp (or Glu) residue, which also functions in coordinating the Mg ion either directly or indirectly via a water molecule and is essential for ATP hydrolysis. In the archaeal ParA protein the Walker B motif consists of residues 140-145 and contains the conserved acidic residue Asp145 that contacts the Mg ion.

While no change was detected in the P-loop near the phosphate moiety of ADP compared to the apo state, a conformational change was detected in the loop, composed of residues 252-262 that surrounds the adenine ring of ADP. In the apo state, residues 261-264 form a  $3_{10}$  helix where in the ADP bound state, the hydroxyl of the ribose ring

would clash with side chain of Ser262 and Leu261 (Figure 31). Upon the ADP binding, the residues that form this  $3_{10}$  helix shift to residues 258-262 to prevent this clash.

### **3.8 Discussion**

To characterize the archaeal ParA at the molecular level, we determined its crystal structures in the apo and ADP bound states. The structure indeed revealed the Walker box fold and was strikingly similar to bacterial ParA homologs that are involved in the partition of bacterial plasmids or chromosomes. Furthermore, recently it has been shown that the chromosome of *Sulfolobus solfataricus* also harbors a segregation system with a putative Walker box protein, SegA, which is required for segregation (Kalliomaas-Sanford et al, 2012). Thus, our findings indicate that bacterial-like Type I Walker-box based partition systems may also be conserved in archaea.

Notably, both apo and ADP bound ParA were dimeric and there was no overall conformational change between these two states. However, to assess if any structural change occurs that may be required for partition would necessitate an ATP bound structure. Indeed, studies in the Schumacher Lab on the pNOB8 ParA protein have captured its structure in its apo, ADP bound and ATP bound states. These structures have revealed that, like the ParA homolog, all states are dimeric. However, only upon ATP binding do large conformational changes occur. These alterations allow the signature lysine from one subunit to interact with the ATP molecule on the adjacent subunit (Schumacher *et al.*, manuscript under review).

Another example of ATP locking in a specific state upon ATP binding is observed in structures of NifH. NifH is a Fe-protein from *Azotobacter vinelandii*. In the NifH structures, the signature lysine is 8.5 Å from the β-phosphate of ADP. However, in the presence of ADP·AlF<sub>4</sub><sup>-</sup> (an ATP analogue) and its partner MoFe protein, each of the monomers of NifH rotates ~13° toward the subunit interface forming a more compact structure, such that the signature lysines are 2.77 Å from the β-phosphate (Schindelin et al., 1997). This rotational movement allows NifH to be active for its function in catalyzing the reduction of atmospheric nitrogen to ammonia.

Although the ATP hydrolysis property of ParA has not been demonstrated in this work, the catalytic residues responsible for ATP hydrolysis in the Walker A' and Walker B motifs, Asp40 and Asp145, are conserved in the archaeal ParA. The structure of ADP bound state also revealed both residues to be located at the nucleotide binding site, suggesting that ParA is at least equipped for an ATPase activity.

### **3.9 Experimental Procedures**

*Expression, Purification, and Crystallization* A synthetic gene, codon optimized for *E. coli* expression of ParA was purchased from Genscript Corporation and subcloned into the pET15b vector such that a hexa-His-tag was expressed for purification (Piscataway, NJ, USA). This was transformed into *E. coli* B834(DE3) and expressed in defined medium supplemented with 90 mg/L of L- Selenomethionine. Cells were grown at 37°C to an OD<sub>600</sub> of 0.5-0.6 and then induced with 1 mM IPTG for 16 hrs at 9°C. His-tagged ParA was purified by using Ni-NTA chromatography and was buffer exchanged

using a size exclusion column equilibrated with 25 mM Tris pH 7.5, 200 mM NaCl, and 5 mM DTT. ParA crystals were grown at room temperature using the hanging drop vapor diffusion method. Crystals were obtained by mixing 2  $\mu$ l of the protein at 15 mg/ml with 2  $\mu$ l of the crystallization buffer, which contained 10% (v/v) 2-propanol, 0.1 M phosphate-citrate pH 4.2, and 0.2 M LiSO<sub>4</sub>. ParA-ADP crystals were grown using a crystallization solution consisting of 0.1 M Tris pH 8.5 and 8% w/v PEG 8000 (Figure 32).

***Structure Determination*** The MAD X-ray intensity data were collected from a selenomethionine-containing ParA crystal at the Advanced Light Source (ALS), beamline 8.3.1 by Dr. Maria Schumacher. The structure was solved by multiwavelength anomalous diffraction (MAD) to 2.45 Å resolution also with the help of Dr. Schumacher. The selenium sites were located using SOLVE (Terwilliger & Berendzen, 1999). Model building was performed by COOT (Emsley et al, 2010), and the model was refined to  $R_{\text{work}}/R_{\text{free}}= 18.9/24.0$  in PHENIX with help of Dr. Tonthat. The data set for the ParA-ADP complex crystal was collected at the Advanced Photon Source (APS), beamline ID. The structure was solved using molecular replacement using the apo structure as a search model. Model building was performed using COOT and PHENIX was used for refinement. See Table 5 for final refinement statistics.

***Size Exclusion Column Chromatography*** The oligomeric state of ParA was determined by size exclusion chromatography. ParA at a concentration of 1 mg/ml was injected into a Superdex S75 column (Amersham Pharmacia Biotech) with a mobile

phase of 25 mM Tris-HCl pH 7.5, and 200 mM NaCl. The elution volume was then plotted against a standard curve to determine the relative molecular weight of the sample. Three protein samples were used to calibrate the column: Cytochrome C (Mr 12 400 kDa), carbonic anhydrase (Mr 29 000 kDa), and bovine serum albumin (Mr 66 000 kDa). The  $K_{Average}$  ( $K_{ave}$ ) was calculated as follow:  $K_{ave}=(V_E - V_O)/(V_T - V_O)$ , where  $V_T$ ,  $V_E$  and  $V_O$  are the total column volume, elution volume and void volume of the column, respectively. The standard plot was generated by graphing the logarithm of the molecular weight (Mr) against the  $K_{ave}$ . The  $K_{ave}$  of each marker as well as the experimental samples were the average value of three experiments.

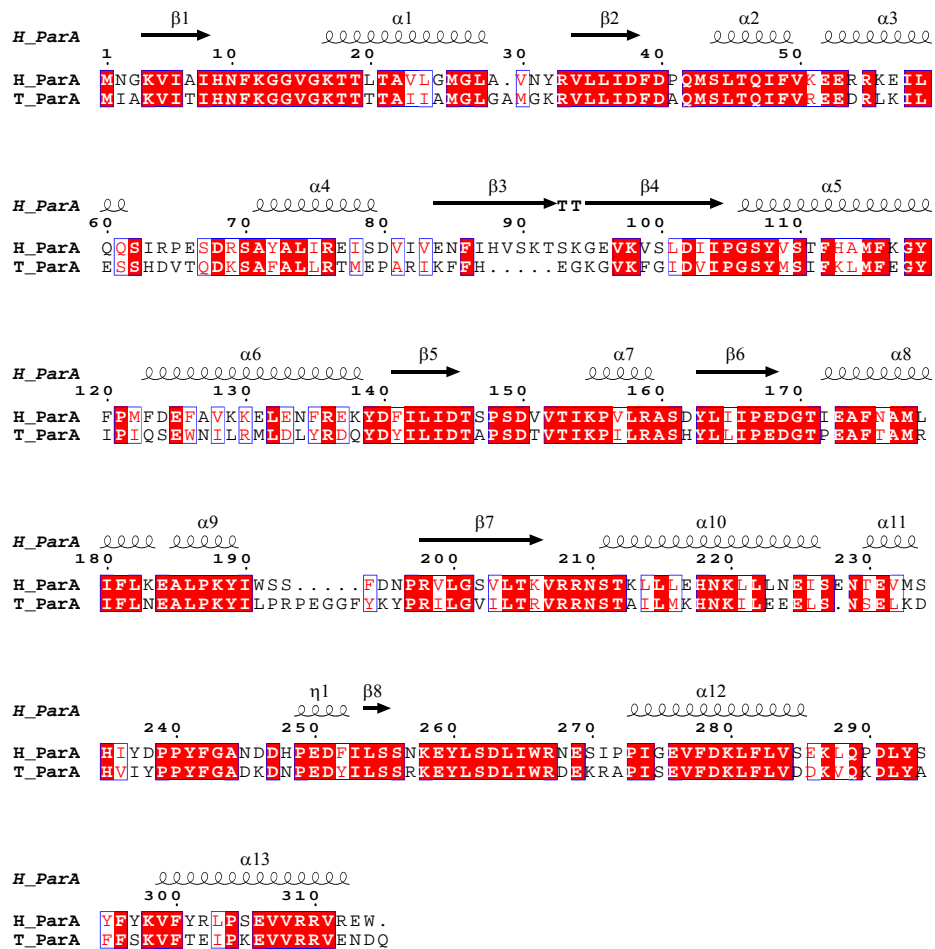


**Figure 21. Sequence alignment of pNOB8 ParA and the ParA homolog.**

Secondary structural elements of ParA homolog are represented above the sequence. The ParA homolog used in this study has 60% sequence identity and 82% similarity to the pNOB8 ParA.

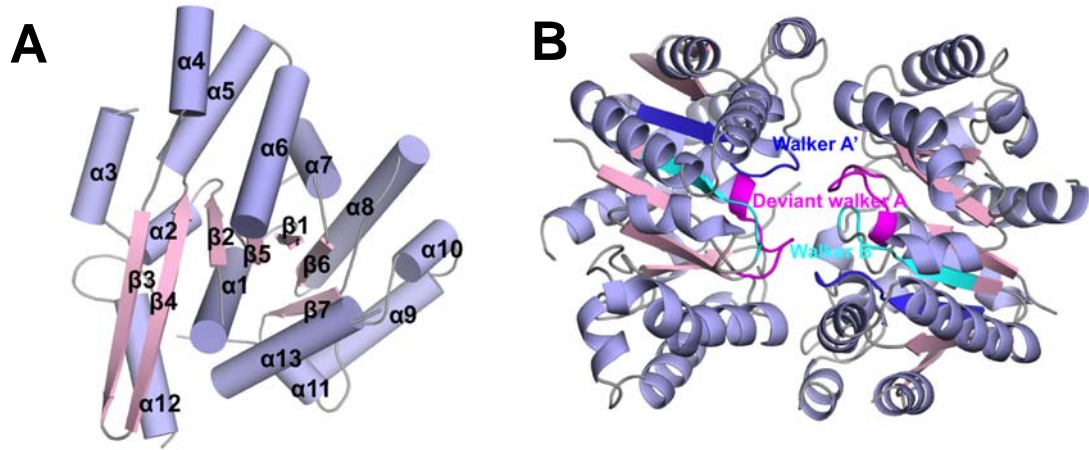


**Figure 22. Overall structure of ParA**

A: Subunit of ParA. The helices are shown as cylinders, colored in light purple and the  $\beta$  strands are colored as pink arrows. Each secondary structure is labeled. Deviant Walker A motif is indicated with magenta. B: Ribbon diagram of the overall structure of ParA dimer. Deviant Walker A motif is colored in magenta, Walker A' in blue, and Walker B in cyan.

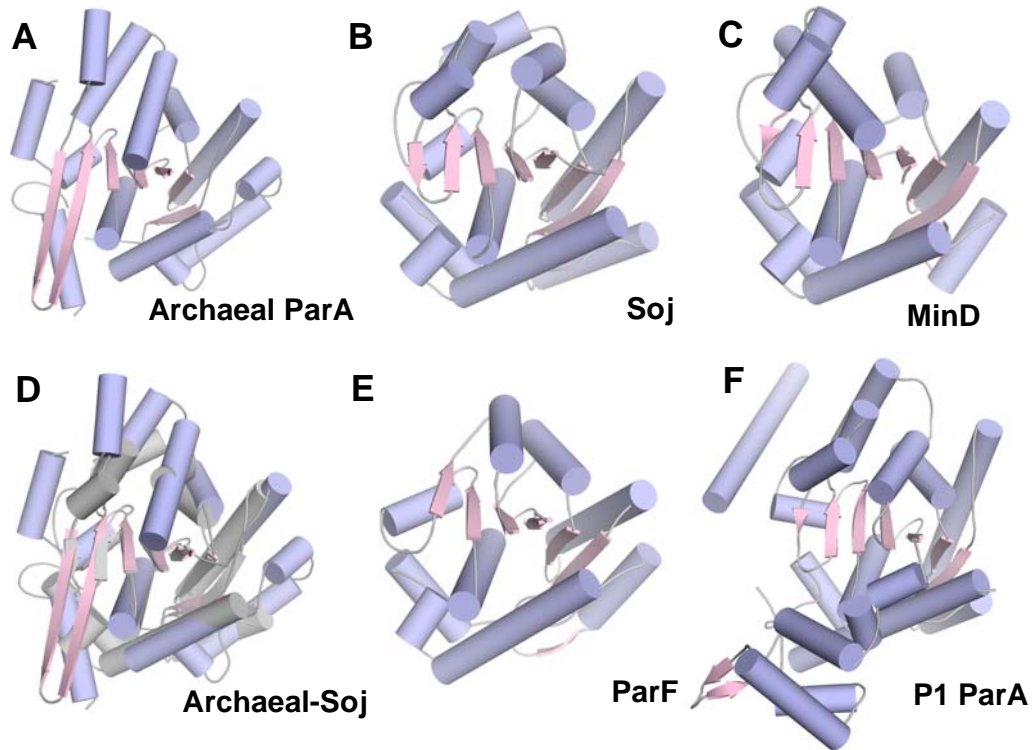


**Figure 23. Structure comparisons of ParA homologs**

The ribbon diagram of (A) ParA, (B) Soj (pdb: 2bek) (C) MinD (pdb: 1g3q) (D): superposition of ParA and Soj (E) ParF (pdb: 4e07) (F) P1 ParA (pdb: 3ez7), shown in the same orientation as (A)

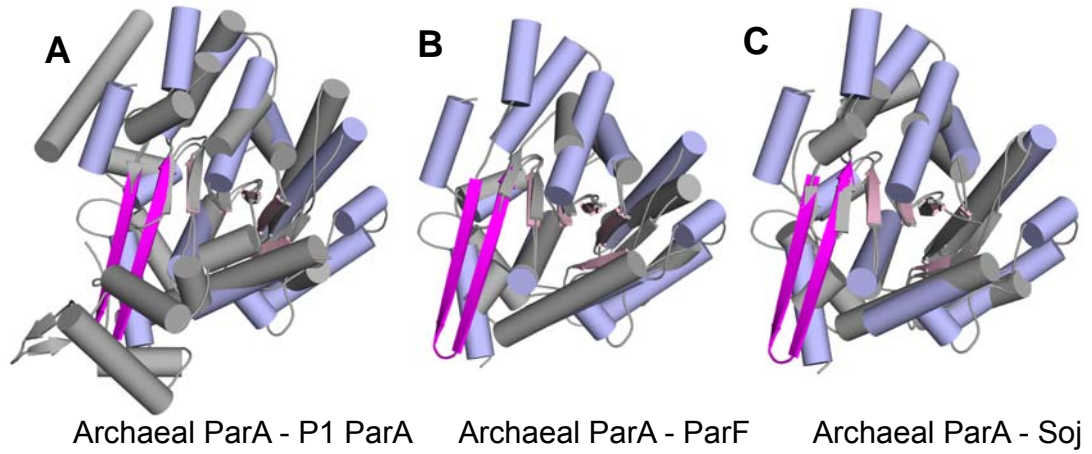


**Figure 24. The insert region**

The overlay of ParA with other ParA homologues from both type Ia and Ib revealed that this region is really unique to ParA. The insert region is colored in magenta. A: Overlay of ParA with P1 ParA (pdb: 3ez7). B: Overlay of ParA with ParF (pdb: 4e07). C: Overlay of ParA with Soj (pdb: 2bek).

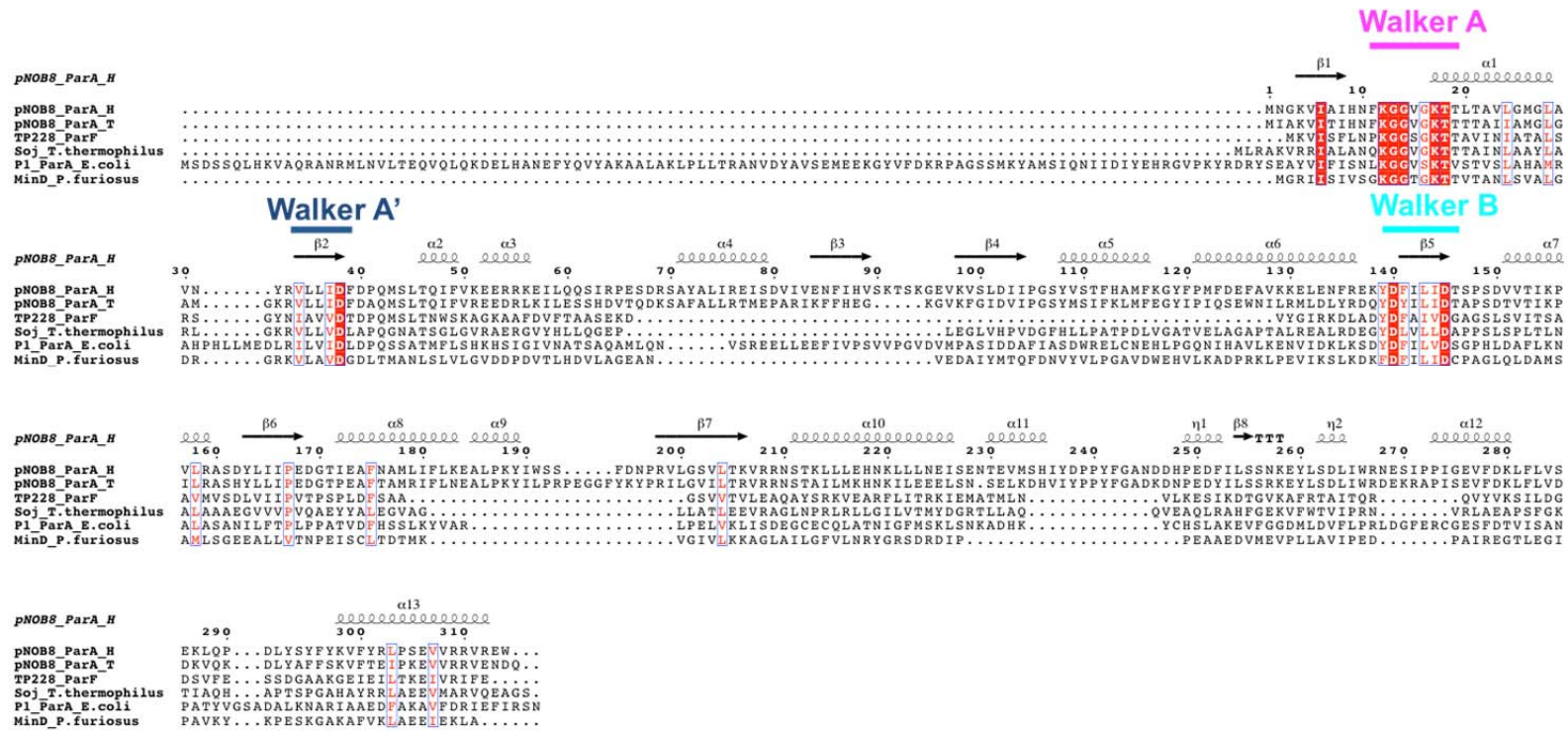
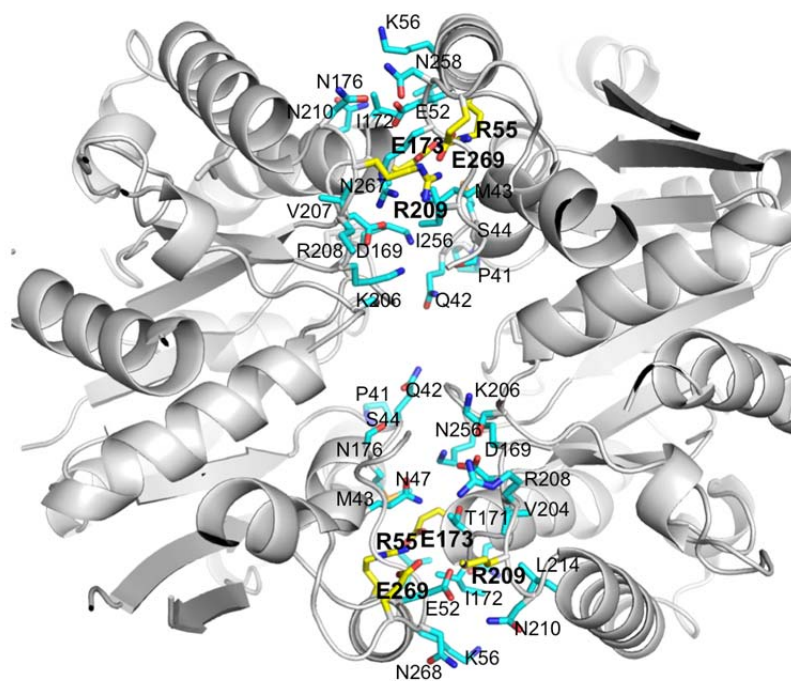


Figure 25. Multiple sequence alignment of pNOB8 ParA and other ParA homologs.

Secondary structural elements of ParA are represented above the sequence. Amino acid residues considered to be similar are in red and the red box represents perfect identity. Multiple sequence alignment of ParA and ParA homologs revealed three conserved motif for ATP binding and ATP hydrolysis, Walker A (indicated in magenta), Walker A' (indicated in dark blue) and Walker B motif (indicated in cyan).



**Figure 26. The Dimerization interface**

The residues involved in the dimerization interface are indicated in cyan. The residues are mostly located in the alpha helices and loops that surround the beta sheet. Four salt bridge interactions were found in the interface. The residues involved in the interactions are Arg55, Glu173, Glu269, and Arg209 (indicated in yellow).

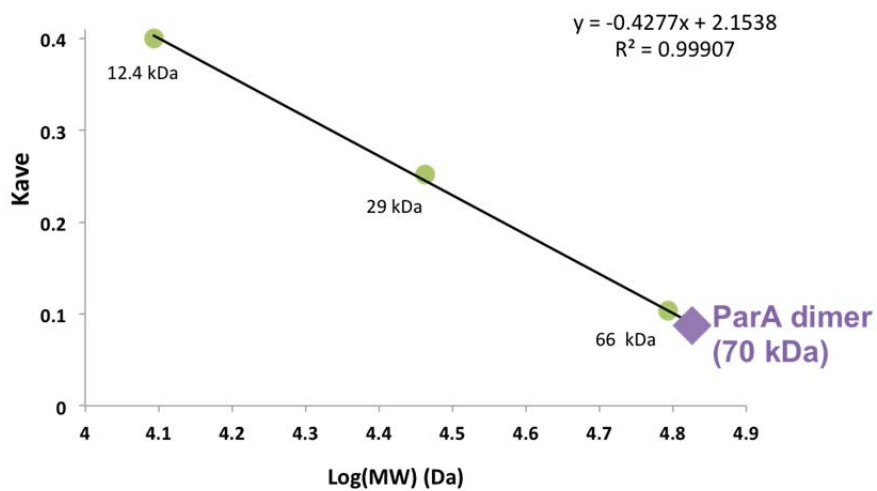


**Figure 27. Oligomeric state of ParA in solution determined by size exclusion chromatography**

The graph illustrates that ParA is dimeric.

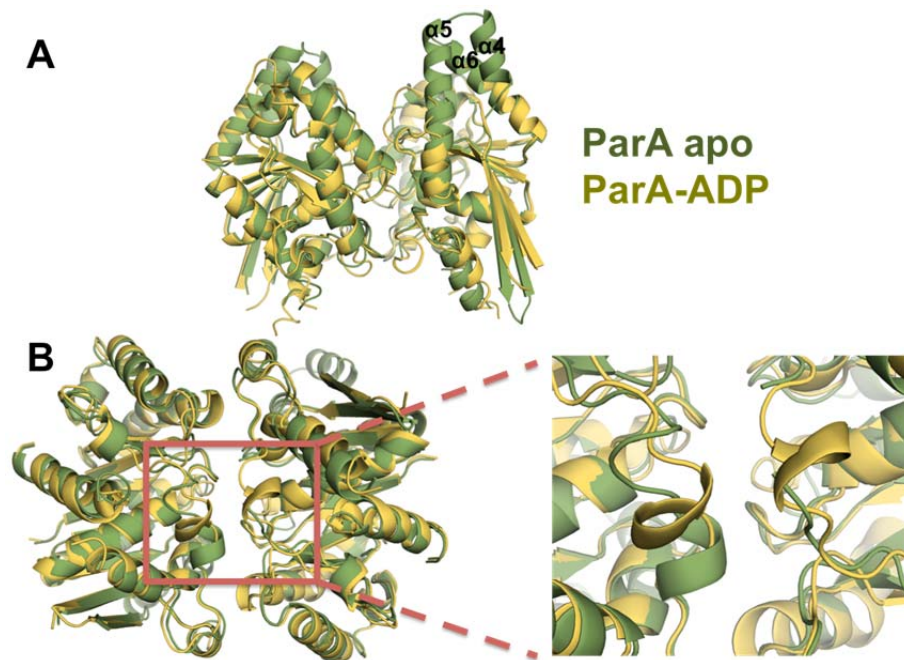


**Figure 28. Comparison between apo ParA and Par-ADP structures**

The structural alignment of ParA apo and ParA-ADP structures. ParA apo structure is in green and ParA-ADP structure is in yellow. A: The helices  $\alpha 4$ ,  $\alpha 5$ , and a part of  $\alpha 6$  are disordered in the ParA-ADP structure while the loop region near the ADP binding site is more ordered. B: Close up of the loops near the ADP binding site.

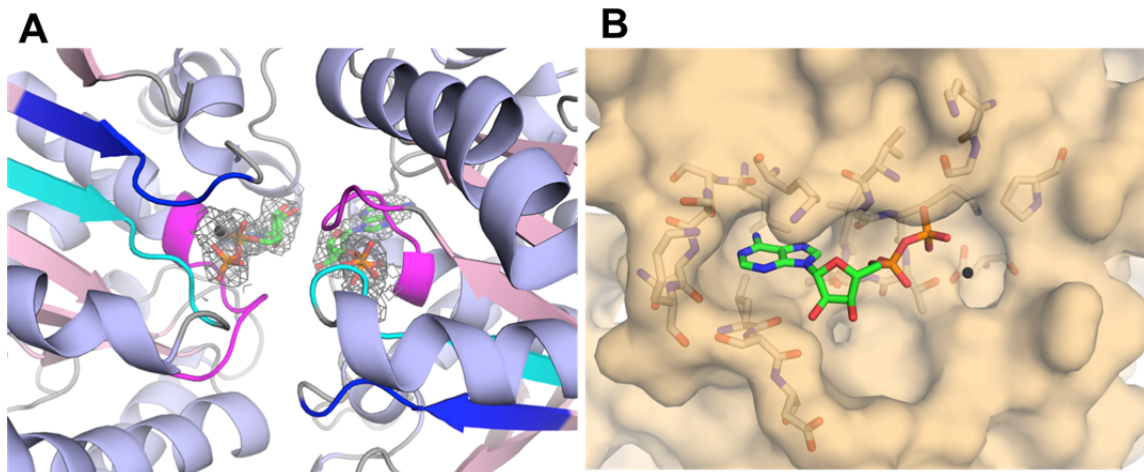


**Figure 29. The ADP binding site**

A: ADP is shown in sticks and the Mg<sup>2+</sup> ion is in black sphere. A fo-fc map (contoured at 3.0  $\sigma$  level) of ADP and magnesium is shown in gray mesh. B: Surface representation of the ADP binding site. The cavity is composed of residues, Lys12-Leu20, Ser44, Asp 145, Pro148, Arg206, Leu254-Lys258, and Leu261-Asp263.

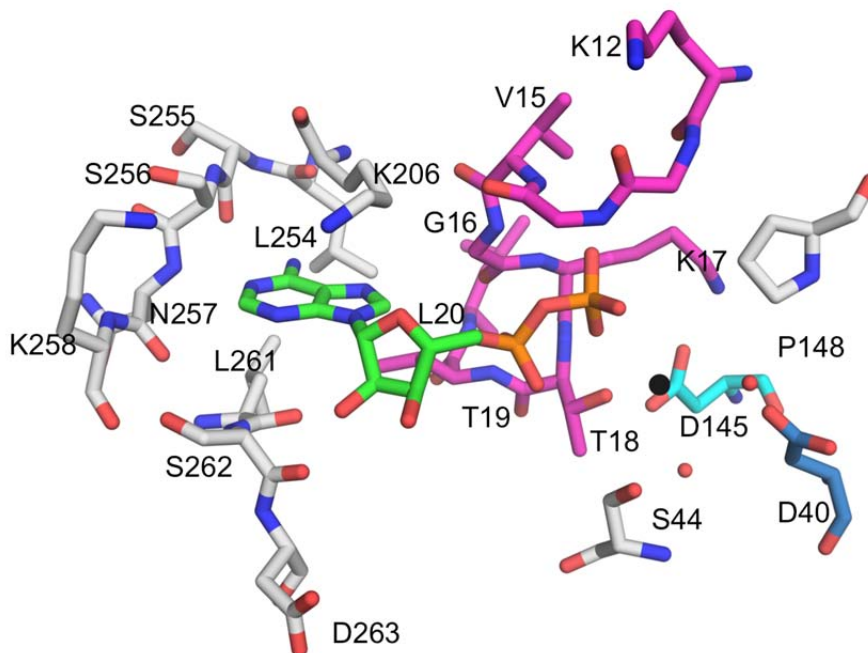


**Figure 30. Close up view of the ADP binding site**

The ADP binding site is composed of residues Lys12-Leu20, Ser44, Asp 145, Pro148, Arg206, Leu254-Lys258, and Leu261-Asp263. The residues from deviant Walker A motif are colored in magenta, Walker A' in blue, and Walker B in cyan.

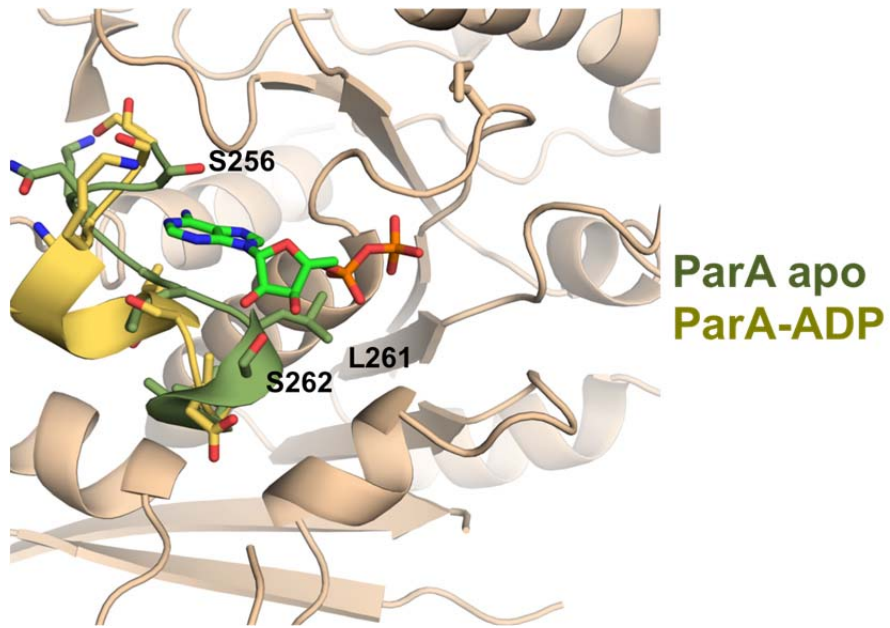


**Figure 31. Loop change upon ADP binding**

The loop from ParA apo structure is colored in green and the loop from ParA-ADP structure is colored in yellow. The residues Ser256-Leu264 form a  $3_{10}$  helix upon ADP binding. In the apo structure, residues 261-264 form a  $3_{10}$  helix where if ADP was bound, the hydroxyl of the ribose ring would clash with side chain of Ser262 and Leu261.

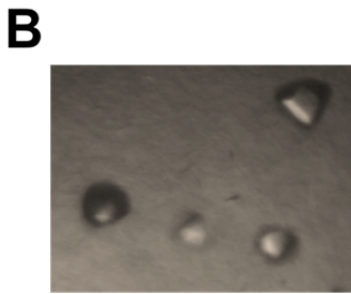
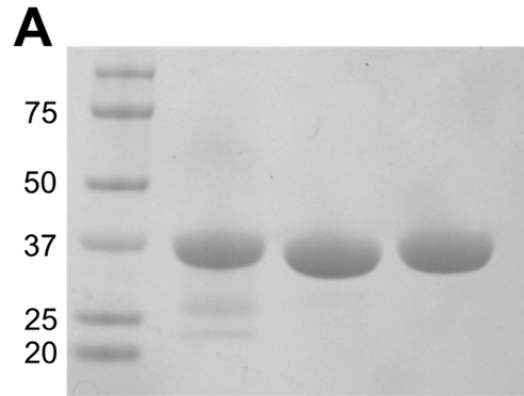


**Figure 32. Purification and crystallization of ParA**

A: SDS-PAGE gel showing purified ParA, 36 kD in size. B: The crystal of ParA was grown in solution that contained 10% (v/v) 2-propanol, 0.1 M phosphate-citrate pH 4.2, and 0.2

**Table 5. Crystallographic statistics for ParA apo and ParA-ADP structures**

	ParA apo			ParA-ADP
<b>Data Collection</b>	Peak	Remote	Inflection	
Space group	P3(1)21	P3(1)21	P3(1)21	P3(2)21
a, b, c (Å)	89.1	89.1	89.1	90.3
	89.1	89.1	89.1	90.3
	116.6	116.6	116.6	61.6
$\alpha, \beta, \gamma$ (°)	90, 90, 120	90, 90, 120	90, 90, 120	90, 90, 120
Resolution (Å)	2.45	2.45	2.45	2.74
Unique reflections	20619	20626	20614	7638
Completeness (%)	99.9	99.9	99.8	96.5
Redundancy	10.2	10.1	10.2	3.4
$R_{\text{merge}}$ (%)	8.8	8.8	8.5	8.3
<b>MAD phasing</b>				
No. of Se sites	12			
Figure of merit	0.6063			
<b>Refinement</b>				
Resolution (Å)	2.45			2.74
Rwork/Rfree (%)	19.0/24.0			22.9/27.7
<b>Ramachandran Analysis</b>				
Most favored (%)	97			97
Disallowed (%)	0			0
<b>RMSD</b>				
Bond lengths (Å)	0.9			1.404
Bond angles (Å)	0.005			0.008

<sup>a</sup> $R_{\text{merge}} = \frac{\sum_{hkl} \sum_i |I_i(hkl) - I(hkl)|}{\sum_{hkl} \sum_i I_i(hkl)}$ , where  $I_i(hkl)$  is observed intensity and  $I(hkl)$  is the final average value of intensity. <sup>b</sup>Values in parentheses are for the highest resolution shell. <sup>c</sup>Figure of Merit =  $\langle |\sum P(\alpha) e^{i\alpha} / P(\alpha)| \rangle$ , where  $\alpha$  is the phase and  $P(\alpha)$  is the phase probability distribution. <sup>d</sup> $R_{\text{work}} = \frac{\sum ||F_{\text{obs}}| - |F_{\text{calc}}||}{\sum |F_{\text{obs}}|}$  and  $R_{\text{free}} = \frac{\sum ||F_{\text{obs}}| - |F_{\text{calc}}||}{|F_{\text{obs}}|}$ , where all reflections belong to a test set of 5% data randomly selected data.

## Chapter 4. Functional studies of ParA

The stable inheritance of genomic material in bacterial low copy number plasmids is achieved by the components encoded by *par* loci: an NTPase, a centromere binding protein, and a DNA centromere site. Three types of *par* system have been defined to date by the nature of the NTPase. Type I systems encode NTPases called ParA with deviant Walker box motifs, Type II systems use actin-like proteins called ParM, and Type III utilizes TubZ proteins with tubulin-like folds. The partitioning mechanism of Type II has been fairly well characterized. Bidirectional elongation of ParM filament capped between two partition complexes pushes the plasmids apart to opposite cell poles.

The recently recognized Type III partition system has also been suggested to undergo a filamentous mechanism where the treadmilling TubZ filaments carry the plasmid to the cell pole. The Type I partition system is the most abundant and common in bacterial plasmids and chromosomes, however the mechanism of Type I systems is less understood.

An important characteristic of plasmids maintained by ParA-type systems is their regular positioning over the nucleoid (Adachi et al, 2006; Ebersbach et al, 2006; Hatano et al, 2007; Ringgaard et al, 2009). Studies have shown that ParA dynamically oscillates across the nucleoid in the presence of ParB and the DNA centromere site. ParA mutants lacking this property had defects in plasmid partition, suggesting that the movement of ParA is somehow related to partitioning. However how ParA dynamics

facilitate partitioning is still unclear. Studies on different ParA homologs have shown that they can form polymers in the presence of ATP (Barilla et al, 2005; Bouet et al, 2007; Bouet & Funnell, 1999; Ebersbach et al, 2006; Lim et al, 2005). Based on the findings that ParM and TubZ have the ability to form filaments and that their partition functions are dependent on their nucleotide binding state suggests that the partitioning mechanism of Type I may resemble that of Type II if ParA polymers are physiologically relevant. However, ParA is distinct from ParM and TubZ in that it harbors nonspecific DNA binding activity (Havey et al, 2012; Hester & Lutkenhaus, 2007; Ringgaard et al, 2009; Vecchiarelli et al, 2010). This *in vitro* DNA binding activity is consistent with the nucleoid co-localization that is observed *in vivo*. It is speculated that this nonspecific binding allows ParA proteins to bind to the chromosomal nucleoid and use it as a track to move between cell poles, carrying the plasmid cargo in its wake.

In the previous chapter, we examined structures of the archaeal ParA and found that its overall structure is similar to bacterial ParA homologs. This suggests that the ParA-type system may be conserved in archaea. In this chapter, we investigate whether the archaeal ParA shares similar properties with the bacterial ParA homologs using biochemical analyses. We examined the ATP-dependent nonspecific DNA binding activity of ParA by fluorescence polarization based DNA binding assays. Based on our previously determined crystal structure, we made mutations in the deviant Walker A motif, the insert region, and the dimerization interface to ascertain their effects on DNA binding. Furthermore, a characterization of ATP/ADP binding was carried out using

ITC. Finally, ATP-dependent polymer formation of ParA was investigated using negative stain electron microscopy.

#### ***4.1. ATP-dependent nonspecific DNA binding studies using fluorescence polarization based DNA binding assays***

In order to examine the DNA binding properties of ParA, fluorescence polarization based DNA binding studies were carried out. First, we wanted to see whether the DNA binding property required the presence of ATP. Each assay was carried out with 1 nM oligonucleotide (23 bp) in the binding buffer containing 25 mM Tris pH 7.5, 100 mM NaCl, and 2mM of AMPPNP or ADP. The non-hydrolyzable ATP analogue, AMPPNP, was used to prevent ATP hydrolysis. The buffer without the nucleotides was used as a control experiment. During the titration of ParA, binding of the protein to the fluorescently labeled DNA increases the size of the particle and this lead to the increase in anisotropy. This change in anisotropy was monitored and interpreted as a consequence of protein-DNA complex formation. As shown in Figure 33A, ParA bound DNA nonspecifically only in the presence of 2 mM AMPPNP with a  $K_d$  of 3.8  $\mu$ M. There was no binding in solution that had 2 mM ADP or no nucleotides.

To confirm whether the binding is nonspecific, another set of experiments was performed with increasing NaCl concentrations (100 mM, 200 mM, and 300 mM). Since nonspecific DNA binding typically involves ionic interactions between basic residues and the acidic DNA phosphate backbone, increasing the salt concentration in the buffer should reduce the nonspecific DNA binding of ParA. Indeed, in Figure 33B, we demonstrated that increasing the salt concentration of the binding buffer decreases the

DNA binding affinity of ParA. From both sets of experiments, we conclude that ParA binds DNA nonspecifically in an ATP-dependent manner.

## **4.2. Site-directed mutagenesis studies**

### **4.2.1 ATP binding site (deviant Walker A motif)**

In order to understand the effect of ATP binding on the nonspecific DNA binding activity of ParA, mutations on the deviant Walker A motif (KGGxxK[T/S]) were made (Figure 34). The second residue of the deviant walker box motif, K12 is the signature lysine of this motif, and is predicted to be crucial for ATP hydrolysis while K17 is predicted to be responsible for ATP binding. The result showed that the K12 to alanine mutant retained nonspecific DNA binding activity, while mutating K17 to alanine completely abrogated the DNA binding activity (Figure 35). These results suggest that ATP is indeed required for ParA's nonspecific DNA binding activity.

### **4.2.2 Insert region**

In the previous chapter, we noted a region in the structure that varies significantly between pNOB8 structures and other ParA homologs. This is the so-called insert region, and in the ParA homolog structure consists of two long antiparallel beta strands that protrude from the structure. This region is nearby the winged HTH region of P1 ParA after the two structures are superimposed, and moreover, the region was suggested to be flexible and may only fold upon binding to another protein or DNA. To test whether this region is involved in DNA binding, we looked for basic residues in the sequences of this region and found three lysines, K91, K94, and K98, and mutated them

to alanine (Figure 34). The result of the DNA binding assays revealed that mutations on the basic lysine residues, K91, K94, and K98 to alanine had no effect on the DNA binding activity of ParA (Table 6). This suggests that this insert region does not function in nonspecific DNA binding.

### **4.2.3 Dimerization interface**

Mutations were made to residues involved in the ParA dimerization interface to assess their function in DNA binding. The residues that are involved in the dimerization interface of ParA are negatively or positively charged and mostly located in the loops between  $\beta 6$ - $\alpha 8$ ,  $\beta 7$ - $\alpha 10$  and the loop just before  $\alpha 11$  (Figure 34). Particularly, there are four salt bridges that seem to stabilize the dimer of ParA. These interactions are located between residues, E173-R55 and R209-E269. We mutated R55, E173, and E269 to alanine and tested their affect on DNA binding. The results showed that the DNA binding affinity of the mutants were the same as wildtype ParA (Table 6). This suggests that mutating just one residue is not sufficient to break the dimerization interface of ParA.

### ***4.3 ATP/ADP binding studies using Isothermal Titration Calorimetry***

To characterize adenine nucleotide binding by ParA, we employed Isothermal Titration Calorimetry (ITC). Instead of using a non-hydrolyzable ATP to prevent ATP hydrolysis in the solution, we used the K12A mutant (ATP non-hydrolyzable mutant) to carry out the ATP binding assays. These experiments showed that ParA K12A binds ATP with a stoichiometry of 1:1 ratio and an equilibrium dissociation constant ( $K_d$ ) of 3.8

$\mu\text{M}$  (Figure 36). The same experiment was carried out to test ADP binding by ParA. The binding isotherm revealed that ParA K12A binds ADP with a stoichiometry of 1:1 ratio. The result is consistent with the structural studies in the previous chapter, where ParA-ADP dimer structure had two molecules of ADP bound. The equilibrium dissociation constant for ADP binding by ParA is  $2.4 \mu\text{M}$ .

#### **4.4. ATP-dependent polymerization of ParA**

Lastly, negative stain electron microscopy was used to investigate whether ParA can form polymers in the presence of ATP with the help of Dr. Milam from the Erickson Lab. The images revealed that ParA at a concentration of  $2 \mu\text{M}$  forms bundles of filaments in the presence of  $1 \text{ mM MgCl}_2$  and  $2 \text{ mM AMPPNP}$  or  $2 \text{ mM ATP}$  (Figure 37B, 37C), while showing an absence of filament in the presence of  $2 \text{ mM ADP}$  or no nucleotide (Figure 37A, 37D). Next, we lowered the concentration to  $1 \mu\text{M}$ . Even at a lower concentration, we observed bundles of filaments but we also observed individual filaments in the bundle (Figure 38). This suggests that ParA has the tendency to polymerize in bundles of filaments in the presence of ATP.

#### **4.5 Effect of DNA on ParA polymer formation**

The *in vivo* substratum of ParA proteins is nucleoid DNA. Thus, we next used the same approach to examine the effect of DNA on ATP-dependent polymer formation by comparing samples that contain ParA-ATP-DNA and ParA-ATP-no DNA. Recent studies on different ParA homologs have suggested that DNA appears to have different effects on ParA polymerization. For example, Soj of *Thermus thermophilus* and  $\delta$  of

*Streptococcus pyogenes* pSM19035 only form polymers on DNA while SopA filament formation seems to be antagonized by its interaction with DNA. However, these studies used different lengths and sizes of DNA. To try and better mimic the nucleoid, we first used a linearized pUC9 plasmid, 2.7 kilobase (kb) pairs in size. Interestingly, we find that ParA still forms polymers in the presence of nonspecific DNA, but there is a striking difference in the shapes and the pattern of ParA polymers between the sample with ParA-ATP (Figure 39A) and that with ParA-ATP bound to plasmid DNA. The images in Figure 39B and 39C indicate that in the presence of plasmid DNA, ParA appears to align along the DNA in a regular pattern. We could not see any sign of regular aggregates or polymers in the images of ParA-ATP in the presence of 16 base pairs of DNA oligonucleotides with random sequences (Figure 39D). These data indicate that the size of the DNA substrate and possibly its three dimensional structure greatly impacts the polymerization properties of ParA.

## **4.6 Discussion**

### **4.6.1 DNA binding by ParA and ParA homologs**

Here we demonstrated the ATP-dependent nonspecific DNA binding activity of archaeal ParA. In the presence of AMPPNP and  $Mg^{2+}$ , ParA showed the ability to bind DNA nonspecifically. No binding was observed in the presence of ADP or no nucleotide in the binding buffer. Next, in order to confirm whether ATP binding is really crucial to ParA's nonspecific DNA binding activity, we made two mutants on the deviant Walker A motif. Mutation of K17 to alanine abolished DNA binding suggesting that indeed,

ATP binding is critical for DNA binding. Additionally, the K12 to alanine mutation had no effect on DNA binding, which indicates that ATP hydrolysis is not required for DNA binding. This ATP-dependent nonspecific DNA binding activity has been observed in both Type Ia and Type Ib ParA homologs (Bouet et al, 2007; Pratto et al, 2008; Ringgaard et al, 2009; Vecchiarelli et al, 2010).

How is this nonspecific DNA binding relevant to DNA partitioning? The *in vitro* nonspecific DNA binding is consistent with the co-localization of ParA with the nucleoid (Hester & Lutkenhaus, 2007; Leonard et al, 2005; Ringgaard et al, 2009). ParA may use the nucleoid DNA as a track to move along the axis of the cell from one pole to the other. This is also supported by the studies that showed dynamic oscillation of ParA proteins across the nucleoid (Lim et al, 2005; Marston & Errington, 1999; Quisel et al, 1999). Moreover, several studies have shown that nonspecific DNA binding is essential to the partitioning process. Indeed, when a surface exposed arginine in Soj was mutated it eliminated DNA binding (Hester & Lutkenhaus, 2007). An F SopA mutant (K340A) that had a mutation located at the C-terminus of the protein, was unable to bind DNA and also had a severe defect in partition *in vivo* (Castaing et al, 2008). The mutants used in both of these studies were shown to form dimers and were able to bind and hydrolyze ATP, indicating the partitioning defect resulted from the abrogation of DNA binding. Similar to bacteria, archaea also lack a true nucleus and nuclear envelope. Thus, the nonspecific DNA binding activity of archaeal ParA proteins indicate that they therefore could utilize the nucleoid DNA as a track for DNA cargo movement.

Furthermore, the ATP hydrolysis activity of different ParA proteins has been shown to be essential for the partition process (Barilla et al, 2005; Fung et al, 2001; Pratto et al, 2008). For example, the catalytically inactive  $\delta$  protein (K36A) was shown to be defective in plasmid partitioning (Pratto et al, 2008). Several studies have also revealed that while ParA proteins alone have weak ATPase activity, this activity is significantly stimulated in the presence of both non-specific DNA and ParB (Davis et al, 1992; Watanabe et al, 1992). It was further demonstrated that the ATPase activity of ParA is stimulated by a putative arginine finger located at the N-terminus of its partner ParB protein (Barilla et al, 2007; Pratto et al, 2008). This suggests that ParB proteins promote the conversion of ParA-ATP to ParA-ADP, potentially causing the detachment of ParA from the nucleoid (Ringgaard et al, 2009; Vecchiarelli et al, 2010). However, how ATPase activity generates the force for plasmid partition is still unclear.

#### **4.6.2 Assembly of proteins in the Walker-type family of proteins**

Here, we observed that ParA form polymers in the presence of AMPPNP or ATP and magnesium at a physiologically relevant concentration ( $\leq 5 \mu\text{M}$ ). Moreover, in the presence of DNA, more regular linear aggregates of structures were observed. This suggests that ParA does not form a long and discrete filament like ParM, but rather bundles together to form irregular polymers. It can be speculated that ParA may have the tendency to form aggregates so it can simultaneously interact with the partition system for more stability. This is supported by the study on pB171 *par* locus, where it was suggested that filament bundling may reduce the detachment rate of the plasmid

from the filament end (Ringgaard et al, 2009). This is more optimal for pNOB8 system since the partition complex has two protein components, ParB and AspA to provide more stability and strength for numbers of contacts with the ParA polymer.

Polymerization of ParA has been demonstrated in a numbers of studies (Barilla et al, 2005; Bouet et al, 2007; Dunham et al, 2009; Ebersbach et al, 2006; Havey et al, 2012; Pratto et al, 2008), although the protein concentrations used in the experiments were far above physiological relevant concentrations. Hence, whether polymerization is required for Type I partition is still controversial. However, some studies support a role for polymerization. For example, discrete linear ParA structures were observed by super-resolution fluorescence imaging in *Caulobacter crescentus* (Ptacin et al., 2010). A study of the *Vibrio cholera* chromosome II ParA2 protein showed that it formed helical filaments on double-stranded DNA using electron microscopy (Hui et al., 2010). Moreover, *in vivo* imaging of fluorescently labeled pB171 ParA revealed helical, filamentous structures that colocalized with the nucleoid (Ringgaard et al., 2009). In the same study, a pulling mechanism was proposed. In this mechanism, ParA-ATP binds to the nucleoid DNA and polymerizes on the nucleoid. Once ParB stimulates its ATP hydrolysis, ParA starts to depolymerize and the retraction of the ParA polymer generates the pulling force for plasmid movement.

In the diffusion ratchet mechanism, ParA-ATP dimers are thought to mediate partition. Similarly to the polymerization or pulling model, here ParA-ATP binds to the nucleoid nonspecifically. In this case, it is thought the ParA dimers form a gradient-like

distribution on the nucleoid. Furthermore, in the study of P1 ParA, a slow conformational change from ParA-ATP to ParA-ATP\* was proposed. As a consequence of this putative conformational change, a time delay is provided between the release of ParA-ADP from the nucleoid and rebinding of ParA-ATP\* to the nucleoid. This time delay generates an uneven distribution of nucleoid bound ParA-ATP dimers and hence, according to this model, provides the motive force for plasmid partition (Vecchiarelli et al, 2010). The dynamic interactions of F- and P1-plasmid partition systems have been recapitulated *in vitro* using total internal reflection fluorescence microscopy (TIRFM) using purified components inside a DNA-carpeted flow cell as an artificial nucleoid surface (Hwang et al, 2013; Vecchiarelli et al, 2013). However, the shortcoming of the *in vitro* system used in these studies was that the partition complexes were only transiently tethered to the DNA carpet and the plasmid diffused away from the carpet (Hwang et al, 2013). It was hypothesized that the surface confinement was required to maintain contact between the plasmid and the DNA carpet. To mimic surface confinement on the nucleoid, magnetic beads coated with plasmid partition complexes were used and a magnetic force perpendicular to the DNA-coated flow cell surface was applied. The result revealed a directed cargo motion driven by a surface ATPase gradient, which suggested that physical confinement is another key requirement for ParA-mediated plasmid segregation by such a diffusion-ratchet model (Vecchiarelli et al, 2014). Indeed, the shortcomings of this model reside in the fact that the characteristics of a magnetic bead differ from those of a DNA molecule, and the magnetic force used here to confine

the beads to the DNA-carpeted surface may not recapitulate the situation in cells (Kiekebusch & Thanbichler, 2014).

These findings have called into question the relevance of ParA polymerization in Type I segregation. However, a recent mathematical modeling study suggested that rather than localizing all over the nucleoid, ParA-ATP dimers may be organized in a 1D-like structure along the nucleoid. One potential explanation for this was that ParA-ATP structures are sensitive to the overall nucleoid architecture (Ietswaart et al, 2014). Thus, the question of how the chromosomal architecture may affect ParA function also needs to be addressed.

#### **4.7 Experimental procedures**

*Expression and Purification of ParA* The gene expressing ParA was obtained as a codon-optimized gene from Genscript and cloned into pET15b. The resulting construct was transformed into BL21(DE3). For protein expression, 250 ml of LB medium with 100 µg/ml ampicillin was inoculated with one colony of the pET15b-*parA* construct and was grown overnight at 37 °C. This 250 ml culture was used to inoculate 9 L of LB. The resultant cells were grown at 37 °C to an OD<sub>600</sub> of 0.6 and then induced with 0.5 mM IPTG for 16 hrs at 9 °C and harvested by centrifugation. For purification, cells were resuspended in buffer A (25 mM Tris pH 7.5, 300 mM NaCl, 2 mM BME, and 5% glycerol), lysed and centrifuged. The supernatant was loaded onto a Ni-NTA column and washed with buffer A containing 7 mM Imidazole. The protein was eluted with

buffer A containing 300 mM Imidazole. Buffer exchange and protein concentration were carried out using Amicon ultra centrifugation filters (Millipore).

*DNA binding studies* A DNA oligodeoxynucleotide (23 bp) with the sequence, 5'-TGC TCT ATG ATT AAC ATA GAG CA -3', labeled with 6-carboxyfluorescein at the 3'-end was used for fluorescence polarization (FP) studies. The labeled DNA was annealed with the unlabeled complementary strand with the sequence, 5'-TGC TCT ATG TTA ATC ATA GAG CA -3'. The DNA binding assay was carried out at 25 °C in 1 ml binding buffer containing 25 mM Tris pH 7.5, 100 mM NaCl, and 1 mM MgCl<sub>2</sub> with 1 nM labeled DNA and 2 mM of AMPPNP or ADP. The non-hydrolyzable ATP analogue, AMPPNP, was used to prevent ATP hydrolysis in the solution. An assay was performed using buffer without the magnesium and the nucleotides as a control. Samples were excited at 490 nm, and the fluorescence emission was measured at 520 nm. Each assay was carried out with 1 nM oligonucleotide in the binding buffer and ParA (at 1 mg/ml, 26 μM) was titrated into the reaction mixture. Changes in fluorescence millipolarization ( $mP = P \cdot 10^{-3}$ , where P is polarization) upon ParA addition were monitored using a Panvera Beacon 2000 (Panvera Corporation). The data were normalized using the equation,  $(P - P_0) / (P_{\max} - P_0)$ , and analysed with KaleidaGraph and fitted to a simple bimolecular binding model by nonlinear least squares regression using the following equation such that the  $K_d$  values represent the protein concentration at half-maximal DNA binding (Lundblad et al, 1996):

$$A = \frac{[L][A_f - A_b]}{K_d + [L]} + A_b$$

(A= Measured anisotropy, [L]= ligand concentration, A<sub>f</sub>= Anisotropy of free fluorescent molecules, A<sub>b</sub>= Anisotropy of bound fluorescent molecules)

**Site-directed mutagenesis** Mutagenesis of ParA was performed by following the instructions provided with the QuickChange site-directed mutagenesis kit (Stratagene). PCR was carried out in a 50 µl mixture using 100 ng template plasmid DNA, 200 ng of each primer, 10 nmol of dNTP mix, and 2.5 U of cloned *Pfu* DNA polymerase in *Pfu* polymerase buffer. Primers used for mutagenesis are listed in Table 7. After PCR, 1 µl of DpnI was added to the PCR reaction and was incubated at 37 °C for one hour. The mixture was then transformed into DH5α competent cells. The mutation was verified by DNA sequencing. All mutants were expressed and purified by the same method as described above.

**Isothermal Titration Calorimetry (ITC)** Protein samples were dialyzed into buffer containing 25 mM Tris pH 7.5 and 150 mM NaCl and thoroughly degassed before use. The concentration of protein samples was determined by Bradford assay. All ITC measurements were performed at 25 °C using a VP-ITC calorimeter (Microcal). 28 5-µl injections of the 0.5 mM ATP were automatically injected into 470 µl of 26 µM of ParA with an interval of 250 sec at a constant stirring rate of 250 rpm or 28 5-µl injections of the 0.5 mM ADP were automatically injected into 470 µl of 260 µM of ParA. All data were collected and analyzed using the manufacturer-supplied software package, Origin 7.0 (OriginLab Corp.). The resulting isotherms were fit to one-site independent binding

model during iterative fitting until the model best fit the data. Control experiments were carried out by titrating the binding buffer into the cell containing solution of ParA in the cell.

*Filament Formation and Electron Microscopy* ParA at 2  $\mu$ M was incubated in 25 mM Tris pH 7.5, 100 mM NaCl, 1 mM MgCl<sub>2</sub>, and 2 mM AMPPNP or 2 mM ATP or 2 mM ADP for 30 minutes at 37 °C before application to EM grids. ParA-DNA polymers in the presence of ATP were prepared with 1  $\mu$ M ParA in 25 mM Tris pH 7.5, 100 mM NaCl, 1 mM MgCl<sub>2</sub>, and 2 mM ATP with a linearized pUC9 plasmid DNA (2.7 kilobase pairs) at a ratio of 30:1 (wt/wt). This mixture was incubated at 37 °C for 30 min before application to EM grids. For negative staining, grids covered with a thin carbon film were made hydrophilic by exposure to UV light and ozone using a Spectroline 11SC-1 Pencil shortwave UV lamp (catalog number 11-992-30; Fischer Scientific, Pittsburgh, PA) and UVP Pen-Ray lamp power supply (catalog number UVP99 0055 01; Fischer Scientific). The grids were treated for 45 min and negatively stained using three drops of 2% uranyl acetate. Images were collected on a Philips EM420 equipped with a CCD camera.

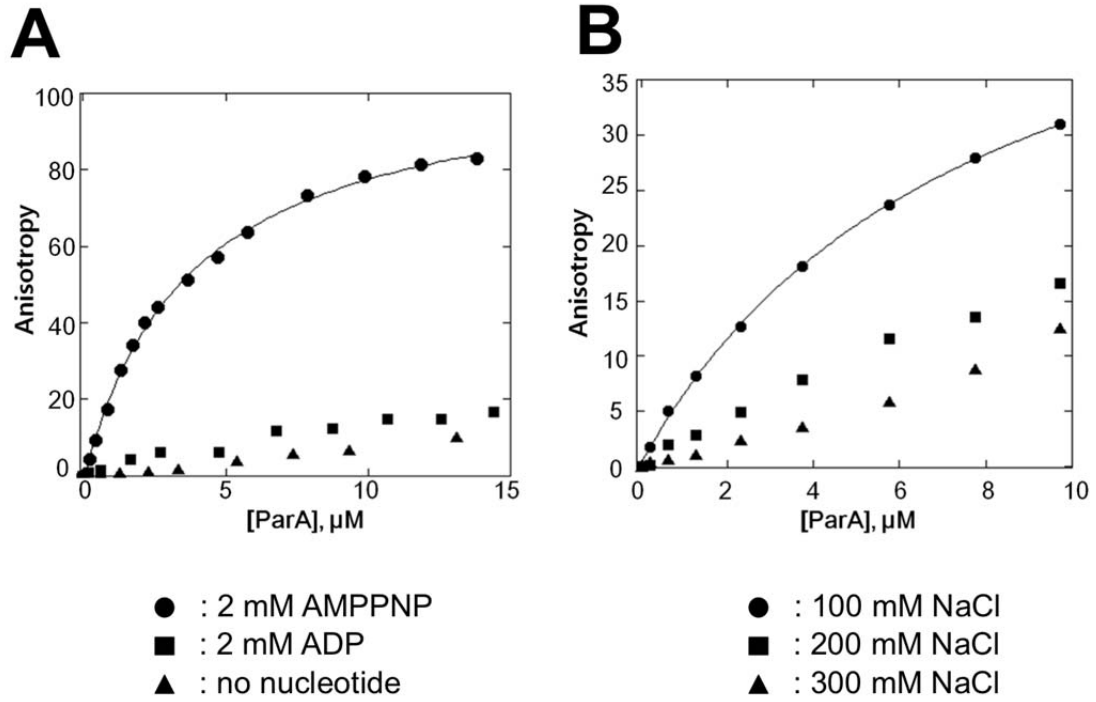


**Figure 33. ATP-dependent nonspecific DNA binding activity of ParA.**

A: Each assay was carried out with 1 nM oligonucleotide in the binding buffer containing 25 mM Tris pH 7.5, 100 mM NaCl, and 2mM of AMPPNP or ADP or no nucleotide. B: Salt-dependent nonspecific DNA binding activity of ParA.

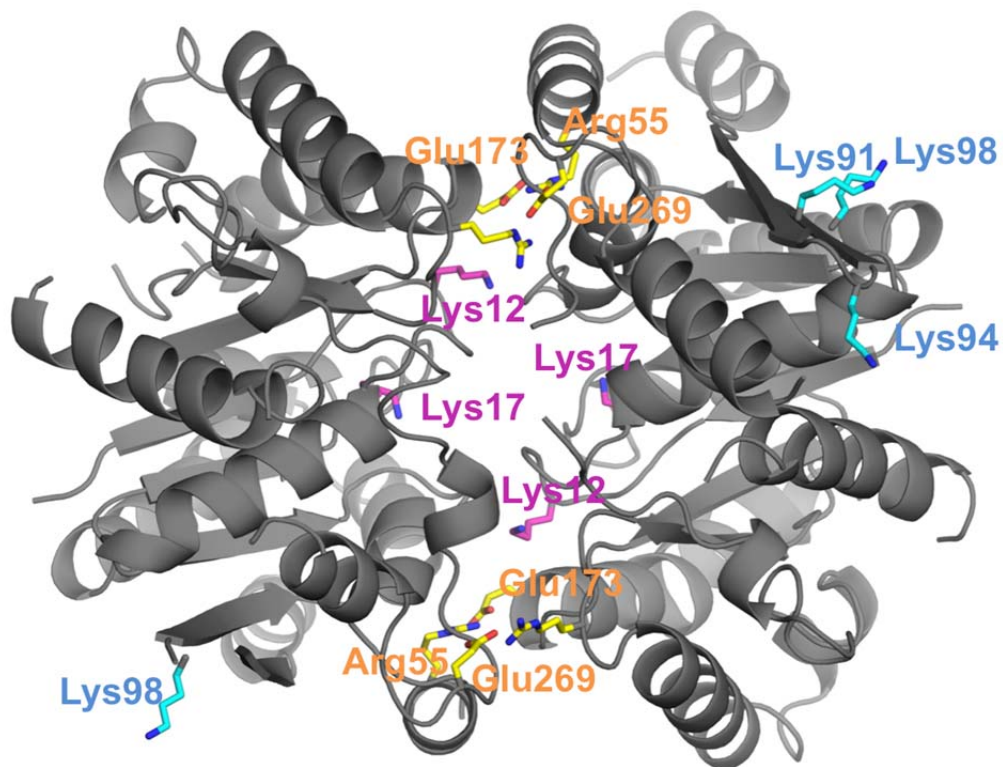


**Figure 34. Structure based site-directed mutagenesis studies**

The residues of deviant Walker A motif are indicated in magenta, the basic residues from the insert region are indicated in cyan, the residues in dimerization interface are indicated in yellow.

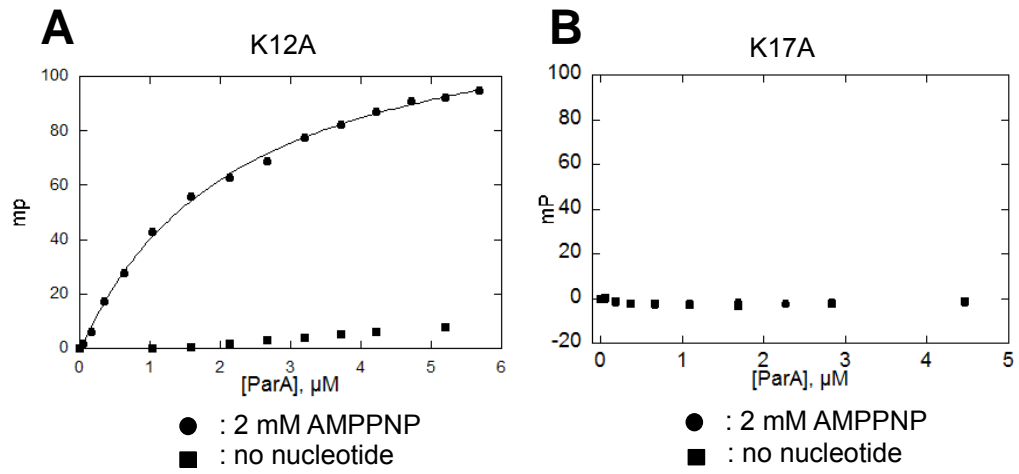


**Figure 35. Site-directed mutagenesis studies on deviant Walker A motif.**

A: Effect of ATP binding on DNA binding activity. B: Effect of ATP binding on DNA binding activity.

**Table 6. DNA binding studies of ParA mutants**

	$K_d$ ( $\mu\text{M}$ )
Wildtype	$3.5 \pm 0.2$
K12A	$2.4 \pm 0.3$
K17A	N/D
R55A	$1 \pm 0.8$
K91A	$6.2 \pm 0.1$
K94A	$2.4 \pm 0.4$
K98A	$1.5 \pm 0.4$
E173A	$3.5 \pm 0.2$
E269A	$1.1 \pm 0.7$

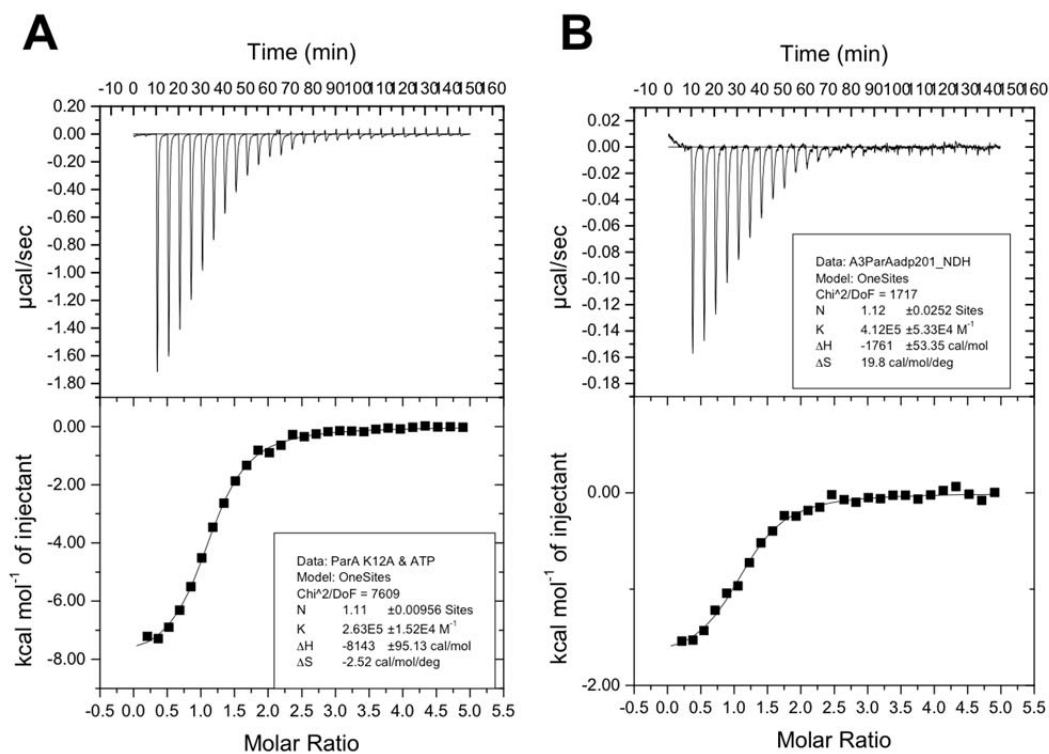


**Figure 36. ITC isotherms of ATP binding and ADP binding of ParA**

Representative experiments are shown. In each case the heat signal is shown (upper panels) together with the binding isotherm derived from this signal. A: ParA (26  $\mu\text{M}$ ) in the cell, ATP (500  $\mu\text{M}$ ) in the syringe. B: ParA (26  $\mu\text{M}$ ) in the cell, ADP (500  $\mu\text{M}$ ) in the syringe.

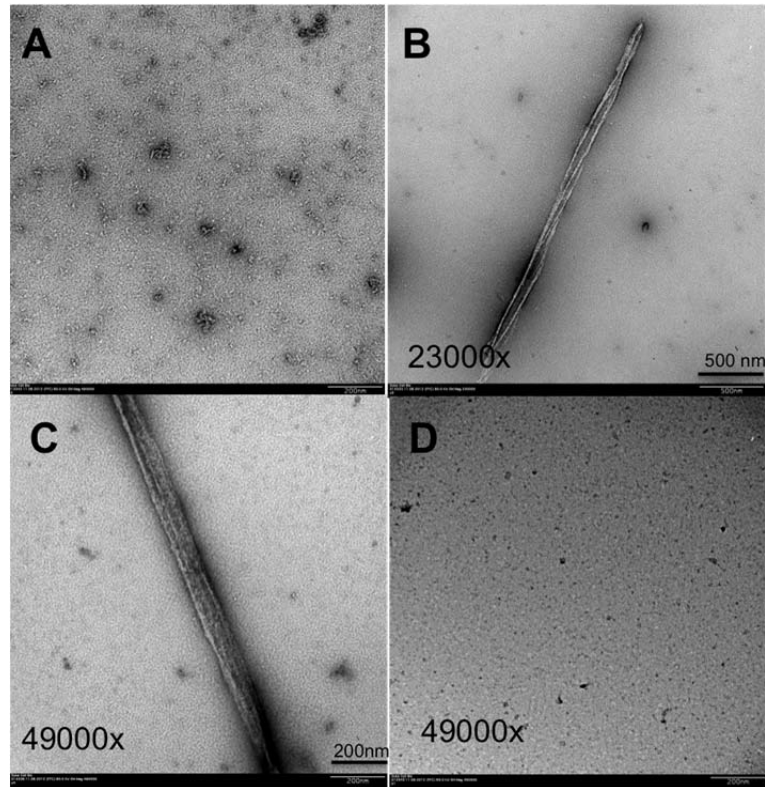


**Figure 37. ATP-dependent polymerization of ParA**

Negative Stain Electron Microscopy images of ParA polymers *in vitro*. A: ParA in the presence of 2 mM ADP and 1 mM MgCl<sub>2</sub> showing an absence of filaments. B: ParA filaments at 2 μM concentration in the presence of 2 mM AMPPNP, 1 mM MgCl<sub>2</sub> C: 2 mM ATP and 1 mM MgCl<sub>2</sub> D: ParA in the presence of 2 mM ADP and 1 mM MgCl<sub>2</sub> also showing an absence of filaments.

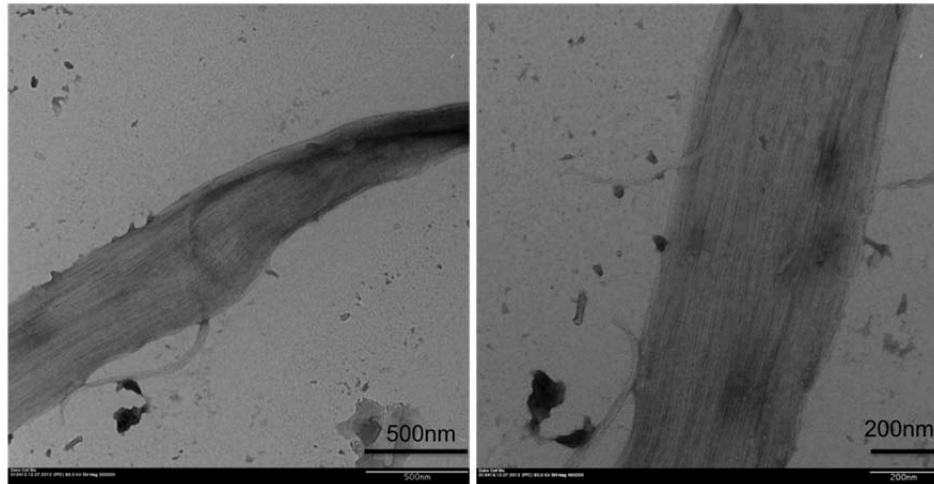


**Figure 38. ATP-dependent polymer formation at 1  $\mu$ M protein concentration**

ParA at 1  $\mu$ M concentration revealed the individual single filaments in the presence of 1 mM MgCl<sub>2</sub> and 2 mM AMPPNP.

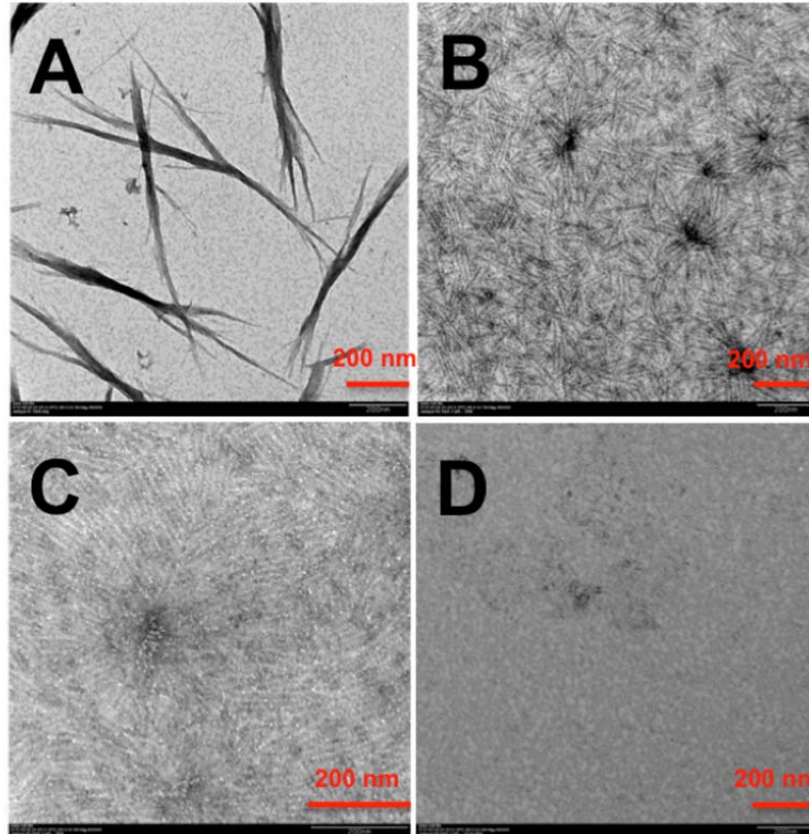


**Figure 39. Negative stain electron micrographs of ParA incubated with ATP in the absence and presence of DNA *in vitro*.**

A: ParA polymers in the presence of ATP with no DNA showing irregular shapes of polymers. B: ParA in the presence of ATP and plasmid DNA. C: B at higher magnification D: ParA in the presence of ATP, magnesium, and the oligonucleotides of 16 base pairs.

**Table 7. Primers used for site-directed mutagenesis**

	Forward	Reverse
K91A	CTTCATCCATGTTAGTGCGAC CTCCAAAGGCGAAG	CTTCGCCTTTGGAGGTCGCACTA ACATGGATGAAG
K94A	CATGTTAGTAAAACCTCCGC AGGCGAAGTTAAAGTCTCC	GGAGACTTTAACTTCGCCTGCGG AGGTTTTACTAACATG
K12A	GGTAAAGTTATCGCAATCCA CAATTCGCAGGCGGTGTTGG TAAAA	TTTTACCAACACCGCCTGCGAAA TTGTGGATTGCGATAACTTTACC
K17A	CAAAGGCGGTGTTGGTGCAA CGACGCTGACGGCG	CGCCGTCAGCGTCGTTGCACCA ACACCGCCTTTG
R55A	CCAAATCTTTGTTAAAGAAG AACGTGCCAAAGAAATTCTG CAGCAAAGTATC	GATACTTTGCTGCAGAATTTCTT TGGCACGTTCTTCTTTAACAAG ATTTGG
E173A	GGAAGATGGCACCATTGCAG CATTCAACGCTATG	CATAGCGTTGAATGCTGCAATG GTGCCATCTTCC
E269A	GATCTGGCGCAACGCATCCA TTCCGCCGA	TCGGCGGAATGGATGCGTTGCG CCAGATC

## Chapter 5. Discussion and Conclusion

DNA partition is essential for the faithful inheritance of the genome and is necessary for the survival of organisms across all kingdoms. To date, nothing has been known at the molecular level regarding the DNA segregation machinery of archaea.

This work has focused on a homolog of the pNOB8 ParA protein. The segregation cassette on the pNOB8 plasmid is similar to bacterial systems in that it encodes ParA, a Walker box ATPase, and ParB. Additionally, the cassette contains a third required protein component called AspA. Thus, this archaeal segregation cassette is atypical in that it has a tricistronic architecture, unlike the more typical bicistronic architecture found in bacteria. Here, we have structurally and biochemically characterized a pNOB8 ParA homolog. The structure of this ParA revealed that it is structurally similar to the bacterial ParA proteins. Moreover, its abilities to bind DNA nonspecifically and to form polymers in the presence of ATP were also similar to what has been observed in bacterial ParA proteins. Recent data has shown that chromosome of *Sulfolobus solfataricus* also employs a Walker-based segregation system. Here the ParA and ParB homologs have been called SegA and SegB, respectively (Kalliomaa-Sanford et al, 2012). Thus, this indicates that Walker-box-based partition systems may be widely conserved in archaea.

While the motor protein of the pNOB8 partition system shows strikingly similar features to bacteria, there are also some unexpected eukaryotic features in the system. The crystal structure of the C-terminal region of ParB was solved in the lab (Schumacher,

manuscript under review), and the structure shows strong structural homology to CenpA. CenpA is a histone H3 variant, which serves to mark the centromere location in eukaryotes. It is essential for the recruitment and assembly of the eukaryotic chromosome segregation machinery (Sekulic et al, 2010; Tachiwana & Kurumizaka, 2011).

### **5.1 Speculative Model for archaeal ParA mediated partition**

The structural and biochemical data presented in this work together with other studies in the Schumacher lab and experiments on other Type I *par* systems leads to a speculative model for pNOB8 plasmid segregation. In this model, cycles of assembly and disassembly of ParA aggregates generates the force that drives movement of the plasmids over the nucleoid, as shown in Figure 40. In this model ParA would first bind ATP driving it into an active dimer state, allowing ParA to bind the nucleoid. Once the ParA aggregates contact the partition complex, ParA ATP hydrolysis activity is stimulated at the end of the ParA aggregate. This would lead to retraction of ParA and its movement across the nucleoid. As it moves, it would drag the ParB-AspA-plasmid cargo in its wake. This is a highly speculative model and much remains to be studied to arrive at a molecular model for partition.

### **5.2 Comparison with closely related Min System in *E. coli***

The *minCDE* locus of *E. coli* encodes three components required for preventing FtsZ-ring formation at the cell poles: MinD is a Walker box protein (ATPase), like partition ParAs, that oscillates rapidly from one cell pole to the other. MinC inhibits the

formation of the FtsZ-ring, MinE stimulates the ATPase activity of MinD and generates the dynamic oscillation property of the MinCD complex (Raskin & de Boer, 1999). The similarities between the Min system of *E. coli* and ParA-type partitioning systems are intriguing. First, ParA and MinD are both deviant Walker-box ATPases with similar structures. Both proteins have been observed to have dynamic oscillation properties on a cellular binding surface (nucleoid and cell membrane, respectively) (Ebersbach & Gerdes, 2004; Raskin & de Boer, 1999; Ringgaard et al, 2009). Furthermore, the nucleotide binding state determines the subcellular locations of ParA and MinD, where ATP-bound dimers interact with their cellular surface while ATP hydrolysis stimulated by their partner proteins (ParB and MinE, respectively), releases the proteins from their surface bound states (Barilla et al, 2007; Dunham et al, 2009; Leonard et al, 2005; Ma et al, 2004; Pratto et al, 2008). The dynamic oscillatory behavior of ParA and MinD somehow functions to position a specific cellular structure (plasmid and FtsZ ring, respectively) (Raskin & de Boer, 1999; Ringgaard et al, 2009).

### **5.3 ParA-like ATPases in other processes**

Recent studies have reported a new class of ParA-like protein to be involved in protein transport. These proteins have been shown to function in the subcellular localization of the chemotaxis machinery in *Rhodobacter spheroids* (Thompson et al, 2006), cell pole maturation in *Vibrio cholerae* (Ringgaard et al, 2011), and the mediation of the accurate distribution of carboxysomes in the cyanobacterium *Synechococcus* (Savage et al, 2010). The resulting subcellular distributions resemble the equipositioning of plasmids

maintained by ParA-type partitioning systems (Roberts et al, 2012). These examples show that Walker-box proteins have evolved to mediate the transport of a variety of cellular structures.

#### **5.4 Future Directions**

Although the molecular mechanisms involved in plasmid partition by ParA based systems are starting to be resolved, important questions remain. First, the role of polymerization in this form of partition is still unclear. Secondly, how the regular positioning of plasmids are achieved by Walker-type partition systems is still poorly understood. The interaction between the nucleoid bound ParA and plasmid bound partition complex needs to be elucidated to address how ParA ATPase activity is stimulated and how it affects the DNA binding property of ParA. The role of the nucleoid and how its shape contributes to partition also needs to be addressed. *In vitro* reconstitution experiments along with mathematical modeling would be useful in answering some of these questions.

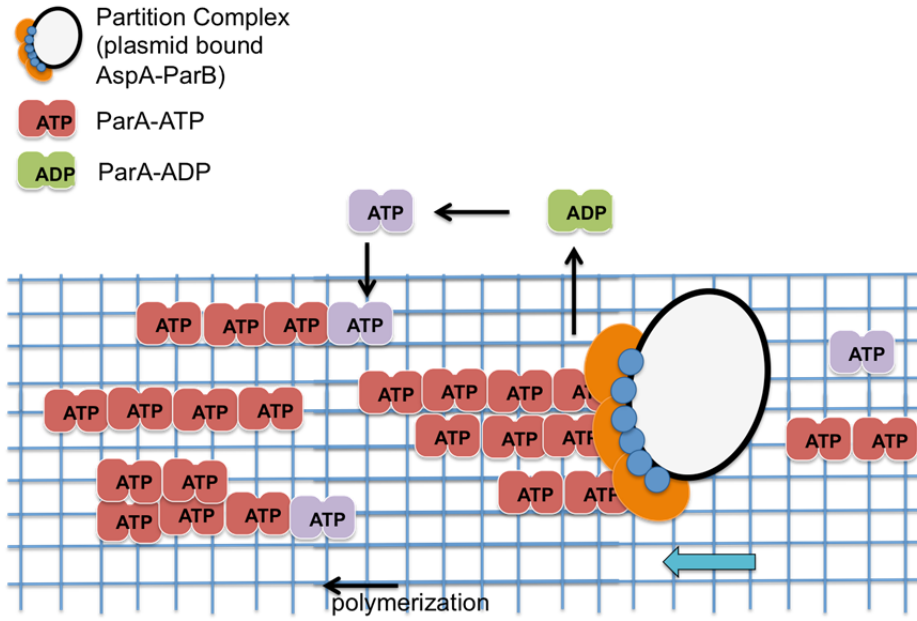


Figure 40. Schematic figure of the speculative model for archaeal ParA mediated partition

## Appendix. Protein-protein interaction studies of RacA and DivIVA

### *Introduction*

DNA segregation is a process essential for the accurate inheritance of the genetic material. This is a challenge in the cells that divide asymmetrically, such as *B. subtilis*. Cell division in the growing cells of *B. subtilis* occurs in the mid-cell by binary fission, while sporulating cells undergo asymmetric cell division leading to the generation of two different sized daughter cells, the forespore (the small sized) and the mother cell. Early in sporulation, the chromosome destined to enter the spore needs to be positioned to the extreme pole of the cell to ensure both the forespore and the mother cell each receive a chromosome. The mechanism of chromosome segregation during sporulation begins with chromosome remodeling. Specifically, chromosomes become condensed to form an elongated, serpentine-like structure known as the axial filament (Ryter et al, 1966), which has *oriC* located at its ends. The axial filament extends from pole to pole, with the *oriC* region of each chromosome anchored at each pole (Hauser & Errington, 1995; Pogliano et al, 2002). Then the septum forms near one pole and traps the *oriC* region of one chromosome (about one third of the chromosome) into the newly formed forespore (Wu & Errington, 1994). The SpoIIIE protein assembles at the edge of the septum into a pore that transverses the septum, and serves to translocate the remaining portion of the chromosome across the septum into the forespore (Wu & Errington, 1994; Wu & Errington, 1997) (Figure 41).

RacA is 184 residue sporulation-specific protein that has both specific and nonspecific DNA binding activity. It binds with high specificity to GC-rich regions near the *oriC* with the consensus, TGACGCCGGCGTCA (Ben-Yehuda et al, 2003). Importantly, fluorescence microscopy studies showed that RacA is essential for the formation of the axial filament, which is required to efficiently trap the chromosome into the forespore. Moreover, RacA was shown to localize to the cell poles. Its polar localization function is needed for the anchoring of the segregating chromosome at cell poles. This polar targeting was suggested to be dependent on its interaction with DivIVA (Wu & Errington, 2003).

DivIVA is located at mid-cell during cell division and at the cell poles in mature cells. DivIVA is also responsible for the polar localization of the cell division inhibitor MinCD in *B. subtilis* (Edwards & Errington, 1997; Marston & Errington, 1999). During sporulation DivIVA acts as an anchor for the *oriC* region at the cell poles in preparation for asymmetric cell division (Thomaides et al, 2001). Crystal structures of DivIVA domains revealed that its N-terminal lipid-binding domain (LBD) forms a parallel coiled-coil. Mutagenesis studies showed this region is essential for membrane binding. Although it was at low resolution, the crystal structure of the C-terminal domain (CTD) of DivIVA displayed a curved tetramer formed by two parallel coiled-coils. It was suggested that this DivIVA domain interacts with other proteins (Oliva et al, 2010).

Our lab has recently determined structures of RacA bound to its cognate DNA site (Schumacher, manuscript in preparation). Interestingly, these structures showed

that the N-terminal region of RacA, which contains a HTH domain, binds DNA both specifically and nonspecifically. Furthermore, these structures unveiled a mechanism for how RacA forms the axial filament when bound to the chromosome. These findings combined with previous data from other labs showing that a truncated RacA protein lacking the HTH domain localized only to the cell suggests that the C-terminal region of RacA is responsible for polar localization, probably via interaction with other proteins, while the N-terminal domain binds DNA and forms the axial filament (Ben-Yehuda et al, 2003). Further support for this model, are data revealing a positive interaction between DivIVA and RacA by bacterial two-hybrid interaction assays (Lenarcic et al, 2009). However, to date there are no biochemical data showing a direct interaction between DivIVA and RacA. To determine if the RacA C-terminal domain does in fact bind directly to the DivIVA C-terminal domain, we employed ITC. Specifically, we analyzed the ability of the DivIVA C-terminal region (59-164) and the RacA C-terminal region (70-184) to interact (Figure 42).

## **Result**

As shown in the Figure 43, the result of ITC experiment demonstrated that indeed, the RacA and DivIVA C-terminal regions interact. The molar ratio of the two binding curves is 0.88 and 0.82, which suggest that RacA and DivIVA interact with a stoichiometry of 1:1. The  $K_d$  of both experiments is 1.9  $\mu\text{M}$  and 1.5  $\mu\text{M}$ .

## ***Discussion***

Here, we have demonstrated a direct protein-protein interaction between the RacA and DivIVA C-terminal regions using ITC. Previous studies indicated that RacA is a kinetochore-like protein, which assembles into an adhesive patch that anchors the *oriC* region of the chromosome to the cell pole via an interaction with DivIVA (Ben-Yehuda et al, 2003). Our data begin to provide a molecular picture of how this essential cell division protein, RacA, mediates its unusual functions.

## ***Experimental Procedures***

*Expression and purification of DivIVA and RacA C-terminal domains.* A gene encoding the DivIVA C-terminal domain was obtained from Genscript and subcloned into pET15b. This construct was transformed into C41(DE3) cells. For protein expression, 250 ml of LB supplemented with ampicillin was inoculated with one colony containing the pET15b-DivIVA construct and was grown overnight at 37 °C. This 250 ml culture was used to inoculate 9 L of LB medium. Cells were grown at 37 °C to an OD<sub>600</sub> of 0.6 and then induced with 0.5 mM IPTG for 16 hrs at 15 °C and harvested by centrifugation. The cells were resuspended in buffer A (25 mM Tris pH 7.5, 300 mM NaCl, 2 mM BME, and 5% glycerol), lysed and centrifuged. The supernatant, which contained the protein, was loaded onto a Ni-NTA column and washed with A buffer containing 20 mM imidazole. The protein was eluted with buffer A containing 300 mM imidazole and was further purified using size exclusion chromatography. The RacA C-

terminal domain was expressed and purified using the same protocol that was employed for obtaining pure DivIVA C-terminal domain.

*Isothermal Titration Calorimetry (ITC)* To carry out the ITC experiments, protein samples were dialyzed into a buffer containing 25 mM Tris pH 7.5 and 150 mM NaCl and thoroughly degassed. The concentration of protein samples was determined by Bradford assays. All ITC measurements were performed at 25 °C using a VP-ITC calorimeter (Microcal). 28 5- $\mu$ l injections of the 450  $\mu$ M DivIVA were injected into 470  $\mu$ l of 10  $\mu$ M of RacA with an interval of 250 sec at a constant stirring rate of 250 rpm and 28 5- $\mu$ l injections of the 680  $\mu$ M RacA (DivIVA) were injected into 470  $\mu$ l of 10  $\mu$ M of DivIVA. All data were collected and analyzed using the manufacturer-supplied software package, Origin 7.0 (OriginLab Corp.). The resulting isotherms were fit to one-site, independent binding models. Control experiments were carried out (Figure 44) by titrating RacA/DivIVA into binding buffer alone( 25 mM Tris pH 7.5 and 150 mM NaCl).

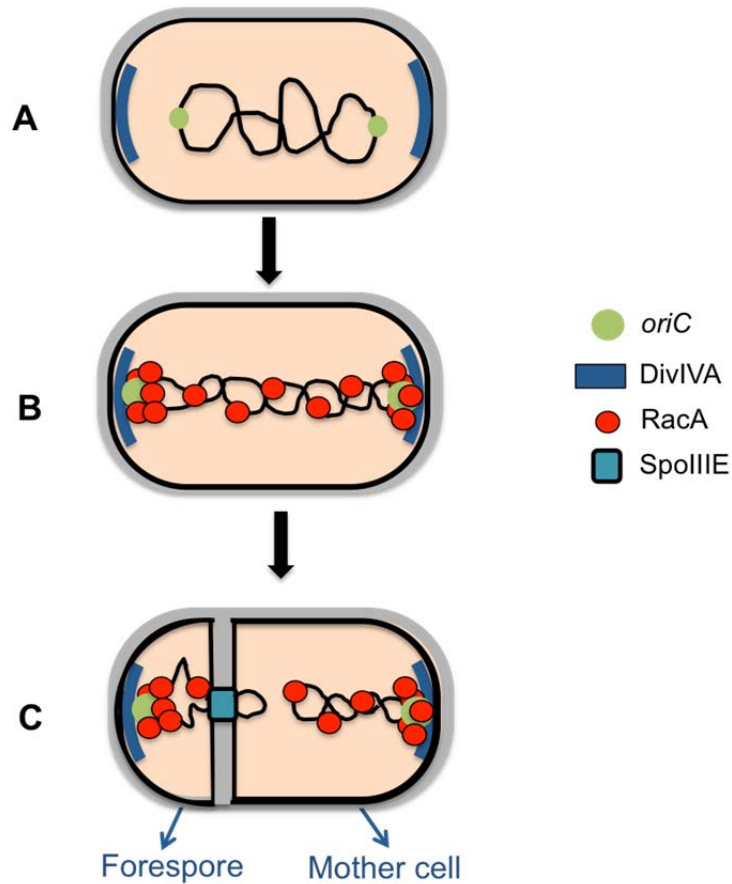


**Figure 41. Chromosome segregation during sporulation in *B. subtilis***

A: The chromosomes become remodeled into axial filament by the action of RacA (indicated by red circle) with *oriC* region (indicated by green circle) located at its ends. B: The axial filament extends from pole to pole, with *oriC* region of each chromosome anchored at extreme ends of the sporangium. C: Polar septum forms and traps 1/3 of chromosome into newly formed forespore, the other 2/3 left in mother cell. SpoIIIE protein (indicated by blue-green rectangle) pumps this 2/3 of chromosome across the septum into the forespore (Errington, 2003).

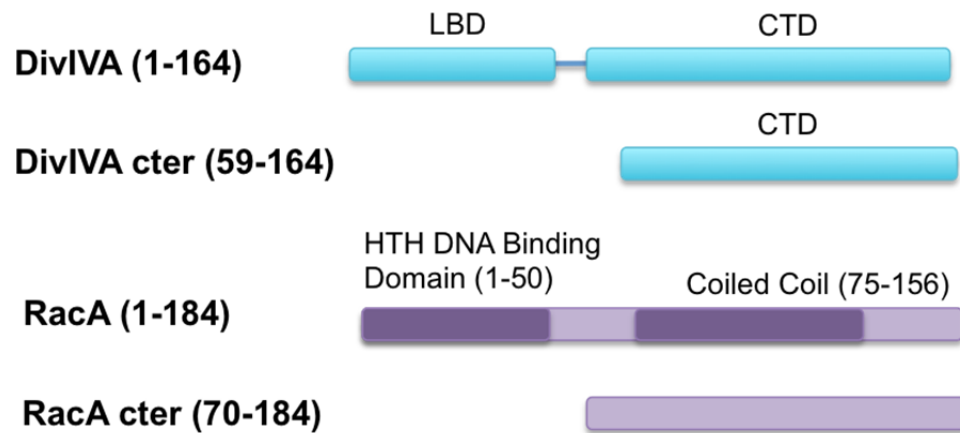


**Figure 42. Constructs of DivIVA (59-164) and RacA (70-184) used for the interaction studies.**

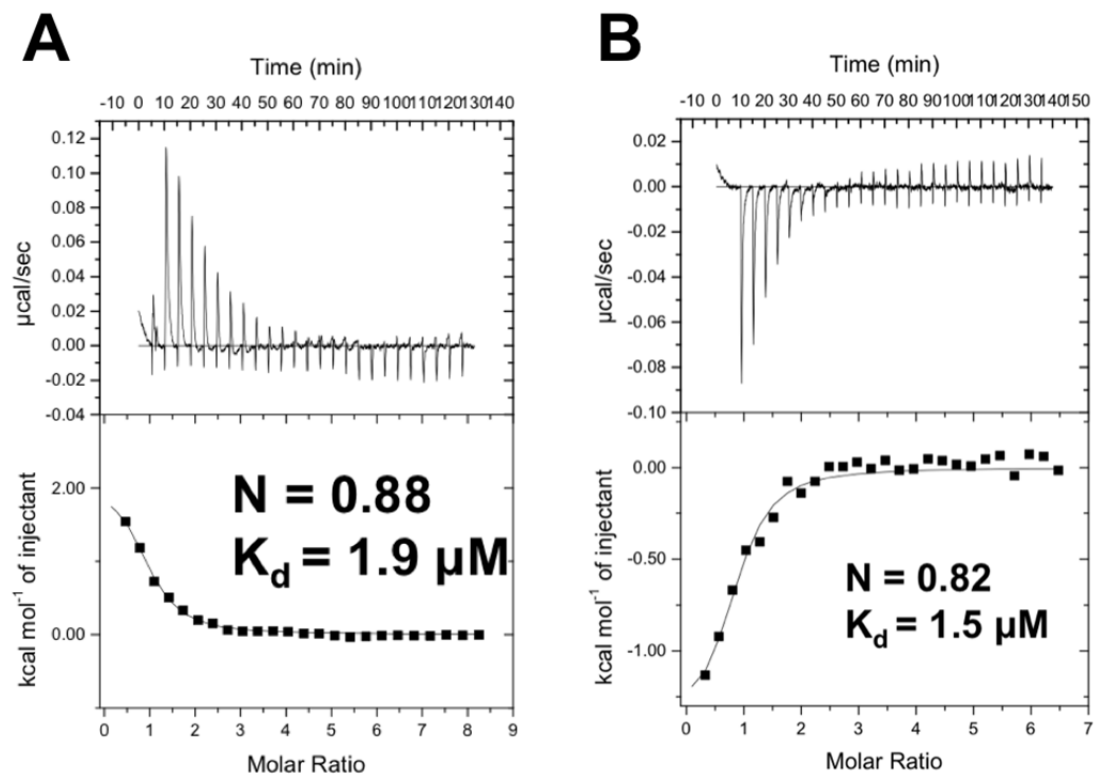


**Figure 43. ITC isotherms of DivIVA and RacA interactions.**

Representative experiments are shown. In each case the heat signal is shown (upper) together with the binding isotherm derived from this signal. A: DivIVA(450  $\mu\text{M}$ ) in the syringe, RacA (10  $\mu\text{M}$ ) in the cell. B: RacA (680  $\mu\text{M}$ ) in the syringe, DivIVA (10  $\mu\text{M}$ ) in the cell.

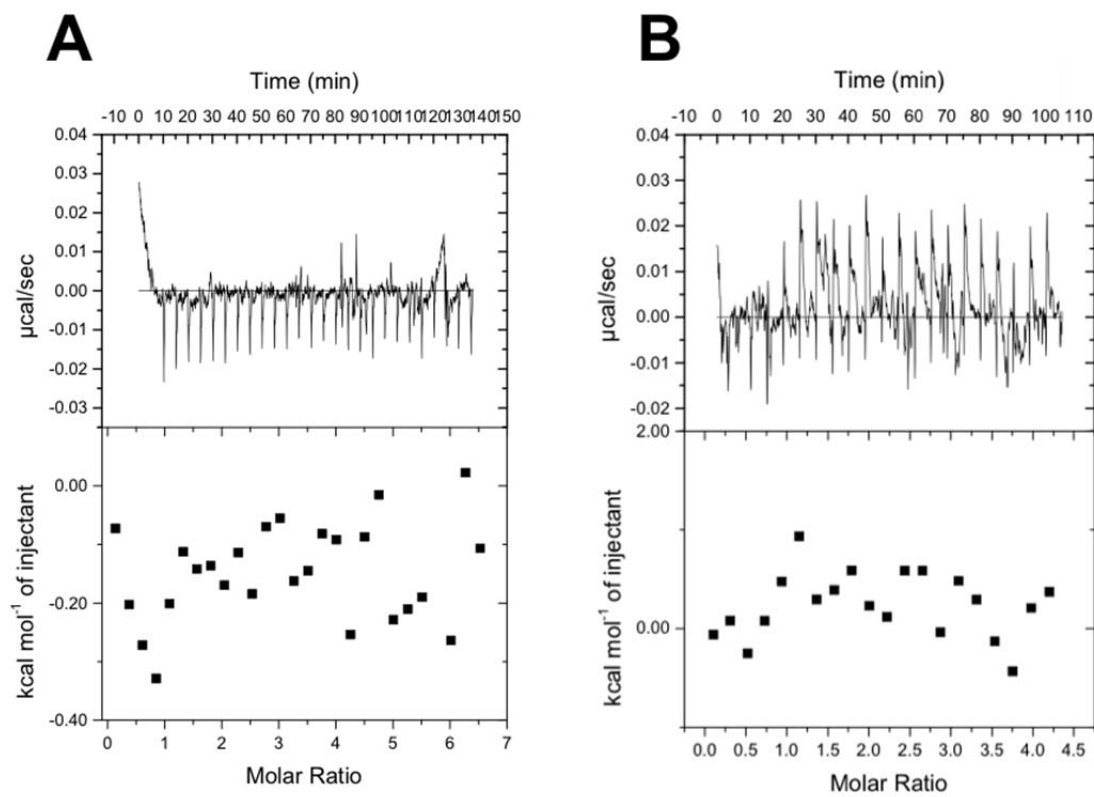


Figure 44. ITC control experiments.

A: RacA control. B: DivIVA control.

## References

- Adachi S, Hori K, Hiraga S (2006) Subcellular positioning of F plasmid mediated by dynamic localization of SopA and SopB. *Journal of molecular biology* **356**: 850-863
- Barilla D, Carmelo E, Hayes F (2007) The tail of the ParG DNA segregation protein remodels ParF polymers and enhances ATP hydrolysis via an arginine finger-like motif. *Proceedings of the National Academy of Sciences of the United States of America* **104**: 1811-1816
- Barilla D, Rosenberg MF, Nobbmann U, Hayes F (2005) Bacterial DNA segregation dynamics mediated by the polymerizing protein ParF. *The EMBO journal* **24**: 1453-1464
- Ben-Yehuda S, Rudner DZ, Losick R (2003) RacA, a bacterial protein that anchors chromosomes to the cell poles. *Science* **299**: 532-536
- Bouet JY, Ah-Seng Y, Benmeradi N, Lane D (2007) Polymerization of SopA partition ATPase: regulation by DNA binding and SopB. *Molecular microbiology* **63**: 468-481
- Bouet JY, Funnell BE (1999) P1 ParA interacts with the P1 partition complex at parS and an ATP-ADP switch controls ParA activities. *The EMBO journal* **18**: 1415-1424
- Brochier-Armanet C, Boussau B, Gribaldo S, Forterre P (2008) Mesophilic Crenarchaeota: proposal for a third archaeal phylum, the Thaumarchaeota. *Nature reviews Microbiology* **6**: 245-252
- Campbell CS, Mullins RD (2007) In vivo visualization of type II plasmid segregation: bacterial actin filaments pushing plasmids. *The Journal of cell biology* **179**: 1059-1066
- Castaing JP, Bouet JY, Lane D (2008) F plasmid partition depends on interaction of SopA with non-specific DNA. *Molecular microbiology* **70**: 1000-1011
- Chen Y, Erickson HP (2008) In vitro assembly studies of FtsZ/tubulin-like proteins (TubZ) from Bacillus plasmids: evidence for a capping mechanism. *The Journal of biological chemistry* **283**: 8102-8109
- Davis MA, Martin KA, Austin SJ (1992) Biochemical activities of the parA partition protein of the P1 plasmid. *Molecular microbiology* **6**: 1141-1147
- Driessen RP, Dame RT (2011) Nucleoid-associated proteins in Crenarchaea. *Biochemical Society transactions* **39**: 116-121

- Dunham TD, Xu W, Funnell BE, Schumacher MA (2009) Structural basis for ADP-mediated transcriptional regulation by P1 and P7 ParA. *The EMBO journal* **28**: 1792-1802
- Ebersbach G, Gerdes K (2004) Bacterial mitosis: partitioning protein ParA oscillates in spiral-shaped structures and positions plasmids at mid-cell. *Molecular microbiology* **52**: 385-398
- Ebersbach G, Ringgaard S, Moller-Jensen J, Wang Q, Sherratt DJ, Gerdes K (2006) Regular cellular distribution of plasmids by oscillating and filament-forming ParA ATPase of plasmid pB171. *Molecular microbiology* **61**: 1428-1442
- Edmondson SP, Kahsai MA, Gupta R, Shriver JW (2004) Characterization of Sac10a, a hyperthermophile DNA-binding protein from *Sulfolobus acidocaldarius*. *Biochemistry* **43**: 13026-13036
- Edwards DH, Errington J (1997) The *Bacillus subtilis* DivIVA protein targets to the division septum and controls the site specificity of cell division. *Molecular microbiology* **24**: 905-915
- Emsley P, Lohkamp B, Scott WG, Cowtan K (2010) Features and development of Coot. *Acta crystallographica Section D, Biological crystallography* **66**: 486-501
- Errington J (2003) Regulation of endospore formation in *Bacillus subtilis*. *Nature reviews Microbiology* **1**: 117-126
- Fogel MA, Waldor MK (2006) A dynamic, mitotic-like mechanism for bacterial chromosome segregation. *Genes & development* **20**: 3269-3282
- Fung E, Bouet JY, Funnell BE (2001) Probing the ATP-binding site of P1 ParA: partition and repression have different requirements for ATP binding and hydrolysis. *The EMBO journal* **20**: 4901-4911
- Garner EC, Campbell CS, Mullins RD (2004) Dynamic instability in a DNA-segregating prokaryotic actin homolog. *Science* **306**: 1021-1025
- Garner EC, Campbell CS, Weibel DB, Mullins RD (2007) Reconstitution of DNA segregation driven by assembly of a prokaryotic actin homolog. *Science* **315**: 1270-1274

- Gerdes K, Howard M, Szardenings F (2010) Pushing and pulling in prokaryotic DNA segregation. *Cell* **141**: 927-942
- Gerdes K, Larsen JE, Molin S (1985) Stable inheritance of plasmid R1 requires two different loci. *Journal of bacteriology* **161**: 292-298
- Gerdes K, Moller-Jensen J, Bugge Jensen R (2000) Plasmid and chromosome partitioning: surprises from phylogeny. *Molecular microbiology* **37**: 455-466
- Golovanov AP, Barilla D, Golovanova M, Hayes F, Lian LY (2003) ParG, a protein required for active partition of bacterial plasmids, has a dimeric ribbon-helix-helix structure. *Molecular microbiology* **50**: 1141-1153
- Guo L, Feng Y, Zhang Z, Yao H, Luo Y, Wang J, Huang L (2008) Biochemical and structural characterization of Cren7, a novel chromatin protein conserved among Crenarchaea. *Nucleic acids research* **36**: 1129-1137
- Hatano T, Yamaichi Y, Niki H (2007) Oscillating focus of SopA associated with filamentous structure guides partitioning of F plasmid. *Molecular microbiology* **64**: 1198-1213
- Hauser PM, Errington J (1995) Characterization of cell cycle events during the onset of sporulation in *Bacillus subtilis*. *Journal of bacteriology* **177**: 3923-3931
- Havey JC, Vecchiarelli AG, Funnell BE (2012) ATP-regulated interactions between P1 ParA, ParB and non-specific DNA that are stabilized by the plasmid partition site, parS. *Nucleic acids research* **40**: 801-812
- Hester CM, Lutkenhaus J (2007) Soj (ParA) DNA binding is mediated by conserved arginines and is essential for plasmid segregation. *Proceedings of the National Academy of Sciences of the United States of America* **104**: 20326-20331
- Holm L, Rosenstrom P (2010) Dali server: conservation mapping in 3D. *Nucleic acids research* **38**: W545-549
- Huffman JL, Brennan RG (2002) Prokaryotic transcription regulators: more than just the helix-turn-helix motif. *Current opinion in structural biology* **12**: 98-106

- Hwang LC, Vecchiarelli AG, Han YW, Mizuuchi M, Harada Y, Funnell BE, Mizuuchi K (2013) ParA-mediated plasmid partition driven by protein pattern self-organization. *The EMBO journal* **32**: 1238-1249
- Ietswaart R, Szardenings F, Gerdes K, Howard M (2014) Competing ParA structures space bacterial plasmids equally over the nucleoid. *PLoS computational biology* **10**: e1004009
- Kahsai MA, Vogler B, Clark AT, Edmondson SP, Shriver JW (2005) Solution structure, stability, and flexibility of Sso10a: a hyperthermophile coiled-coil DNA-binding protein. *Biochemistry* **44**: 2822-2832
- Kallioma-Sanford AK, Rodriguez-Castaneda FA, McLeod BN, Latorre-Rosello V, Smith JH, Reimann J, Albers SV, Barilla D (2012) Chromosome segregation in Archaea mediated by a hybrid DNA partition machine. *Proceedings of the National Academy of Sciences of the United States of America* **109**: 3754-3759
- Kiekebusch D, Thanbichler M (2014) Plasmid segregation by a moving ATPase gradient. *Proceedings of the National Academy of Sciences of the United States of America* **111**: 4741-4742
- Koonin EV (1993) A superfamily of ATPases with diverse functions containing either classical or deviant ATP-binding motif. *Journal of molecular biology* **229**: 1165-1174
- Lenarcic R, Halbedel S, Visser L, Shaw M, Wu LJ, Errington J, Marenduzzo D, Hamoen LW (2009) Localisation of DivIVA by targeting to negatively curved membranes. *The EMBO journal* **28**: 2272-2282
- Leonard TA, Butler PJ, Lowe J (2005) Bacterial chromosome segregation: structure and DNA binding of the Soj dimer--a conserved biological switch. *The EMBO journal* **24**: 270-282
- Lewis RA, Bignell CR, Zeng W, Jones AC, Thomas CM (2002) Chromosome loss from par mutants of *Pseudomonas putida* depends on growth medium and phase of growth. *Microbiology* **148**: 537-548
- Lim GE, Derman AI, Pogliano J (2005) Bacterial DNA segregation by dynamic SopA polymers. *Proceedings of the National Academy of Sciences of the United States of America* **102**: 17658-17663

- Lundblad JR, Laurance M, Goodman RH (1996) Fluorescence polarization analysis of protein-DNA and protein-protein interactions. *Mol Endocrinol* **10**: 607-612
- Lutkenhaus J, Sundaramoorthy M (2003) MinD and role of the deviant Walker A motif, dimerization and membrane binding in oscillation. *Molecular microbiology* **48**: 295-303
- Ma L, King GF, Rothfield L (2004) Positioning of the MinE binding site on the MinD surface suggests a plausible mechanism for activation of the Escherichia coli MinD ATPase during division site selection. *Molecular microbiology* **54**: 99-108
- Marston AL, Errington J (1999) Dynamic movement of the ParA-like Soj protein of B. subtilis and its dual role in nucleoid organization and developmental regulation. *Molecular cell* **4**: 673-682
- Moller-Jensen J, Ringgaard S, Mercogliano CP, Gerdes K, Lowe J (2007) Structural analysis of the ParR/parC plasmid partition complex. *The EMBO journal* **26**: 4413-4422
- Murayama K, Orth P, de la Hoz AB, Alonso JC, Saenger W (2001) Crystal structure of omega transcriptional repressor encoded by Streptococcus pyogenes plasmid pSM19035 at 1.5 Å resolution. *Journal of molecular biology* **314**: 789-796
- Ni L, Xu W, Kumaraswami M, Schumacher MA (2010) Plasmid protein TubR uses a distinct mode of HTH-DNA binding and recruits the prokaryotic tubulin homolog TubZ to effect DNA partition. *Proceedings of the National Academy of Sciences of the United States of America* **107**: 11763-11768
- Oliva MA, Halbedel S, Freund SM, Dutow P, Leonard TA, Veprintsev DB, Hamoen LW, Lowe J (2010) Features critical for membrane binding revealed by DivIVA crystal structure. *The EMBO journal* **29**: 1988-2001
- Pabo CO, Lewis M (1982) The operator-binding domain of lambda repressor: structure and DNA recognition. *Nature* **298**: 443-447
- Pikuta EV, Hoover RB, Tang J (2007) Microbial extremophiles at the limits of life. *Critical reviews in microbiology* **33**: 183-209
- Pogliano J, Sharp MD, Pogliano K (2002) Partitioning of chromosomal DNA during establishment of cellular asymmetry in Bacillus subtilis. *Journal of bacteriology* **184**: 1743-1749

- Poplawski A, Bernander R (1997) Nucleoid structure and distribution in thermophilic Archaea. *Journal of bacteriology* **179**: 7625-7630
- Popp D, Narita A, Oda T, Fujisawa T, Matsuo H, Nitanaï Y, Iwasa M, Maeda K, Onishi H, Maeda Y (2008) Molecular structure of the ParM polymer and the mechanism leading to its nucleotide-driven dynamic instability. *The EMBO journal* **27**: 570-579
- Pratto F, Cicek A, Weihofen WA, Lurz R, Saenger W, Alonso JC (2008) Streptococcus pyogenes pSM19035 requires dynamic assembly of ATP-bound ParA and ParB on parS DNA during plasmid segregation. *Nucleic acids research* **36**: 3676-3689
- Quisel JD, Lin DC, Grossman AD (1999) Control of development by altered localization of a transcription factor in B. subtilis. *Molecular cell* **4**: 665-672
- Raskin DM, de Boer PA (1999) MinDE-dependent pole-to-pole oscillation of division inhibitor MinC in Escherichia coli. *Journal of bacteriology* **181**: 6419-6424
- Ringgaard S, Schirner K, Davis BM, Waldor MK (2011) A family of ParA-like ATPases promotes cell pole maturation by facilitating polar localization of chemotaxis proteins. *Genes & development* **25**: 1544-1555
- Ringgaard S, van Zon J, Howard M, Gerdes K (2009) Movement and equipositioning of plasmids by ParA filament disassembly. *Proceedings of the National Academy of Sciences of the United States of America* **106**: 19369-19374
- Robert X, Gouet P (2014) Deciphering key features in protein structures with the new ENDscript server. *Nucleic acids research* **42**: W320-324
- Roberts MA, Wadhams GH, Hadfield KA, Tickner S, Armitage JP (2012) ParA-like protein uses nonspecific chromosomal DNA binding to partition protein complexes. *Proceedings of the National Academy of Sciences of the United States of America* **109**: 6698-6703
- Robertson CE, Harris JK, Spear JR, Pace NR (2005) Phylogenetic diversity and ecology of environmental Archaea. *Current opinion in microbiology* **8**: 638-642
- Ryter A, Schaeffer P, Ionesco H (1966) [Cytologic classification, by their blockage stage, of sporulation mutants of Bacillus subtilis Marburg]. *Annales de l'Institut Pasteur* **110**: 305-315

- Salje J, Gayathri P, Lowe J (2010) The ParMRC system: molecular mechanisms of plasmid segregation by actin-like filaments. *Nature reviews Microbiology* **8**: 683-692
- Salje J, Zuber B, Lowe J (2009) Electron cryomicroscopy of *E. coli* reveals filament bundles involved in plasmid DNA segregation. *Science* **323**: 509-512
- Savage DF, Afonso B, Chen AH, Silver PA (2010) Spatially ordered dynamics of the bacterial carbon fixation machinery. *Science* **327**: 1258-1261
- Schleper C, Holz I, Janekovic D, Murphy J, Zillig W (1995) A multicopy plasmid of the extremely thermophilic archaeon *Sulfolobus* effects its transfer to recipients by mating. *Journal of bacteriology* **177**: 4417-4426
- Schumacher MA (2008) Structural biology of plasmid partition: uncovering the molecular mechanisms of DNA segregation. *The Biochemical journal* **412**: 1-18
- Schumacher MA (2012) Bacterial plasmid partition machinery: a minimalist approach to survival. *Current opinion in structural biology* **22**: 72-79
- Schumacher MA, Funnell BE (2005) Structures of ParB bound to DNA reveal mechanism of partition complex formation. *Nature* **438**: 516-519
- Schumacher MA, Glover TC, Brzoska AJ, Jensen SO, Dunham TD, Skurray RA, Firth N (2007) Segrosome structure revealed by a complex of ParR with centromere DNA. *Nature* **450**: 1268-1271
- Schumacher MA, Ye Q, Barge MT, Zampini M, Barilla D, Hayes F (2012) Structural mechanism of ATP-induced polymerization of the partition factor ParF: implications for DNA segregation. *The Journal of biological chemistry* **287**: 26146-26154
- Sekulic N, Bassett EA, Rogers DJ, Black BE (2010) The structure of (CENP-A-H4)<sub>2</sub> reveals physical features that mark centromeres. *Nature* **467**: 347-351
- Sengupta M, Nielsen HJ, Youngren B, Austin S (2010) P1 plasmid segregation: accurate redistribution by dynamic plasmid pairing and separation. *Journal of bacteriology* **192**: 1175-1183
- She Q, Singh RK, Confalonieri F, Zivanovic Y, Allard G, Awayez MJ, Chan-Weiher CC, Clausen IG, Curtis BA, De Moors A, Erauso G, Fletcher C, Gordon PM, Heikamp-de Jong I, Jeffries AC, Kozera CJ, Medina N, Peng X, Thi-Ngoc HP, Redder P, Schenk ME,

Theriault C, Tolstrup N, Charlebois RL, Doolittle WF, Duguet M, Gaasterland T, Garrett RA, Ragan MA, Sensen CW, Van der Oost J (2001) The complete genome of the crenarchaeon *Sulfolobus solfataricus* P2. *Proceedings of the National Academy of Sciences of the United States of America* **98**: 7835-7840

Szardenings F, Guymer D, Gerdes K (2011) ParA ATPases can move and position DNA and subcellular structures. *Curr Opin Microbiol* **14**: 712-718

Tachiwana H, Kurumizaka H (2011) Structure of the CENP-A nucleosome and its implications for centromeric chromatin architecture. *Genes & genetic systems* **86**: 357-364

Terwilliger TC, Berendzen J (1999) Automated MAD and MIR structure solution. *Acta crystallographica Section D, Biological crystallography* **55**: 849-861

Thomaides HB, Freeman M, El Karoui M, Errington J (2001) Division site selection protein DivIVA of *Bacillus subtilis* has a second distinct function in chromosome segregation during sporulation. *Genes & development* **15**: 1662-1673

Thompson SR, Wadhams GH, Armitage JP (2006) The positioning of cytoplasmic protein clusters in bacteria. *Proceedings of the National Academy of Sciences of the United States of America* **103**: 8209-8214

Toro E, Hong SH, McAdams HH, Shapiro L (2008) *Caulobacter* requires a dedicated mechanism to initiate chromosome segregation. *Proceedings of the National Academy of Sciences of the United States of America* **105**: 15435-15440

van den Ent F, Moller-Jensen J, Amos LA, Gerdes K, Lowe J (2002) F-actin-like filaments formed by plasmid segregation protein ParM. *The EMBO journal* **21**: 6935-6943

Vecchiarelli AG, Han YW, Tan X, Mizuuchi M, Ghirlando R, Biertumpfel C, Funnell BE, Mizuuchi K (2010) ATP control of dynamic P1 ParA-DNA interactions: a key role for the nucleoid in plasmid partition. *Molecular microbiology* **78**: 78-91

Vecchiarelli AG, Hwang LC, Mizuuchi K (2013) Cell-free study of F plasmid partition provides evidence for cargo transport by a diffusion-ratchet mechanism. *Proceedings of the National Academy of Sciences of the United States of America* **110**: E1390-1397

Vecchiarelli AG, Neuman KC, Mizuuchi K (2014) A propagating ATPase gradient drives transport of surface-confined cellular cargo. *Proceedings of the National Academy of Sciences of the United States of America* **111**: 4880-4885

- Wardleworth BN, Russell RJ, Bell SD, Taylor GL, White MF (2002) Structure of Alba: an archaeal chromatin protein modulated by acetylation. *The EMBO journal* **21**: 4654-4662
- Watanabe E, Wachi M, Yamasaki M, Nagai K (1992) ATPase activity of SopA, a protein essential for active partitioning of F plasmid. *Mol Gen Genet* **234**: 346-352
- Woese CR, Fox GE (1977) Phylogenetic structure of the prokaryotic domain: the primary kingdoms. *Proceedings of the National Academy of Sciences of the United States of America* **74**: 5088-5090
- Woese CR, Kandler O, Wheelis ML (1990) Towards a natural system of organisms: proposal for the domains Archaea, Bacteria, and Eucarya. *Proceedings of the National Academy of Sciences of the United States of America* **87**: 4576-4579
- Wu LJ, Errington J (1994) Bacillus subtilis SpoIIIE protein required for DNA segregation during asymmetric cell division. *Science* **264**: 572-575
- Wu LJ, Errington J (1997) Septal localization of the SpoIIIE chromosome partitioning protein in Bacillus subtilis. *The EMBO journal* **16**: 2161-2169
- Wu LJ, Errington J (2003) RacA and the Soj-Spo0J system combine to effect polar chromosome segregation in sporulating Bacillus subtilis. *Molecular microbiology* **49**: 1463-1475
- Yamaichi Y, Niki H (2000) Active segregation by the Bacillus subtilis partitioning system in Escherichia coli. *Proceedings of the National Academy of Sciences of the United States of America* **97**: 14656-14661

## **Biography**

Jeehyun Lee was born in Seoul, Korea. She graduated Seoul National University in 2006 with the degree of Bachelor of Science in Applied Biology and Chemistry. She then went on and earned the degree of Master of Science in Agricultural Biotechnology, at Seoul National University in 2008. She came to United States in the fall of 2010 to start her doctoral studies in Structural Biology and Biophysics program at Duke University. She joined the Schumacher Lab in the Department of Biochemistry in 2011 and is currently a member in the lab under the guidance of Dr. Maria A Schumacher.